Development and Assessment of Renewable Energy Based Integrated Systems for Dimethyl Ether Production

By

Magd N. DinAli

A Thesis Submitted in Partial Fulfilment
Of the Requirements for the degree of
Master of Applied Science
In
Mechanical Engineering

Faculty of Engineering and Applied Science
University of Ontario Institute of Technology

Oshawa, Ontario, Canada

THESIS EXAMINATION INFORMATION

Submitted by: **Magd DinAli**

Master of Applied Science in **Mechanical Engineering**

Thesis title: Development and Assessment of Renewable Energy Based Integrated Systems for Dimethyl Ether Production

An oral defense of this thesis took place on December 4, 2018 in front of the following examining committee:

Examining Committee:

Chair of Examining Committee	Dr. Martin Agelin-Chaab
Research Supervisor	Dr. Ibrahim Dincer
Examining Committee Member	Dr. Dipal Patel
Examining Committee Member	Dr. Shaghayegh Bagheri

The above committee determined that the thesis is acceptable in form and content and that a satisfactory knowledge of the field covered by the thesis was demonstrated by the candidate during an oral examination. A signed copy of the Certificate of Approval is available from the School of Graduate and Postdoctoral Studies.

Abstract

Dimethyl-ether (DME) is considered to be one of the most promising, renewable alternative fuels. This thesis studies, develops, analyzes and assesses the performance of three dimethyl-ether production integrated systems, where dimethyl-ether is produced from carbon dioxide and renewable hydrogen. The three systems are fully operated by waste heat and renewable energy. The first system consists of a proton exchange membrane electrolyzer system, carbon capturing system and heat recovery from cement furnace, methanol synthesis system and dimethyl-ether synthesis system. The second system consists of a solar heliostat field, solid oxide steam electrolyzer, carbon capturing and heat recovery system from steel furnace, methanol synthesis system and dimethyl-ether synthesis system. The third system consists of gas turbine cycle, Cu-Cl thermochemical hydrogen production cycle, carbon capturing system and heat recovery from gas turbine exhaust gas, methanol synthesis system, dimethyl-ether synthesis system and multi-effect desalination system. Modeling studies and simulations are performed using both Aspen Plus, and Engineering Equation Solver software packages. These three systems are thermodynamically assessed based on energy and exergy efficiencies. The overall system's energy and exergy efficiencies resulted in 40.46 % and 52.81 for the first system, 28.75% and 32.54% for the second system, and 39.72% and 55.2 % for the third system.

Keywords: Dimethyl-ether; exergy; desalination; multi-generation; renewable energy; waste heat recovery

Table of Contents

Table of Figures

Table of Tables

Nomenclature

$\dot{E}x$	Exergy rate (kW)
ex	Specific exergy (kJ/kg)
h	Specific enthalpy (kJ/kg)
HHV	Higher heating value (kJ/kg)
LHV	Lower heating value (kJ/kg)
$\dot{m}$	Mass flow rate (kg/s)
$\dot{Q}$	Heat rate (kW)
s	Specific entropy (kJ/kg K)
T	Temperature (^{o}C or K)
$\dot{W}$	Work rate (kW)
x	Mole fraction of constituent j in the flow

Subscripts

abs	Absorber
cc	Combustion chamber
ch	Chemical
comp	Compressor
cond	Condenser
cv	Control volume
d	Destroyed
DC	Distillation column
e	Exit
en	Energy
EH	Electric heater
el	Electrolyzer
ex	Exergy
Hel	Heliostat field
i	Inlet

IC	Intercooler
LA	Lean amine
MeOH	Methanol
Mix	Mixture stream
Ph	Physical
RA	Rich amine
Reb	Reboiler
Rec	Recycle stream
s	Source
SG	Steam generator
Unrec	Unreacted gases stream

Acronyms

CCS	Carbon capturing system
Cu-Cl	Copper-Chlorine
DME	Dimethyl ether
EES	Engineering Equation Solver
GOR	Gain output ratio
HRSG	Heat recovery steam generator
HX	Heat exchanger
MED	Multi effect desalination
PEM	Proton exchange membrane
PPM	Parts per million
PR	Performance ratio
PV	Photovoltaic
REGEN	Regenerator
SOSE	Solid oxide steam electrolyzer

Acknowledgment

I would like to express my sincere gratitude to my academic supervisor Professor Dr.Ibrahim Dincer for his continuous support in my thesis study and research, for his patience, motivation and immense knowledge. His guidance has significantly improved my thesis research quality and content and encouraged me to work, produce and publish.

Nobody has been more important to me in the pursuit of this degree than the members of my family. I would like to thank my parents, whose love and guidance are with me in whatever I pursue. I wish to thank my loving and supportive brother Amr.

I am grateful to all of those with whom I have had the pleasure to work within ACE 3030 lab and CERL lab during this project. I would especially like to thank Anna Crivellari, Haris Ishaq, Maan Alzareer, Osamah Siddiqui and Sherif Saifeldin.

Chapter 1 : Introduction

Energy is one of the most critical needs to mankind for sustainability and continuous development. The world`s population is significantly growing and energy demand is growing accordingly. In this chapter, the different energy resources are reviewed and presented with their associated challenges. The significance of using renewable energy resources is also discussed. The importance of dimethyl ether production as promising fuel is also articulated in motivation. And the objectives of the present study are elucidated.

1.1 Energy Resources and Challenges

The growth of global energy demand is significantly increasing due to the population growth and industrial expansion all over the world. The world currently is highly dependent on fossil fuels to meet this huge energy demand. US Department of Energy [1] presented that the most widely used resources for energy production are mainly from fossil fuel resources as shown in Figure 1.2. As a result of the huge consumption of conventional fuel, fossil fuel reservoirs are depleting significantly.

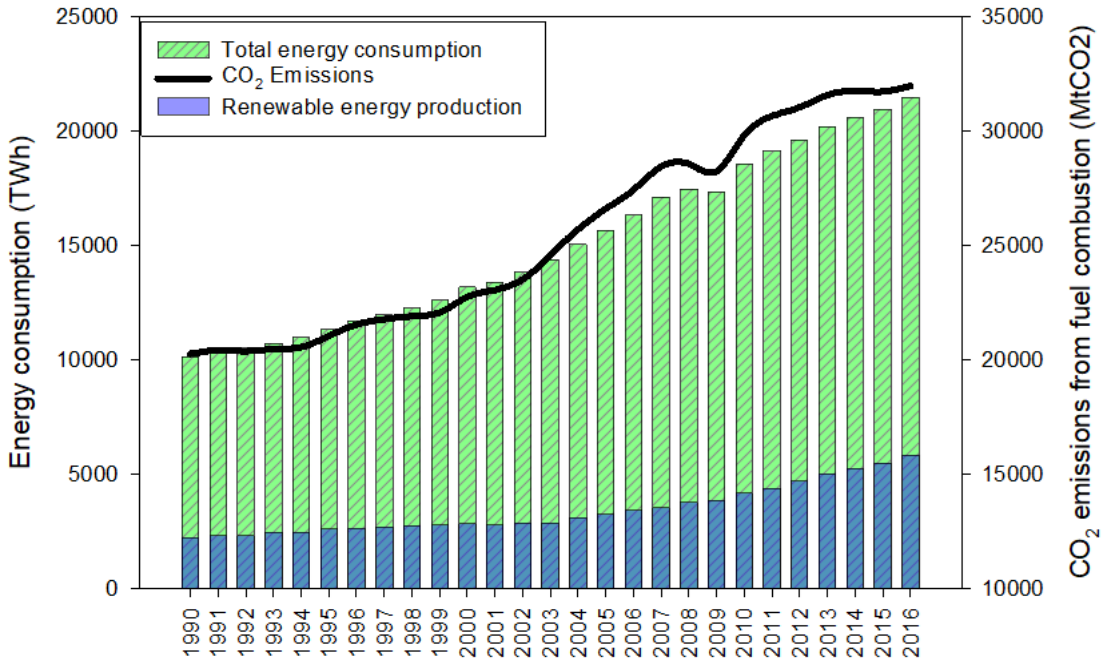

Figure 1.1 Global energy production growth & CO2 emissions from fossil fuels between 1990-2017[2]

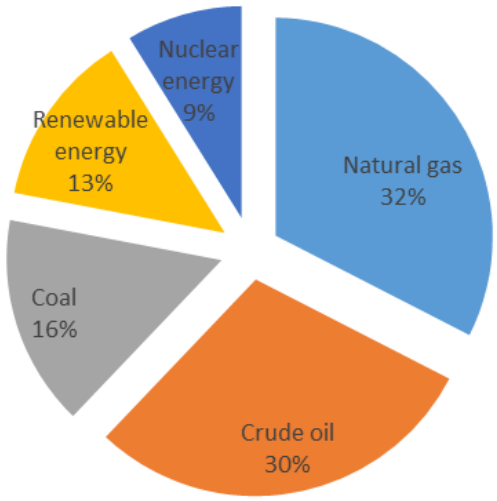

Figure 1.2 Primary energy production resources (data from [1])

Furthermore, the global energy demands for energy are projected to have an increase of 50% by 2030 [1]. The concern of limited fossil fuel resources has encouraged many research studies in this area to look for other energy resources that are renewable. For instance, solar photovoltaic energy, solar thermal energy, wind energy, geothermal energy and hydropower energy. However, these resources are intermittent due to environmental and time changes and would require energy storage systems. Consequently, it would significantly increase the investment cost. Furthermore, biomass represented by wood, crops and forestry waste are considered one of the renewable fuels with high potential of energy which can be converted by three main thermal processes which are combustion, gasification, and pyrolysis [3]. Despite the high potential of energy that biomass fuel has, still it has some challenges needs to be further investigated in terms of processing such as the mass transfer limitation, quality of syngas microbial catalyst and product recovery[4]. Moreover, Hydrogen can be considered as one of the renewable energy sources. There are many processes that can be used for hydrogen production, some of them are utilizing fossil fuel such as natural gas steam reforming, coal gasification and biomass gasification. While other processes can produce hydrogen without using fossil fuel through water electrolysis. However, storing hydrogen is very challenging due to its low density, which requires compressing it to very high pressure, And it has a highly explosive nature[5]. Table 1.1 exhibits the different properties of different renewable and non-renewable fuels.

Table 1.1 Properties of various fuels [6]

Fuel	LHV [MJ/kg]	Octane number	Cetane number	Density [kg/m^3]
Hydrogen	120.21	>125	NA	0.09
Gasoline	43.44	90-100	NA	745
Diesel	42.50	15-25	40-50	848
LPG	46.60	109	NA	508
LNG	48.62	>127	<10	450
CNG	45.71	>127	<10	174
Methanol	19.5	112	5	768
DME	27.60	35	55-60	668

1.2 Motivation

The concern of storing and handling hydrogen is reaching to technical challenges in terms of weight and volume, efficiency, durability of hydrogen storage, and driving range for transportation systems. Also, the effect of global warming significantly affecting the life on earth due to the endless increase in carbon emissions. The motivation is to obtain clean energy resources that are environmentally friendly and produce a fuel that is easy to store and handle. Dimethyl ether offers promising properties that overcome hydrogen limitations as shown in Figure 1.3. In addition, dimethyl ether gives a significant opportunity to reduce the dependence on fossil fuels, minimize the environmental impact of fuel combustion and implement more environmentally friendly energy alternative that is Practical and feasible in for implementation, production and use. In addition, it is also able to utilize renewable energy resources for synthesis. Therefore, dimethyl ether fuel from renewable energy has become the main subject of this research. The energy systems developed and studied in this research should be able to fulfill the growing energy demands in an efficient and environmentally friendly manner. The availability of renewable energy in different forms on earth and the carbon emissions from different industries have driven this thesis into

considering different renewable energy sources as well as different waste flue gas emissions.

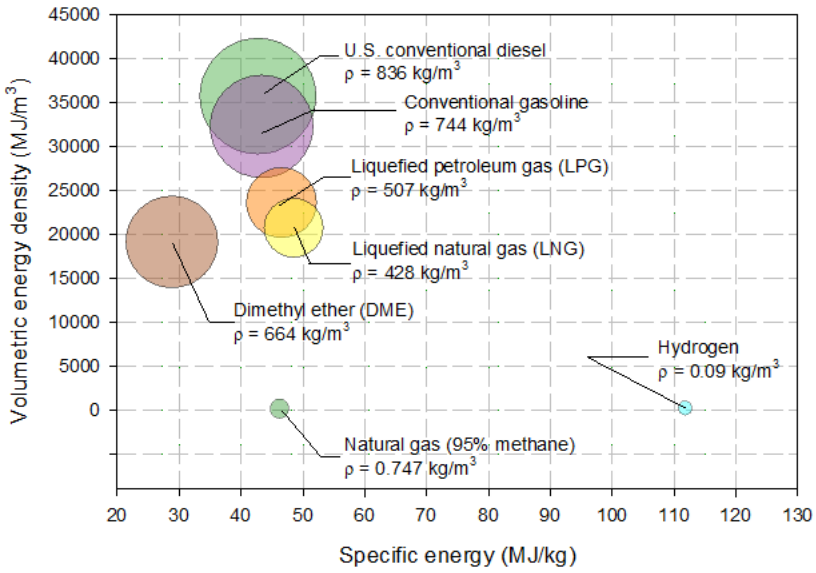

Figure 1.3 Specific energy, energy density and density of different fuels

1.3 Objectives

Based on the literature review, there are few studies in the literature that considered proposing renewable energy based DME production systems, where comprehensive energy and exergy analyses are required. The thermodynamic analyses are very important steps to assess any energy system before proceeding to any further steps. Thus, this study conducts detailed thermodynamic analyses for three different DME production energy systems. The proposed systems will be simulated and modeled through Aspen plus and Engineering equation solver software.

The specific objectives of this thesis study are described as follows:

- To propose different methods for producing hydrogen. One system produces hydrogen through PEM electrolyzer which is powered by PV solar energy. Another system, produce hydrogen through solid oxide electrolyzer which is powered using solar thermal energy source. The third system produces hydrogen through the Cu-Cl cycle which is thermochemical decomposition of water, powered by waste heat and PV solar energy.

- To develop three different energy systems for DME production. These three systems should produce DME in high purity to be used as fuel. The main subsystems of these three energy systems are waste heat source, carbon capturing unit, hydrogen production system and DME production plant.
- To model the proposed conceptual systems using Aspen plus process simulation software. Some systems are modeled through engineering equation solver (EES).
- To validate the results of the subsystems developed within the systems with published data. All the assumptions considered in the modeling process of the systems are validated with the published data in the literature.
- To perform detailed energy and exergy analyses for proposed energy systems through carrying detailed energy and exergy analyses for each subsystem of the integrated systems, evaluating energy and exergy efficiencies for each component and exergy destruction rates.
- To perform comprehensive parametric studies on the proposed systems by investigating the effect of different key parameters on the performance of each subsystem and observe the variation of their energy and exergy performances.

This research will begin by developing the conceptual systems for DME production plant by selecting the best possible combination of the main subsystems and the proper waste heat source. Then, the following chapters will analyze these systems through energy and exergy analyses. An important requirement of this research is to produce DME with high quality and purity to be used as a fuel for transportation and other industrial practices.

Chapter 2 : Literature Review

This chapter provides a literature review on the different process such as, hydrogen production technologies, carbon capturing methods from industrial waste, and waste heat recovery from different industries and the potential of energy recovery from this waste. Also, this chapter discusses the different methods and techniques for DME production from hydrogen. DME is considered to be a clean fuel because of its low exhaust emissions, does not produce particulate matter, low CO_2 emissions and high thermal efficiency. Furthermore, it can be used for different application such as, transportation, domestic applications and power generation as well.

2.1 Use of Renewable Energy in Hydrogen Production

Hydrogen is a very rich chemical storage medium due to its very high specific energy having higher heating value (HHV) of 39.42 kWh/kg which is around 2.5 times that of gasoline and methane[7]. There are two main streams for producing hydrogen from renewable energy: electrolysis and thermochemical water decomposition cycle. Electrolysis is one of the significant methods to produce hydrogen from water by applying direct electric current on the water to dissociate. The decomposed hydrogen has a high purity that can reach 99.9 vol%. Water electrolysis using renewable energy is now attracting interests since it is considered the only way to produce sustainable hydrogen without emissions or consumption of fossil fuel. The basic principle of water electrolysis as to circulate a direct current through water to dissociate it to hydrogen and oxygen. The electrodes need to be immersed in the electrolyte and need to be corrosion resistant. Furthermore, electrodes need to be separated by diaphragm or membrane to avoid the recombination of hydrogen and oxygen. There are three techniques for water electrolysis from the technological point of view, alkaline electrolyzer, proton exchange membrane (PEM) electrolyzer, and solid oxide electrolyzer. Alkaline electrolysis commonly uses liquid electrolyte KOH with a concentration of 30-40% and electrode are separated by a porous membrane that conducts hydroxyl ions. Typical operating conditions for alkaline electrolyzer is 70-90 ^{o}C with a cell voltage of 1.85-2.2 V and conversion efficiency is in the range 60-80% [8]. Gandia et al. [9] conducted several experiments on commercial alkaline water electrolysis of 5kW under typical dynamic conditions of wind energy

systems. They found that the efficiency of hydrogen production varies between 74% and 79%. Proton exchange membrane (PEM) electrolysis technology is presented in the literature as a very efficient alternative to the conventional alkaline electrolysis. It offers a number of advantages over traditional technologies such as higher energy efficiency, greater production rate, more compact design and fast response time in startup and shutting down which makes it suitable for intermittent available sources of electricity like renewable energy [8]. Meng Ni et al. [10] developed an electrochemistry model to analyze the characteristics of PEM electrolyzer. The results obtained from the model found a good agreement with experimental data in the literature. Meng et al. [11] also have performed detailed energy and exergy analyses to identify the losses and optimize the PEM electrolyzer performance for hydrogen production. Moreover, he conducted parametric analyses to study the effect of design parameters on plant energy efficiency. The third technology which is solid oxide electrolyzer. High temperature electrolysis has been under development since 1980 [12].The main advantage for high temperature electrolysis is that part of the energy demand for water splitting is obtained from high temperature heat source thus, electrolysis is performed at lower electricity consumption. Many research are mainly focusing on the use of solar thermal energy or waste heat for the high temperature electrolysis process. Houijia et al. [13] investigated the capability of renewable energy especially, solar thermal energy to provide SOSE with steam and power. The receiver to hydrogen production efficiency was 26% while solar to hydrogen production efficiency was 18%. AlZahrani and Dincer have developed an electrochemical and thermodynamic model for high temperature solid oxide electrolyzer for hydrogen production. In their model, they incorporated energy and exergy analyses along with optimization and sensitivity analyses to highlight the optimum performance. The energy and exergy analyses obtained in his model was 85% and 83% respectively. The other technology which is thermochemical water splitting allows to achieve the appreciable amount of hydrogen at a lower temperature compared to thermal water decomposition [14]. Research in Thermochemical hydrogen production has received great attention in recent years. Doizi et al. [15] have investigated the potential, scaling and optimization of the distillation column in Sulphur-iodine thermochemical cycle. Le Duigou and his team have studied the use of solar energy and other renewable resources in thermochemical cycles for large-scale

hydrogen production [16]. Research is also been conducted to lower the required temperature for thermochemical cycles to increase the efficiency [17]. On the other hand, other researchers have looked for alternative cycles that require lower temperatures. For instance, the copper-chlorine thermochemical cycle requires heat at a temperature of 550 °C [18]. Many research have been conducted on the Cu-Cl cycle to study the different designs of the cycle and examine the performance improvement possibilities [19,20].

2.2 Waste Heat Recovery from Industrial Plants

Industrial waste heat is any heat generated or produced from industrial processes without being utilized. This heat can be in the form of combustion gas, heated products, cooling water from compressors or any other component. The distribution of recoverable waste heat from different processes has been estimated based on data collected between 2012 and 2013 is shown in Figure 2.1.Various studies have shown that 20 to 50% of the industrial consumption is discarded as waste heat [21]. Although some heat losses are inevitable, plants can reduce their losses either by improving their efficiencies or installing heat recovery technologies. Jouhara et al. [22] have presented a review paper discussing the different technologies and applications for waste heat recovery. There are many factors that affect waste heat recovery feasibility depending on the source, and the process to which heat will be transferred to. These factors include, heat quantity, heat temperature or quality of the heat, composition, minimum allowed temperature, and availability of the source. Semkov et al. [23] have investigated the role of heat recovery in efficiency improvement, fuel consumption reduction and reducing emissions. Haris et al. [24–26] have studied the integration of different waste heat sources such as the gas melting furnace, and steel furnace with hydrogen production through thermochemical Cu-Cl Cycle. Also, he was able to integrate Rankine cycles for the purpose of power generation and reverse osmosis system for a seawater desalination to achieve higher overall energy and exergy efficiencies. Gude [27] provided a review about the use of renewable energy and waste heat in the desalination process with the incorporation of thermal energy storage. The paper discussed the thermal energy demands of the different desalination processes as well as the different working temperature ranges for each desalination process. Also, the paper demonstrated the different possible energy storage options for the desalination process. Quoilin et al. [28] have presented thermo-economic optimization of organic Rankine cycle operated by waste

heat recovery. In this study they have considered different working fluids as well as different working conditions. Wang et al. [29] have carried multi-objectives optimization for organic Rankine cycle fluid selection using waste heat recovery. The study concluded the optimal fluid for each temperature range. Bell [30] has investigated the potential of recovering waste heat using thermoelectric generators to produce electricity, heat and cooling. Bruckner et al. [31] have performed a general economic analysis for three different waste heat applications, the maximum investment cost was estimated for each application and compared with conventional investment cost.

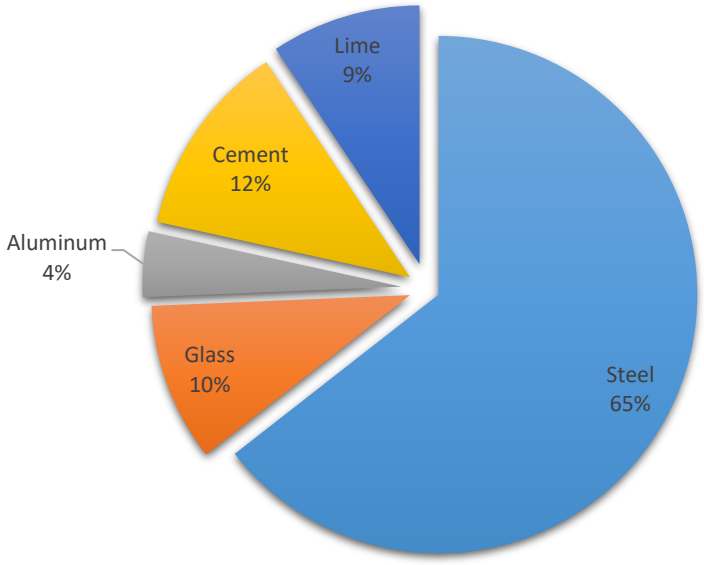

Figure 2.1 Distribution of recoverable waste heat from different processes (data from [21])

Despite the different opportunities for waste heat recovery, there are concomitant obstacles to waste heat recovery in terms of cost, composition, application, and accessibility. Cost barriers can be represented by long payback period and material constraints and cost. Temperature barriers are represented by lack of an end use for low temperature heat, material mechanical- thermal stresses- and chemical-corrosion- properties and heat transfer rate. Application barriers are represented by equipment design according to the process needs and process control. And finally, accessibility barriers can be denoted by limited space, transportability, and inaccessibility.

2.3 Carbon Capturing from Industrial Flue Gases

Carbon dioxide (CO_2) is one of the most significant greenhouse gasses in the atmosphere. The global amount of CO_2 emissions is drastically growing over the years. Figure 2.2 describes the Distribution of Carbon dioxide emission over the different industrial countries. Metal industry and refineries are the largest main contributor to CO_2 emissions. These two sectors produce annually about 11 GT/yr. Steel and iron alone emit 2.3 GT/yr, cement sector accounts for 2 GT/yr, and petrochemical refineries and chemical process emit around 2.3 GT/yr [32–34]. CO_2 capturing is considered to be a promising approach to significantly reduce CO_2 emissions.

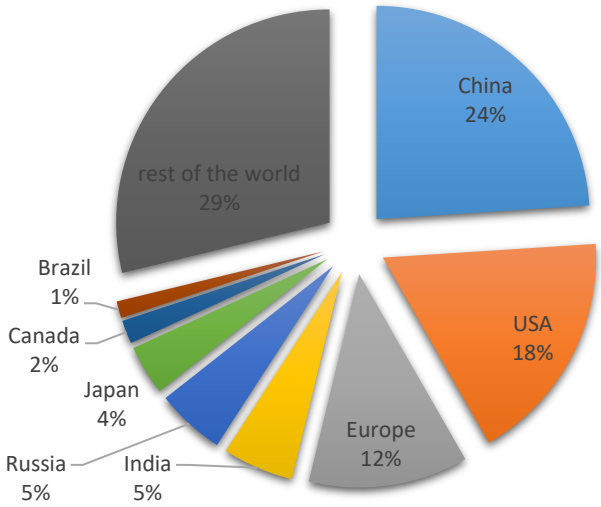

Figure 2.2 Distribution of carbon dioxide emissions over various industrial countries (data from[32])

Kuramochi et al.[22] presented a comparative assessment on energy requirements of different carbon capturing technologies for each industrial flue gas based on different parameters such as capacity factors, energy prices, compression pressure and grid electricity CO_2 intensity. Olaleye and Wang [35] have presented advanced exergy analysis of post-combustion carbon capturing based on chemical absorption. Chemical absorption of monoethanolamine (MEA) is considered to be one of the most matured and preferred technologies for carbon capture. The study also proposed strategies to reduce exergy destruction of the system. Arachchige [36] performed aspen plus simulation for carbon

capturing from a gas-fired power plant and performed a parametric study for the key parameters of the system.

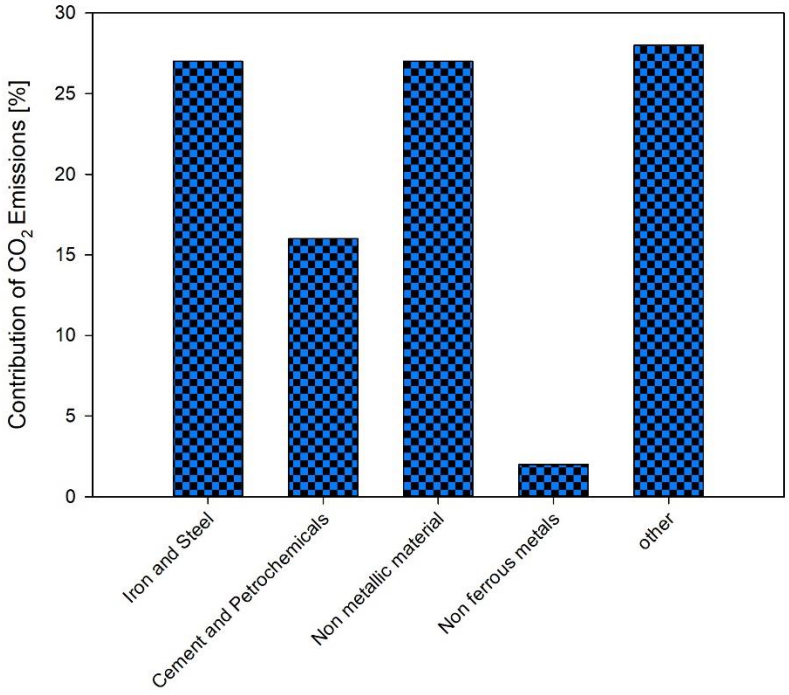

Figure 2.3 Distribution of carbon dioxide emissions from the various industries (data from [32])

2.4 Dimethyl ether Production Methods

DME is one of the promising fuels among various clean and low carbon fuels. DME can be used as a diesel substitute in diesel engines and gas turbines. Also, it can blend with LPG and used in gasoline engine [37,38]. Diesel engines working 100% on DME have resulted in smoke-free combustion with no particulate matter and reduced ignition delay [39]. Furthermore, DME is portable which means it can be stored and used everywhere without establishing a fixed network and safe as long as it is handled properly. It can be synthesized from a variety of feedstocks like biomass, coal, natural gas, and hydrogen. DME synthesis methods can be classified into two main categories according to the use of raw materials into direct and indirect methods. However, there are other routes as well.

2.4.1 Indirect synthesis method

DME has been produced traditionally in two steps in which methanol is synthesized in the first step from syngas, after methanol is purified, methanol will be converted to DME in another reactor through a process called methanol dehydration [40,41]. Methanol

dehydration process is usually preferred to be at a lower temperature to avoid the formation of other byproducts.

The process reactions for DME indirect synthesis can be expressed as:

Methanol synthesis from CO_2:

$$CO_2 + 3H_2 \rightarrow CH_3OH + H_2O$$

Methanol dehydration

$$2CH_3OH \rightarrow CH_3OCH_3 + H_2O$$

2.4.2 Direct synthesis method

A more recent method has combined both methanol synthesis and methanol dehydration in one step through a single reactor [42].

The process reactions for DME direct synthesis can be expressed as:

$$3CO + 3H_2 \rightarrow CH_3OCH_3 + CO_2$$

$$2CO + 4H_2 \rightarrow CH_3OCH_3 + H_2O$$

Chen et al. [43] have performed thermodynamic analyses on one step DME synthesis to minimize Gibbs free energy. Although direct synthesis method allows higher conversion of CO and simpler reactor which results in lower DME production cost, the separation process of DME from unreacted gas and produced CO_2 is more complex. Another novel method proposed DME synthesis from methane in two steps process in the presence of hydrogen and oxygen and different catalysts [44]. However, the main issue is corrosion. Azizi et al. [45] have presented a review paper about technologies and challenges of DME production. In their study they exhibited the different synthesis methods and their associated types of reactors, catalyst and operating conditions.

An open literature review has revealed gaps in the previous studies regarding the production of DME utilizing renewable energy resources and industrial waste heat. These two sources of energy represent a great potential for such a process like DME synthesis. This thesis will examine the capability of utilizing renewable energy and industrial waste heat in DME production and some other useful commodities such as power and fresh water. The main outcome of this research is to study the overall system performance of three renewable energy based integrated systems for DME production.

Chapter 3 : Systems Development

This chapter describes the three different sustainable systems developed and proposed in this study. Production of Dimethyl ether is the primary purpose of the proposed systems. However, there are some additional products such as electricity and fresh water. The main inputs of the three systems can be represented by waste flue gas from different industries such as steel, cement and exhaust gas power plants. Moreover, different forms of renewable energy are incorporated as well. The first system is PV solar based DME production system, the second system is solar thermal based DME production plant and the third system is thermochemical based solar assisted DME production system. This chapter describes each system in a separate subsection.

3.1 Photovoltaic Based DME Production Plant (System 1)

In this system, the input thermal energy is provided by the waste flue gas from a cement plant and the electrical work is supplied through photovoltaic solar panels. The main output of this system is the production of DME, which is the major focus of this study. Flue gas is released from the furnace at a temperature of 370 ^{o}C [21]. Recovered waste heat provides distillation columns with the required heat for the synthesis process. Flue gas then passes through carbon capturing plant to split carbon dioxide for the DME synthesis process. Hydrogen is produced through Proton Exchange Membrane electrolyzer. Both carbon dioxide and hydrogen are fed to methanol synthesis process in a process called carbon hydrogenation. Then, the produced methanol undergoes a process called methanol dehydration to produce dimethyl ether. Each subsystem of the integrated system is explained below. Figure 3.1 shows the overall schematic of system 1.

3.1.1 Cement furnace exhaust gas

Flue gas produced from Cement furnace exchanges heat with water in a heat exchanger to produce steam. Steam is then derived to the boiler of unreacted methanol distillation to provide 27.95 kW of heat. Further, steam is sent to the methanol reactors where it passes through the reactors water jackets recovering the rejected heat. After that, steam is derived to methanol distillation column providing 39.9 kW. Finally, steam passes through the regenerator of carbon capturing unit providing 312 kW.

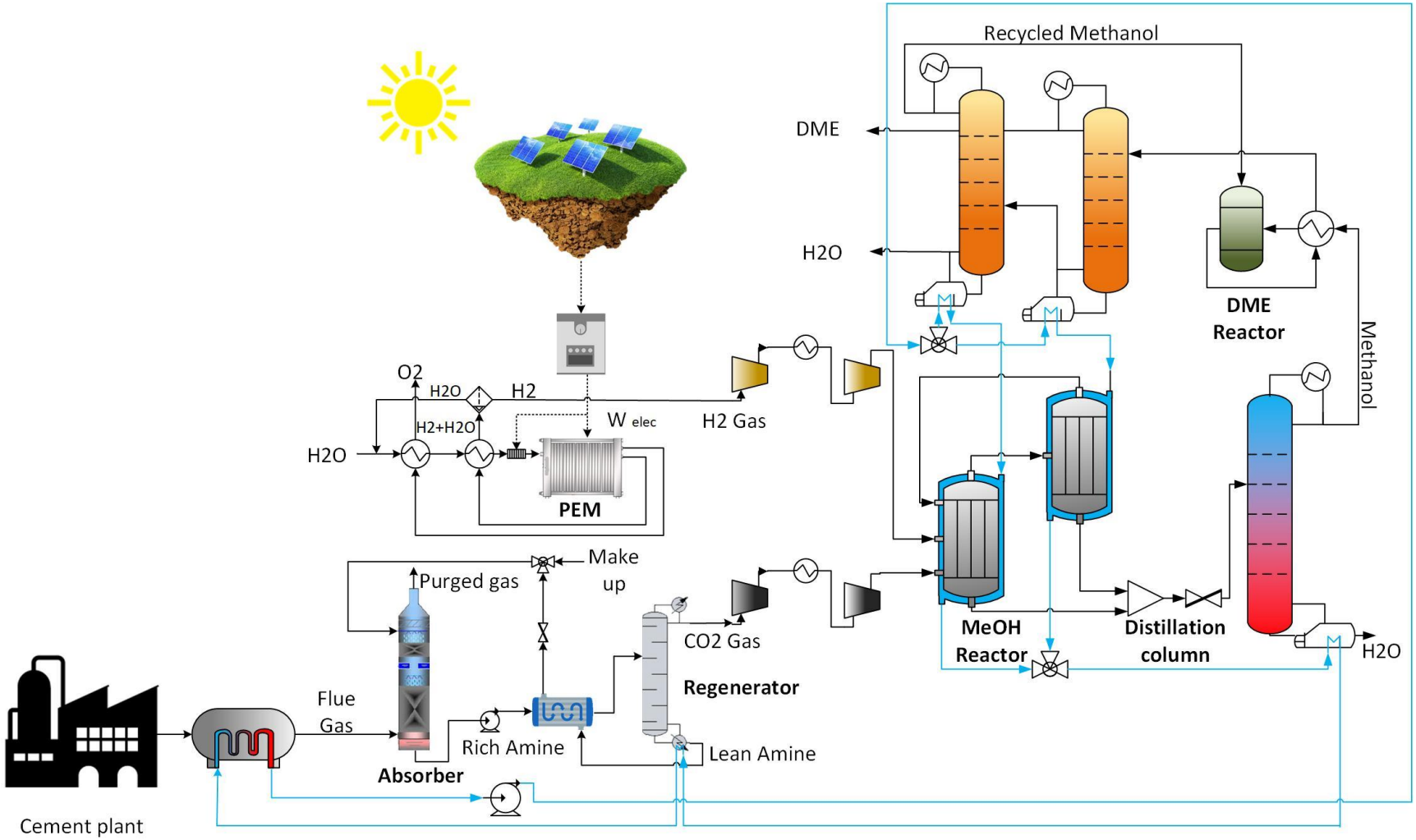

Figure 3.1 Schematic of photovoltaic based DME production plant (System 1).

3.1.2 Carbon capturing plant

After the flue gas gets cooled, cold gas enters the carbon capturing unit. In a chemical absorption process, flue gas enters the absorber from the bottom while the solvent enters the absorber from the top. The reaction occurs between CO_2 and MEA forming CO_2 rich solvent while other gasses are released at the top of the absorber. Rich solvent leaves the absorber to a heat exchanger to increase its temperature before entering the regenerator. Then, the heated rich solvent enters the regenerator at the top. In the regenerator, the regeneration process occurs where separated acid gas (CO_2) leaves regenerator at the top. The lean solvent (MEA) leaves the regenerator from the bottom to the heat exchanger to heat the rich solvent and makeup water is added to the lean solvent before recycling it back to the absorber. Figure 3.2 shows the Aspen flowsheet for carbon capturing and heat recovery system.

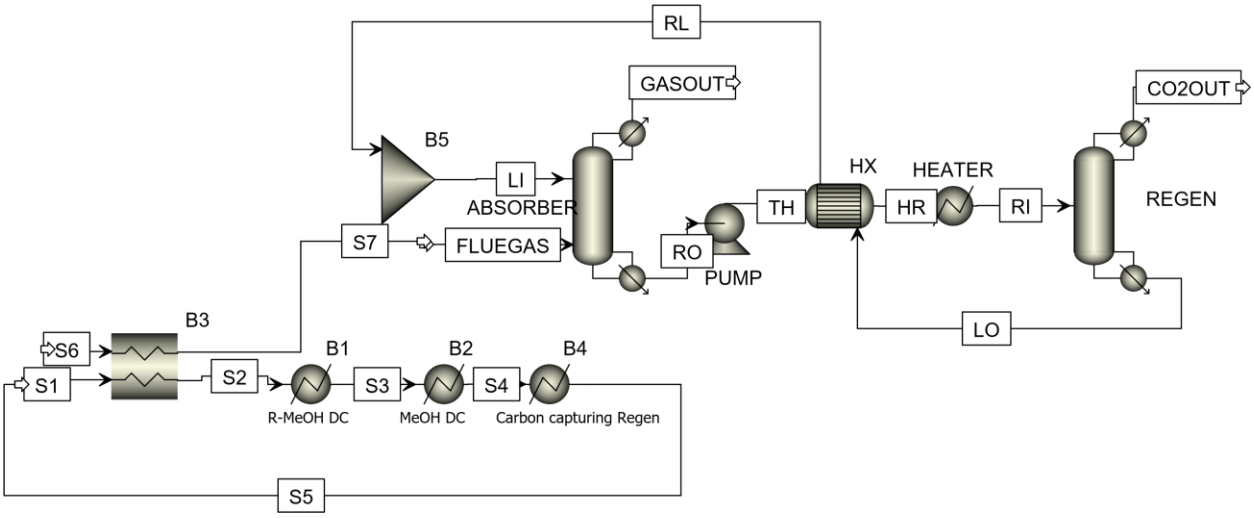

Figure 3.2 Flowsheet of carbon capturing system with flue gas heat recovery for system 1.

3.1.3 PEM hydrogen production plant

PEM hydrogen production plant produces hydrogen using PEM electrolyzer through an electrochemical reaction. Water is fed to the electrolyzer at a temperature of 80 ^{o}C. The electrochemical reaction is performed utilizing the generated electric work from the PV panels. The outputs of the electrolyzer are oxygen with the water stream and hydrogen. Both streams are used to preheat feed water through heat exchangers. The list of parameters and assumptions used PEM electrolyzer modeling are shown in Table 3.1.

Table 3.1 Parameters and assumptions used PEM electrolyzer modeling

Parameters	Value
Operating Temperature T_{PEM}	80 ^{o}C
Operating current density J	2000 A/m^2
Activation energy at the anode $E_{act,a}$	76 kJ/mol
Activation energy at the cathode $E_{act,c}$	18 kJ/mol
Water content at membrane interface-Anode λ_a	14
Water content at membrane interface-cathode λ_c	10
Anode pre-exponential factor J_a^{ref}	1.7×10^5 A/m^2
Cathode pre-exponential factor J_c^{ref}	4.6×10^3 A/m^2
Membrane thickness D	100 µm
Faraday's constant F	96,486 C/mol
Number of cells N_s	30
Stack area A_s	10 m^2

Source: [46]

3.1.4 Methanol synthesis process

The flow sheet in Figure 3.3 shows the main process components. CO_2 and H_2 are fed at 1 bar and then compressed to 50 bar through multistage compressors. Then, both streams are mixed and enter the first reactor at a temperature of 235 ^{o}C as per the kinetic study conducted by Matzen et al. [47] achieving single pass conversion of 47%. There are two output streams for the reactor, one stream contains the reaction product while the other stream contains the unreacted gasses which will be going to the second reactor. The product streams of the second methanol reactor are the unreacted gasses stream which will be recycled back to the first methanol reactor and reaction products stream which will be mixed with the first reactor products. Then the pressure of the combined streams will be reduced to 1 bar and heated to 80 ^{o}C to facilitate the separation of water in a distillation column. Then, the stream enters the distillation column where the distillate will be extracted from the top of the distillation column and water will be extracted from the bottom of the distillation column.

3.1.5 DME synthesis process

DME is produced by the process of methanol dehydration, the reaction temperature is set between 240 ^{o}C and 400 ^{o}C to avoid the formation of byproducts. Methanol is introduced from a methanol synthesis plant at a temperature of 48 ^{o}C. Then stream is heated through a heat exchanger to a temperature of 260 ^{o}C and pressure of 13 bar. Then stream is fed to the DME reactor in an exothermic reaction called methanol dehydration at a conversion rate of 80% as reported by [41] . Product stream passes through a heat exchanger to preheat the DME reactor feed. Then, the product stream is further cooled to 70 ^{o}C to facilitate the separation of DME from the product stream in the distillation column at a pressure of 10 bar. Then, the remaining of the product stream will leave the column from the bottom of the distillation column going to the next distillation column to separate unreacted methanol from water. The distillate (methanol) will leave the column from the top and will be recycled back to the DME reactor. Water will be discarded from the bottom of the column.

3.2 Solar Thermal Based DME Production Plant (System 2)

Exhaust gas from the steel manufacturing process and solar thermal energy are the main sources for thermal energy. Steel waste flue gas comes at a temperature of 982 ^{o}C [21] and solar thermal energy that can produce steam at a temperature up to 600 ^{o}C. The systems composed of hydrogen production plant which is solid oxide electrolyzer in this system and carbon capturing plant from the cooled flue gas in addition to the methanol synthesis and DME synthesis plants. The main outputs of this system are DME which is the main focus of this study as well as electrical energy from the solar heliostat field. Description of the main subsystems is provided below. Figure 3.5 shows the overall schematic of system2.

3.2.1 Steel furnace exhaust gas

Flue gas exhaust from the Steel furnace exchanges heat with water in a heat exchanger to produce steam. Steam is then derived to the boiler of the unreacted methanol distillation column to provide 55.9 kW of heat. Steam is then derived to the methanol reactors passing through the reactors water jackets and recovering the rejected heat. After that, steam is derived to methanol distillation column providing 79.8 kW. Finally, steam passes through regenerator of carbon capturing unit providing 479.3 kW.

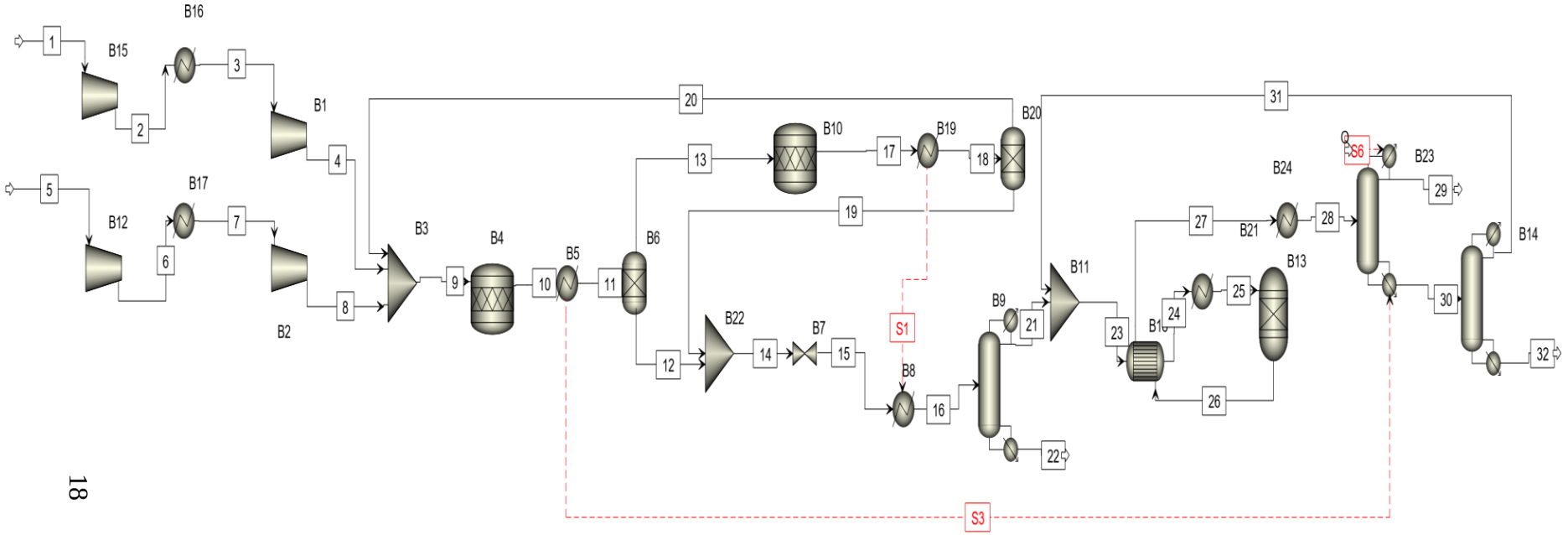

Figure 3.3 Flowsheet of methanol and DME synthesis for system 1.

3.2.2 Carbon capturing plant

After recovering the heat from the steel furnace exhaust gas, gasses are driven to the chemical absorption carbon capturing plant. Flue gasses enter the absorber at the bottom along with the lean amine entering from the top. Lean solvent absorbs carbon dioxide from the flue gasses and the remaining gasses are purged from the top of the absorber. The rich solvent then leaves the absorber to the heat exchanger to be heated to 80 ^{o}C before entering the regenerator. Then, hot rich solvent enters the regenerator to be further heated to release the absorbed CO_2 gas. CO_2 gas is collected from the top of the regenerator and the lean solvent leaves the regenerator to the heat exchanger to give heat to the rich solvent and recycled back to the absorber. Figure 3.4 shows the Aspen flowsheet of carbon capturing system and heat recovery from the flue gas.

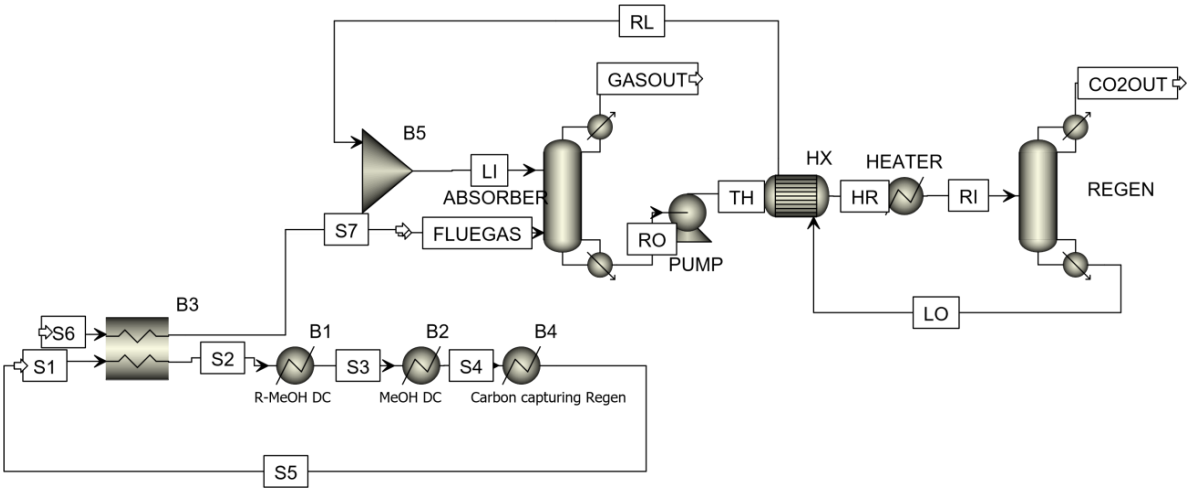

Figure 3.4 Flowsheet of carbon capturing system and heat recovery for system 2.

3.2.3 Solar heliostat field

Heliostat field consists of hundreds of heliostats that reflect and concentrate sunlight into the central receiver. The received solar radiation is partly absorbed by the central receiver while the remaining heat is lost to the environment. The heat absorbed by the central receiver is transferred partly to the thermal energy storage and the remaining to the Rankine cycle steam generator through therminol working fluid. The generated steam is directly fed to the steam turbine at a temperature of 535 ^{o}C and pressure of 12.6 MPa. A bled stream is extracted at a pressure of 300 kPa to provide the necessary heat to solid oxide steam electrolyzer (SOSE) steam generator. The expanded steam is then cascaded back to the condenser at a pressure of 100 kPa.

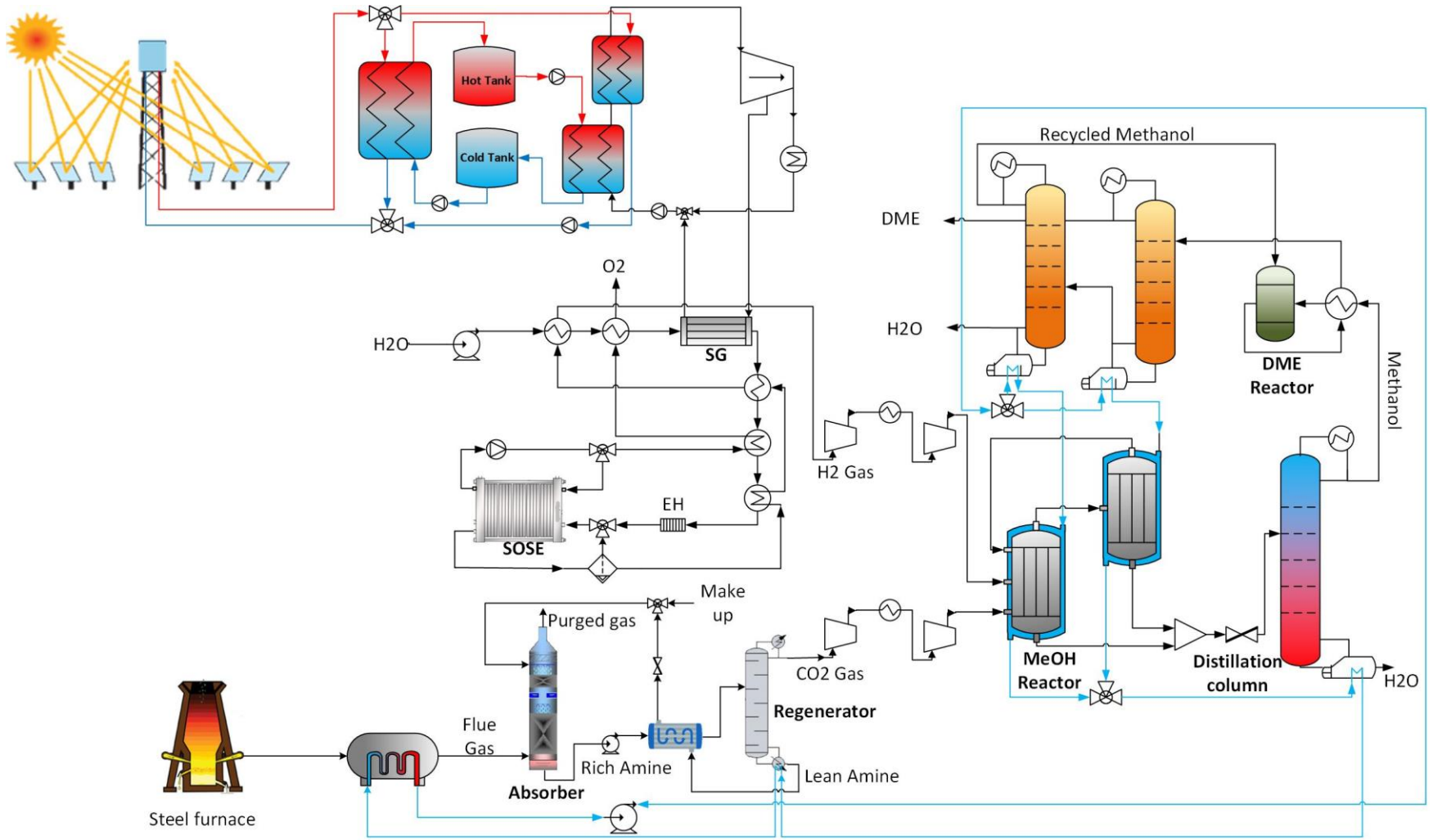

Figure 3.5 Schematic of solar thermal based DME production plant (system 2)

3.2.4 SOSE hydrogen production plant

The hydrogen production system has been developed according to Alzahrani and Dincer [48]. They proposed a novel configuration with the integration of solar energy in a steam generator of the SOSE system. The main inputs for SOSE system are water, electricity and thermal energy. Water is derived through a pump to achieve the required pressure at the electrolyzer. Water is heated through several heat exchangers before passing through the steam generator. Steam is further heated then by exchanging heat with the electrolyzer outputs such as oxygen and hydrogen. Utilizing the high temperature output in preheating the water before entering the electrolyzer decreases the thermal energy demand and thermal losses and increases the efficiency. The list of parameters and assumptions used for the SOSE modeling are listed in Table 3.2.

Table 3.2 Parameters and assumptions used SOSE modeling [49,50]

Parameter	Value
Stack operating temperature	1073 K
Stack operating pressure	180 kPa
Operating current density	5000 A/m^2
H_2O stream composition	90 %
Steam utilization factor	85 %
Pre-exponential exchange current density, anode	2.05×10^9 A/m^2
Pre-exponential exchange current density, cathode	1.34×10^{10} A/m^2
Activation energy at the anode $E_{act,a}$	1.2×10^5 kJ/mol
Activation energy at the cathode $E_{act,c}$	1.0×10^5 kJ/mol
Anode thickness	500 µm
Cathode thickness	50 µm
Electrolyte thickness	50 µm
Pores diameter	0.5 µm
Number of cells	24
Stack area	10

3.2.5 Methanol synthesis plant

The produced hydrogen at a rate of 6 mol/sec and the captured carbon dioxide at a rate of 2 mol/sec enter multi-stage compressors to reach the required pressure for reactions. Then, the compressed gasses enter the first methanol reactor at a temperature of 235 ^{o}C and pressure of 50 bar. The products of the first reactor are methanol as the main product, water and unreacted gas. The produced methanol and water is driven to the distillation column, while the unreacted gas will be driven to a second methanol reactor. The unreacted gas is heated again to the same temperature to produce methanol as a main product and water. Remaining unreacted gas is recycled back to the first reactor. The produced methanol and water mixture is combined with the first reactor product to reduce its pressure to 1 bar through a pressure changer. The products stream is heated then to 80 ^{o}C before entering to the first distillation column. The distillation column is used to separate the produced methanol from the water.

3.2.6 DME synthesis plant

The main purpose of this plant is to convert the produced methanol to DME. The produced methanol needs to be converted to DME through a process called methanol dehydration. Methanol dehydration is basically taking out water from methanol producing DME. The methanol-DME mixture is heated to 260 ^{o}C through a heat exchanger before entering the DME reactor at a pressure of 13 bar. The products of the reactor are DME as the main product, unreacted methanol and water. The product stream exit at a temperature of 299 ^{o}C because the reaction is exothermic. The product stream passes through a heat exchanger to be cooled and heat the feed stream to DME reactor. The cooled product stream is then fed to the second distillation column to separate the produced DME from the mixture at a pressure of 10 bar. Remaining mixture is introduced to the third distillation column in which methanol get separated from water at a pressure of 2.9 bar. The extracted pure methanol from the top of the distillation column is recycled back to the DME reactor. Figure 3.6 shows the Aspen flowsheet for methanol and DME synthesis.

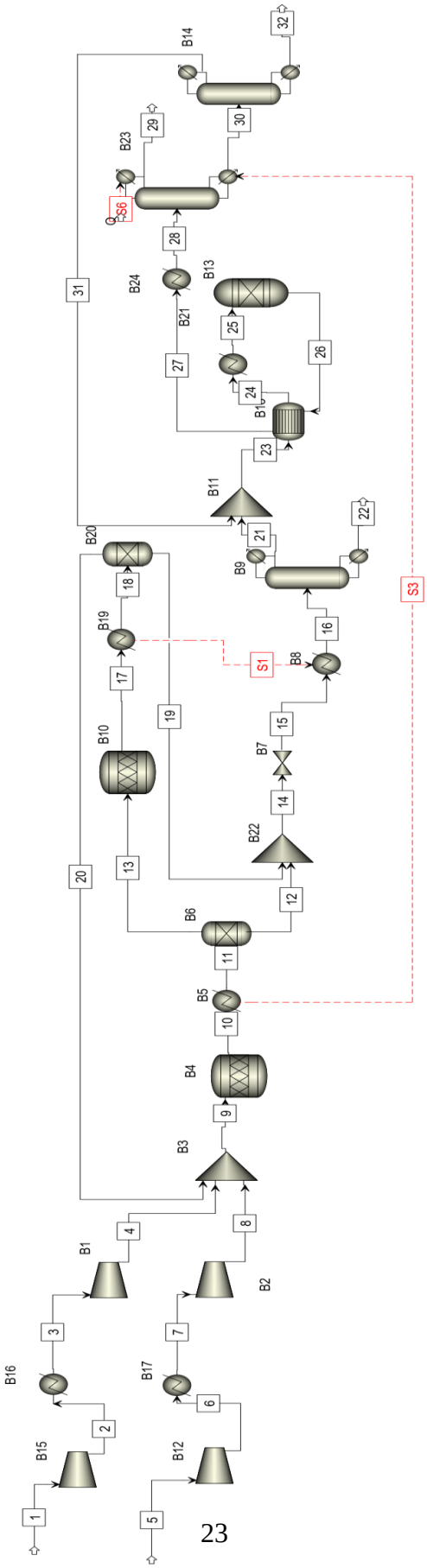

Figure 3.6 Flowsheet of methanol and DME synthesis for system 2.

3.3 Thermochemical Based DME Production Plant (System 3)

In this system, gas turbine exhaust gas is the main source of thermal energy. Flue gas comes out of the turbine at a temperature of 840 ^{o}C exchanging heat with water in heat recovery Steam Generator (HRSG) to produce superheated steam to provide the thermochemical Cu-Cl cycle with the required heat at a temperature of 500 ^{o}C and then supply the remaining processes such as methanol synthesis, DME synthesis and carbon capturing with the necessary heat. Eventually, saturated steam is then fed to the multi effect desalination (MED). Cu-Cl thermochemical cycle is the chosen hydrogen production technology in this system. Four steps configuration Cu-Cl cycle is adopted among the different configurations. The main useful outputs of this system are DME which is the main focus of this study, electricity, and fresh water.

3.3.1 Gas turbine exhaust gas

After the air is compressed, combust and expand in the turbine, Gas turbine exhausts gas usually have high potential energy due to its high temperature which may reach up to 1000 ^{o}C. Heat recovery of gas turbine exhaust gas usually occurs in a specific heat exchanger called HRSG producing high temperature steam. The generated stem pass through the different components in a specific order to maintain the pinch temperature in each component and then condensed in the first effect of the desalination system. For instance, steam is going first to the thermolysis process to provide a heat at a temperature of 500 ^{o}C. Then, steam moves to the hydrolysis process to provide a heat at a temperature of 400 ^{o}C. And then steam moves to lower temperature processes such as Methanol synthesis plant, DME synthesis plant and finally Carbon capturing plant.

3.3.2 Carbon capturing plant

The cooled gas turbine exhaust gas pass to the carbon capturing unit. In a chemical absorption technology, the exhaust gas passes through the absorber. Solvent reacts with carbon dioxide only and remaining gasses leave the system. Then, in order for the rich amine to reject carbon dioxide gas, the solvent needs to be heated. So, rich amine passes through the heat exchanger and further heated in the regenerator. Carbon dioxide will be released at the top of the regenerator and the lean amine is recycled back to the absorber. Figure 3.7 show carbon capturing and the heat recovery subsystem for system 3.

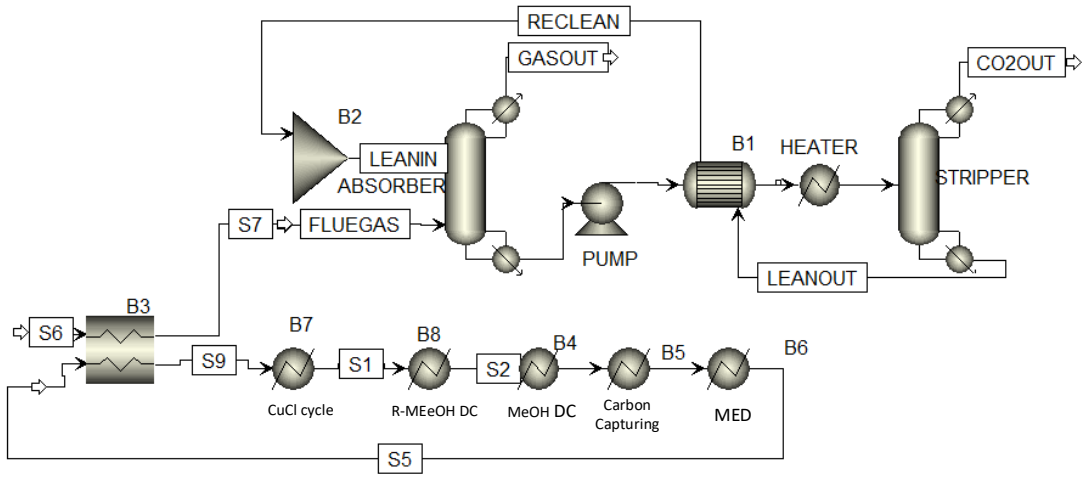

Figure 3.7 Carbon capturing and heat recovery flowsheet for system 3.

3.3.3 Cu-Cl thermochemical cycle

Different studies have been conducted on the Cu-Cl cycle at UOIT clean energy research laboratory [51]. The Cu-Cl cycle in this system is four steps cycle which are named as hydrolysis, thrombolysis, electrolysis, and drying. The list of chemical reactions and operating conditions are demonstrated in Table 3.3. The first process is hydrolysis which takes place between copper dichloride and water at a temperature of 400 ^{o}C to produce copper oxychloride and hydrochloric acid. The second step is thermolysis which occurs for copper oxychloride at a temperature of 500^{o}C to dissociate to oxygen and copper chloride. Then the third step is electrolysis in which copper chloride reacts with hydrochloric acid from the hydrolysis process at a low temperature to produce hydrogen gas and copper dichloride solution. Hydrogen is then extracted and copper dichloride solution goes to the fourth step. The last step is drying in which copper dichloride solution get dried at 80 ^{o}C and water is discarded while solid copper dichloride is sent back to hydrolysis. Figure 3.9 shows the aspen flowsheet for the Cu-Cl cycle developed for the system.

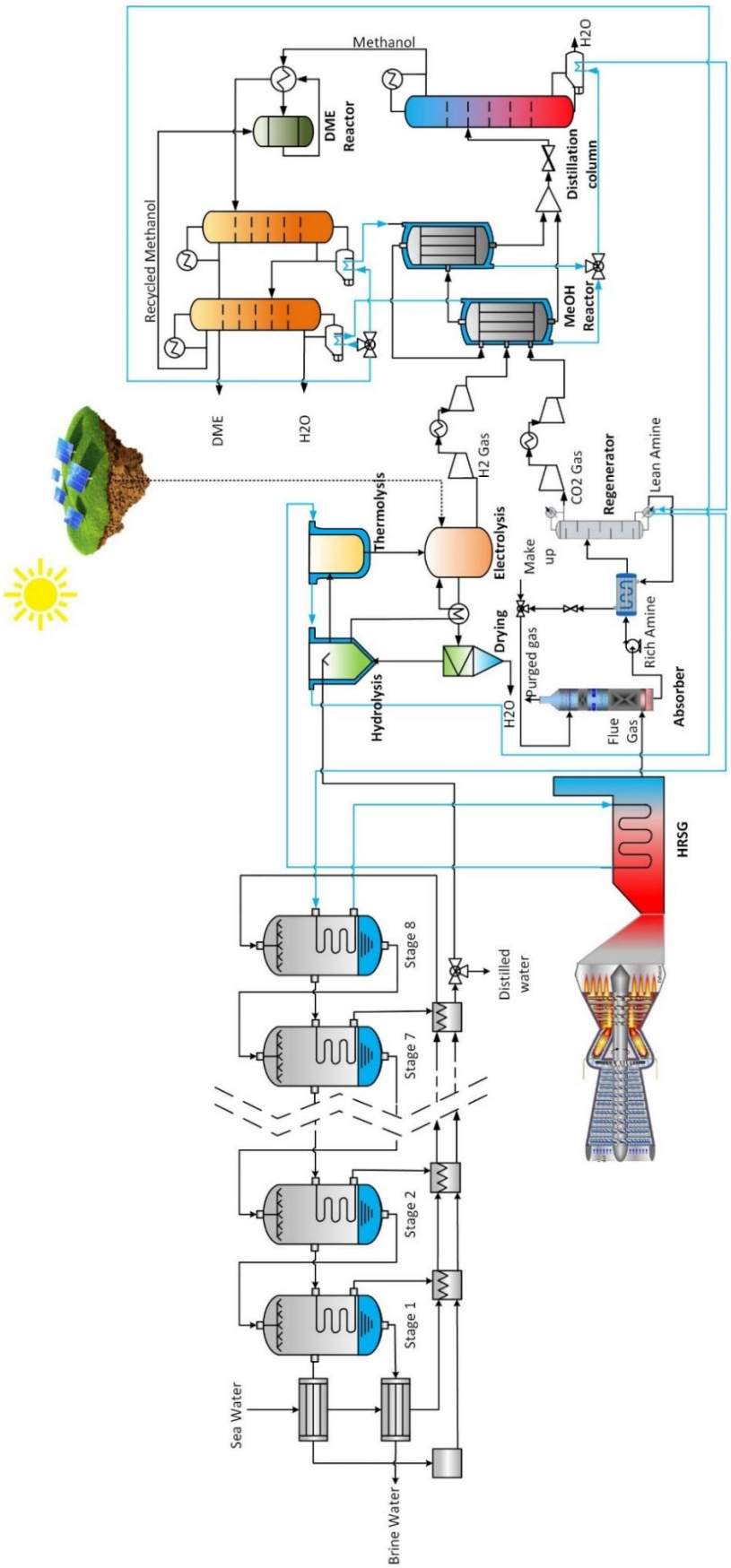

Figure 3.8 Schematic of thermochemical based DME production plant (system 3)

Table 3.3 List of reactions occurring in four-step Cu-Cl cycle

Step	Reactor name	Chemical reaction	Temperature range (°C)
1	Hydrolysis reactor	$H_2O(g) + 2CuCl_2(s) \rightarrow Cu_2OCl_2(s) + 2HCl(g)$	400
2	Cu_2OCl_2 decomposition reactor	$Cu_2OCl_2(s) \rightarrow \frac{1}{2}O_2(g) + 2CuCl(l)$	500
3	Hydrogen production reactor	$2CuCl(aq) + 2HCl(g) \rightarrow 2CuCl_2(aq) + H_2(g)$	<100
4	Dryer	$CuCl_2(aq) \rightarrow CuCl_2(s)$	<100

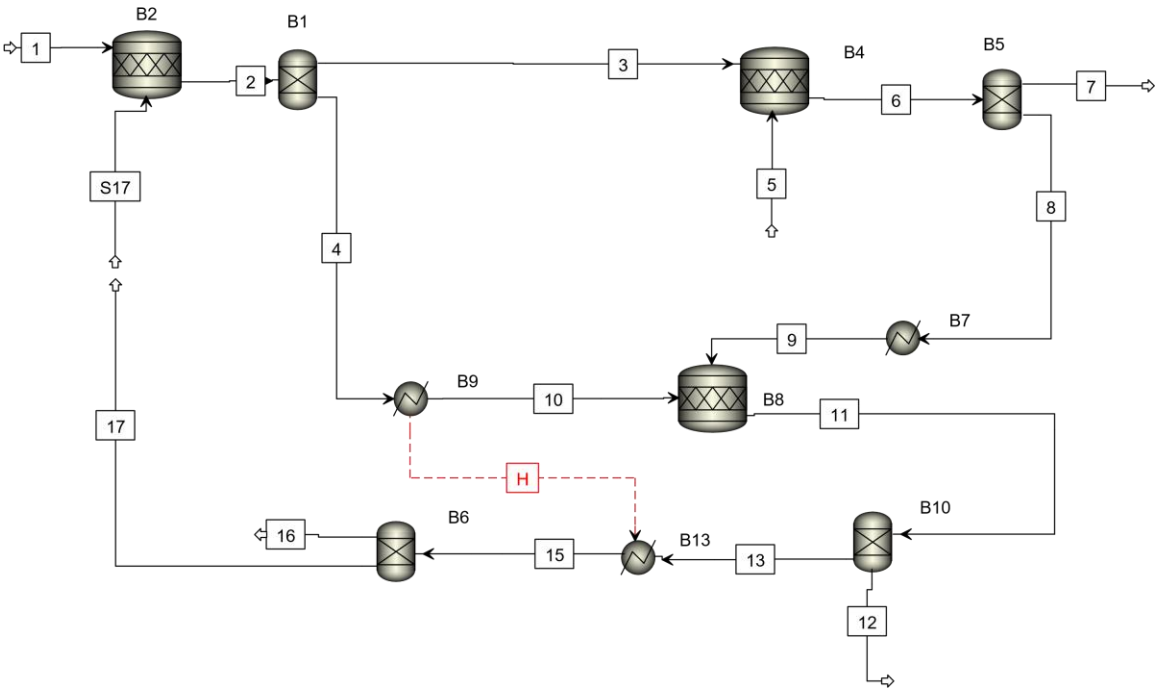

Figure 3.9 Flowsheet of the Cu-Cl cycle.

3.3.4 Methanol synthesis plant

The hydrogen produced through the Cu-Cl thermochemical cycle and carbon dioxide captured from gas turbine exhaust gas is compressed to 50 bar. The compressed gasses are introduced to the first methanol reactor at a temperature of 235 °C and pressure 50 bar producing methanol at a conversion rate of 80% and water and some of the reactant gas

remains unreacted. Products leave the reactor to the first distillation column, while unreacted gasses leave to a second methanol reactor at the same temperature and pressure of the first reactor. Then, second methanol reactor products have methanol besides unreacted gasses which will be recycled back to the first methanol reactor. Products are mixed together before entering the distillation column to separate water from the produced methanol.

3.3.4 DME synthesis plant

In this subsystem, the produced methanol is dissociated to DME and water in a process called methanol dehydration. Methanol produced in the previous subsystem is heated to the required temperature which is 260 ^{o}C through the heat exchanger. Then, the stream is introduced to the DME reactor at a pressure of 13 bar. The products contain the produced DME, water and unreacted methanol. The stream is cooled by providing heat to the feed stream. The stream is then introduced to the second distillation column which will isolate the produced DME. The remaining mixture will exit the distillation column to enter the third distillation column to isolate water from the unreacted methanol which will be recycled back to the DME reactor. Figure 3.10 shows the aspen flowsheet for methanol and DME synthesis for system 3.

3.3.5 Multi Effect Desalination system

It is a process of multi-stage desalination in which the first effect is heated by passing saturated steam in tubes and water sprayed over the tubes forming a vapor that is used as a heating source for the next effect. The main idea of MED is to keep using the same evaporation energy in every effect but with lower temperatures. The configuration considered in this study is a feed forward MED configuration. In the proposed system, saturated steam coming from carbon capturing regenerator enters the first effect of the desalination system to be condensed and deliver the latent heat to it.

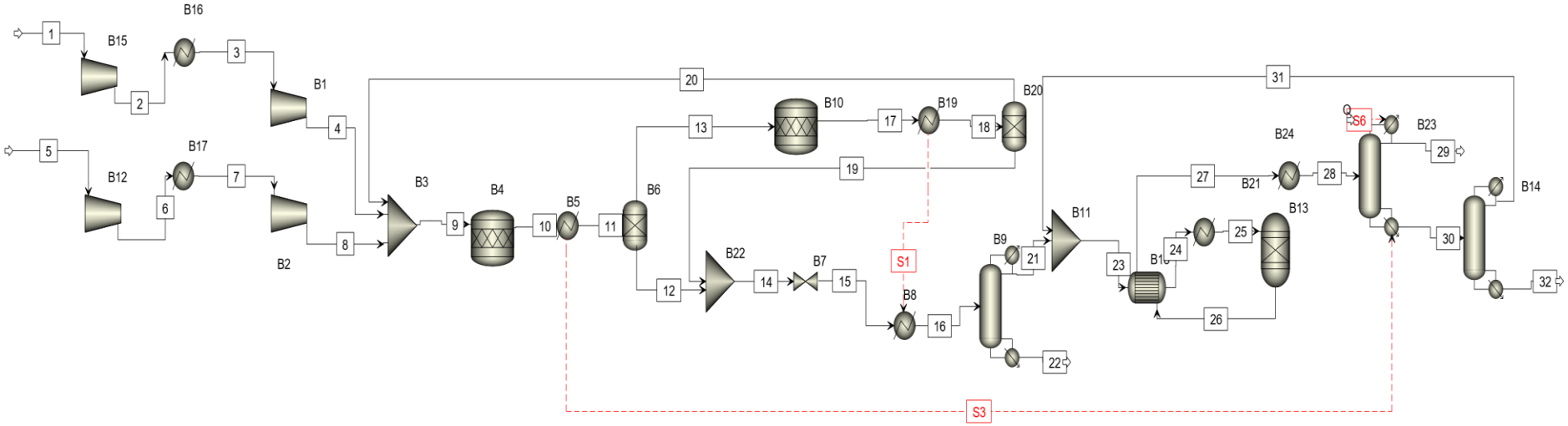

Figure 3.10 Flowsheet of methanol and DME synthesis of system 3.

Chapter 4 : Thermodynamic Analysis

This chapter describes the detailed thermodynamic analyses of the proposed integrated systems. Thermodynamic analyses are represented by comprehensive energy and exergy analyses for the components, subsystems, and overall systems. Major assumptions considered during simulation and modeling are also discussed in this chapter. The fundamental balance equations for a control volume are expressed below.

- Mass balance equation

The general balance equation of mass conservation can be written as:

$$\sum_i \dot{m}_i - \sum_e \dot{m}_e = \frac{dm_{cv}}{dt} \tag{4.1}$$

where m_{cv} represents the mass of the control volume and $\dot{m}$ represents mass flow rate, subscript i is for inlet flow while subscript e is for exit flow.

- Energy balance equation

The general energy balance equation can be represented by the first law of thermodynamics through the following equation:

$$\dot{Q} - \dot{W} + \sum_i \dot{m}_i \left(h_i + \frac{V_i^2}{2} + gZ_i\right) - \sum_e \dot{m}_e \left(h_e + \frac{V_e^2}{2} + gZ_e\right) = \frac{dE_{cv}}{dt} \tag{4.2}$$

where $\dot{Q}$ represent heat transfer rate, $\dot{W}$ represent work rate, E_{cv} represents the energy of the control volume, h represents specific enthalpy, V represents flow velocity from or to control volume, g is gravitational acceleration and Z is the elevation.

- Exergy balance equation

Exergy analysis significantly contributes in improving and optimizing designs because it clearly identifies the locations and causes of thermodynamic losses. There are two main forms of exergy, physical exergy which identifies the work potential of a system with reference to the environment, and chemical exergy which is usually associated with chemical changes or reactions. According to the second law of thermodynamics, the general exergy balance equation can be written as follows:

$$\dot{E}x^{Q} + \sum_i \dot{m}_i ex_i = \sum_e \dot{m}_e ex_e + \dot{E}x_W + \dot{E}x_d \quad (4.3)$$

where ex is the specific exergy which is the summation of physical and chemical exergy and can be written as follows:

$$ex = ex_{ph} + ex_{ch} \quad (4.4)$$

where physical exergy can be expressed as:

$$ex_{ph} = (h - h_0) - T_0(s - s_0) \quad (4.5)$$

where the subscript 0 denotes the property at the reference point. And chemical exergy can be expressed as:

$$ex_{ch} = \sum_j x_j \, ex_{ch}^0 + RT_0 \sum_j x_j \ln(x_j) \quad (4.6)$$

where x_j represents the mole fraction of component, R is universal gas constant, ex_{ch}^0 represents standard specific chemical exergy. $\dot{E}x^{Q}$ is the exergy rate due to heat transfer and can be expressed as :

$$\dot{E}x^{Q} = \dot{Q}_i(1 - \frac{T_0}{T_s}) \quad (4.7)$$

where T_s is the source temperature. $\dot{E}x_W$ is the exergy flow due to work and expressed as:

$$\dot{E}x_W = \dot{W} \quad (4.8)$$

And $\dot{E}x_d$ represent the exergy destruction for the component studied.

4.1 Assumptions

A detailed description of the assumptions considered during the development, modeling and simulation of the proposed systems for DME production is explained in this section. Assumptions of each system are listed separately as given below.

The assumptions considered for system 1 are listed below:

- The system operates in steady-state conditions.
- The changes in kinetic and potential energies are neglected
- No heat losses and pressure drops take place in heat exchangers

- For all the compressors, the isentropic efficiency of 72% is considered.
- The efficiency of the electrical generator is considered as 95%.
- The conversion efficiency of the solar inverter is 95%.
- The starting up time has not been considered.
- The reference environment conditions are taken to be 25^{o}C and 1 atm.
- The property method used in Aspen plus for carbon capturing is ELECNRTL. The ELECNRTL Property Method is the most useful electrolyte property method. It can accommodate both aqueous and mixed solvent systems.
- The property method used in Aspen plus for synthesis is PSRK. The PSRK property method is based on the Predictive Soave-Redlich-Kwong equation-of-state model, which is an extension of the Redlich-Kwong-Soave equation of state.
- NBS/NRC: Steam table correlations (TEAMNBS) is the property method for water analyses.

The assumptions considered for system 2 are listed below:

- The system is working under a steady state condition.
- All the kinetic and potential energy changes are neglected.
- The isentropic efficiency for all the compressors is assumed to be 72%.
- No heat losses were considered in all heat exchangers
- Pressure drop was assumed to be 1% across each heat exchanger.
- The SOSE hydrogen production system is assumed to be working under exothermic conditions.
- The ambient reference state was assumed to have a temperature of 25 ^{o}C and pressure of 1atm.
- The efficiency of the heliostat field was assumed to be 75% [52].
- The absorption efficiency of the solar tower receiver is assumed to be 90% [52].
- The property method used in Aspen plus for carbon capturing is ELECNRTL. The ELECNRTL Property Method is the most useful electrolyte property method. It can accommodate both aqueous and mixed solvent systems.
- The property method used in Aspen plus for synthesis is PSRK. The PSRK property method is based on the Predictive Soave-Redlich-Kwong equation-of-state model, which is an extension of the Redlich-Kwong-Soave equation of state.

- NBS/NRC: Steam table correlations (TEAMNBS) is the property method for water analyses.

The assumptions considered for system 3 are listed below:

- The system is assumed to be working in a steady state condition.
- The gravitational and kinetic energy changes are neglected all over the system.
- All compressors and turbines are assumed to be working adiabatically.
- Neither heat losses nor pressure drop were considered in this system.
- All gas compressors are set to have an isentropic efficiency of 72%.
- For combustion chamber, pressure drop is neglected.
- The isentropic efficiencies for gas turbine system compressor and turbine are set as 83% and 87% respectively.
- The gas turbine is assumed to be working under adiabatic conditions.
- For Copper Chlorine cycle, no heat losses occur in heat exchangers.
- The required electrical work for electrolysis is set as 63 kJ/mol of H_2 [53].
- The Aspen plus property method used for Cu-Cl thermochemical cycle simulation was set as SOLIDS.
- The Aspen plus property method used for methanol and DME synthesis plant simulation is PSRK. The PSRK property method is based on the Predictive Soave-Redlich-Kwong equation-of-state model, which is an extension of the Redlich-Kwong-Soave equation of state.
- The property method used in Aspen plus for carbon capturing is ELECNRTL. The ELECNRTL Property Method is the most useful electrolyte property method. It can accommodate both aqueous and mixed solvent systems.
- NBS/NRC: Steam table correlations (TEAMNBS) is the property method for water analyses.
- The salinity of feed seawater entering the MED system is assumed to be 42000 PPM.
- The salinity of rejected brine water should be no more than 70000 PPM.

4.2 Thermodynamic Analysis of System 1

The first system is producing DME using waste heat from cement furnace and renewable energy through solar PV. The integrated system is composed of four subsystems, named as carbon capturing system, PEM hydrogen production system, methanol synthesis system and DME synthesis system. Thermodynamic analyses represented by energy and exergy balance equations have been performed to assess the performance of each subsystem and the overall integrated system. Mass balance equations and energy balance equations are listed in Table 4.1. Exergy balance equations and exergy efficiency equations are tabulated in Table 4.2.

The distillation columns designs and sizing is a very important process to choose the optimum operating conditions for the distillation column such as the number of stages, feed stage and reflux ratio. The distillation column design and sizing was performed using McCabe and Thiele graphical method.

The energy efficiency of PEM hydrogen production system is can be written as

$$\eta_{PEM,en} = \frac{\dot{m}_{H2} LHV_{H2}}{\dot{Q}_{EH} + \dot{W}_{el}} \tag{4.9}$$

where $\dot{m}_{H2}$ is the mass flow rate of the produced hydrogen, LHV_{H2} is the lower heating value of hydrogen, $\dot{Q}_{EH}$ is the heat rate provided by an electric heater to achieve the working temperature and $\dot{W}_e$ is the electric work provided to the system. While the exergy efficiency of the PEM hydrogen production system can be written as

$$\eta_{PEM,ex} = \frac{\dot{m}_{H2} ex_{H2}}{\dot{E}^{\dot{Q}}{}_{EH} + \dot{W}_{el}} \tag{4.10}$$

where ex_{H2} is the total specific exergy –chemical and physical- of hydrogen, $\dot{E}^{\dot{Q}}{}_{EH}$ is the exergy provided to the system in the form of heat.

The third system is the DME synthesis system. The energy efficiency of the DME synthesis system can be written as

$$\eta_{DME,en} = \frac{\dot{m}_{DME} LHV_{DME}}{Q_{total} + \dot{W}_{Total}} \tag{4.11}$$

where $\dot{m}_{DME}$ is the mass flowrate of produced DME, LHV_{DME} is the lower heating value of the producedDME. The total heat provided during methanol synthesis process is expressed as

$$Q_{total} = \dot{Q}_{B9} + \dot{Q}_{B10} + \dot{Q}_{B23} + \dot{Q}_{B14} \tag{4.12}$$

And total work can be expressed as follows:

$$\dot{W}_{Total} = \dot{W}_{B1} + \dot{W}_{B2} + \dot{W}_{B12} + \dot{W}_{B15} \tag{4.13}$$

And the energy efficiency of methanol synthesis system is can be written as

$$\eta_{DME,ex} = \frac{\dot{m}_{DME} ex_{DME}}{\dot{E}^{\dot{Q}}{}_{Total} + \dot{W}_{Total}} \tag{4.14}$$

where ex_{DME} is the total specific exergy of methanol, $\dot{E}^{\dot{Q}}{}_{Total}$ is the total exergy provided in the form of heat.

The overall energy efficiency for Photovoltaic based DME production system is expressed as follows:

$$\eta_{ov,en,sys1} = \frac{\dot{m}_{\mathrm{DME}}\, LHV_{\mathrm{DME}}}{\dot{Q}_{total} + \dot{W}_{Total}} \tag{4.15}$$

where $\dot{Q}_{total}$ can be expressed as follows:

$$\dot{Q}_{total} = \dot{Q}_{EH} + \dot{Q}_{Regen} + \dot{Q}_{B9} + \dot{Q}_{B10} + \dot{Q}_{B23} + \dot{Q}_{B14} \tag{4.16}$$

Here $\dot{W}_{Total}$ can be expressed as follows:

$$\dot{W}_{Total} = \dot{W}_{p,ccs} + \dot{W}_{el} + \dot{W}_{B1} + \dot{W}_{B2} + \dot{W}_{B12} + \dot{W}_{B15} \tag{4.17}$$

The overall exergy efficiency for Photovoltaic based DME production system is expressed as follows:

$$\eta_{ov,ex,sys1} = \frac{\dot{m}_{\mathrm{DME}}\, ex_{\mathrm{DME}}}{\dot{Ex}^{\dot{Q}}{}_{total} + \dot{W}_{Total}} \tag{4.18}$$

where $\dot{Ex}^{\dot{Q}}{}_{total}$ is the total exergy provided in the form of heat and is expressed as

$$\dot{Ex}_{total}^{\dot{Q}} = \dot{Q}_{EH}\left(1-\frac{T_0}{T}\right)+\dot{Q}_{Regen}\left(1-\frac{T_0}{T}\right)+\dot{Q}_{B9}\left(1-\frac{T_0}{T}\right)+\dot{Q}_{B10}\left(1-\frac{T_0}{T}\right)$$

$$+\dot{Q}_{B23}\left(1-\frac{T_0}{T}\right)+\dot{Q}_{B14}(1-\frac{T_0}{T}) \quad (4.19)$$

(PEM) electrolyzer electrochemical model

The overall electrochemical reaction for water decomposition can be expressed as

$$H_2O \xrightarrow{\Delta H} H_2+\frac{1}{2}O_2 \quad (4.20)$$

here ΔH is the amount of energy supplied to the electrolyzer and can be written as

$$\Delta H = \Delta G + T\Delta S \quad (4.21)$$

where $T\Delta S$ denotes the thermal energy demand and ΔG represent the electrical energy demand (change in Gibbs energy).

Hydrogen production rate through PEM electrolyzer can be expressed as

$$\dot{N}_{H_2} = \frac{J_{el}}{2F} \quad (4.22)$$

where J_{el} is current density in [A/m^2], F represents Faraday constant.

The electrical work provided to the PEM electrolyzer is calculated as

$$\dot{W}_{PEM} = J_{el}V \quad (4.23)$$

Here V represent the electrolyzer cell potential in Volts and can be calculated as

$$V = V_0 + V_{act,a} + V_{act,c} + V_{Ohmic} \quad (4.24)$$

where V_o denotes reversible cell potential and can be expressed by Nernst equation

$$V_0 = \frac{\Delta G}{nF}+\frac{RT}{nF}\ln\left(\frac{(p_{H_2})(p_{O_2})^{0.5}}{p_{H_2O}}\right) \quad (4.25)$$

Here, n is the number of moles transferred and P is the partial pressure.

Table 4.1: Mass balance and energy balance equations for system 1

Sub-system	Component	Mass balance equation	Energy balance equation
Carbon Capturing system	Absorber	$\dot{m}_{fluGas} + \dot{m}_{LA} = \dot{m}_{Gasout} + \dot{m}_{RA}$	$\dot{m}_{fluGas}h_{fluGas} + \dot{m}_{LA}h_{LA} = \dot{m}_{cleanGas}h_{cleanGas} + \dot{m}_{RA}h_{RA}$
	Pump	$\dot{m}_{RA1} = \dot{m}_{RA2}$	$\dot{m}_{RA1}h_{RA1} + \dot{W}_{pump} = \dot{m}_{RA2}h_{RA2}$
	Heat exchanger	$\dot{m}_{LA1} + \dot{m}_{RA1} = \dot{m}_{LA2} + \dot{m}_{RA2}$	$\dot{m}_{LA1}h_{LA1} + \dot{m}_{RA1}h_{RA1} = \dot{m}_{LA2}h_{LA2} + \dot{m}_{RA2}h_{RA2}$
	Regenerator	$\dot{m}_{RA} = \dot{m}_{CO2} + \dot{m}_{LA}$	$\dot{m}_{RA}h_{RA} + \dot{Q}_{Boiler} = \dot{m}_{LA}h_{LA} + \dot{m}_{CO2}h_{CO2}$
PEM Hydrogen production system	Heat exchanger1	$\dot{m}_0 + \dot{m}_8 = \dot{m}_1 + \dot{m}_9$	$\dot{m}_0h_0 + \dot{m}_8h_8 = \dot{m}_1h_1 + \dot{m}_9h_9$
	Heat exchanger2	$\dot{m}_1 + \dot{m}_4 = \dot{m}_2 + \dot{m}_5$	$\dot{m}_1h_1 + \dot{m}_4h_4 = \dot{m}_2h_2 + \dot{m}_5h_5$
	Electric heater	$\dot{m}_2 = \dot{m}_3$	$\dot{m}_2h_2 + \dot{Q}_{EH} = \dot{m}_2h_2$
	PEM electrolyzer	$\dot{m}_{H2O} = \dot{m}_{H2} + \dot{m}_{O2}$	$\dot{m}_{H2O}h_{H2O} + \dot{W}_{elec} = \dot{m}_{H2}h_{H2} + \dot{m}_{O2}h_{O2}$
Methanol synthesis system	H_2 compressor1	$\dot{m}_1 = \dot{m}_2$	$\dot{m}_1h_1 + \dot{W}_{comp1,H2} = \dot{m}_2h_2$
	H_2 compressor2	$\dot{m}_3 = \dot{m}_4$	$\dot{m}_3h_3 + \dot{W}_{comp2,H2} = \dot{m}_4h_4$
	CO_2 compressor1	$\dot{m}_5 = \dot{m}_6$	$\dot{m}_5h_5 + \dot{W}_{comp1,CO2} = \dot{m}_6h_6$
	CO_2 compressor 2	$\dot{m}_7 = \dot{m}_8$	$\dot{m}_7h_7 + \dot{W}_{comp2,CO2} = \dot{m}_8h_8$
	H_2 intercooler	$\dot{m}_2 = \dot{m}_3$	$\dot{m}_2h_2 = \dot{m}_3h_3 + \dot{Q}_{IC,H2}$
	CO_2 intercooler	$\dot{m}_6 = \dot{m}_7$	$\dot{m}_6h_6 = \dot{m}_7h_7 + \dot{Q}_{IC,CO2}$
	MeOH reactor 1	$\dot{m}_{CO2} + \dot{m}_{H2} + \dot{m}_{Rec} = \dot{m}_{MeOH,1} + \dot{m}_{Unrec}$	$\dot{m}_{CO2}h_{CO2} + \dot{m}_{H2}h_{H2} + \dot{m}_{Rec}h_{Rec} = \dot{m}_{MeOH,1}h_{MeOH,1} + \dot{m}_{Unrec}h_{Unrec} + Q_{out}$
	MeOH reactor 2	$\dot{m}_{Unrec} = \dot{m}_{MeOH,2} + \dot{m}_{Rec2}$	$\dot{m}_{Unrec}h_{Unrec} = \dot{m}_{MeOH,2}h_{MeOH,2} + \dot{m}_{Rec2}h_{Rec2} + Q_{out}$
	MeOH distillation column	$\dot{m}_{MeOH,1} + \dot{m}_{MeOH,2} = \dot{m}_{MeOH,Pure} + \dot{m}_{H2O}$	$\dot{m}_{MeOH,1}h_{MeOH,1} + \dot{m}_{MeOH,2}h_{MeOH,2} + \dot{Q}_{reb,DC1} = \dot{m}_{MeOH,pure}h_{MeOH,pure} + \dot{m}_{H2O}h_{H2O} + \dot{Q}_{cond,DC1}$
DME synthesis system	DME reactor	$\dot{m}_{MeOH,Pure} = \dot{m}_{DME,mixture}$	$\dot{m}_{MeOH,Pure}h_{MeOH,Pure} = \dot{m}_{DME,mix}h_{DME,mix}$
	Heat exchanger	$\dot{m}_{23} + \dot{m}_{26} = \dot{m}_{27} + \dot{m}_{24}$	$\dot{m}_{23}h_{23} + \dot{m}_{26}h_{26} = \dot{m}_{27}h_{27} + \dot{m}_{24}h_{24}$
	DME distillation column	$\dot{m}_{DME,mix} = \dot{m}_{MeOH,mix} + \dot{m}_{DME,Pure}$	$\dot{m}_{DME,mix}h_{DME,mix} + \dot{Q}_{reb,DC2} = \dot{m}_{MeOH,mix}h_{MeOH,mix} + \dot{m}_{DME,Pure}h_{DME,Pure} + \dot{Q}_{cond,DC2}$
	Unreacted MeOH distillation column	$\dot{m}_{MeOH,mix} = \dot{m}_{MeOH,Rec} + \dot{m}_{H2O}$	$\dot{m}_{MeOH,mix}h_{MeOH,mix} + \dot{Q}_{reb,DC3} = \dot{m}_{MeOH,Rec}h_{MeOH,Rec} + \dot{m}_{H2O}h_{H2O} + \dot{Q}_{cond,DC3}$

Table 4.2: Exergy balance and exergy efficiency equations for system 1

Sub-system	Component	Exergy balance equation	Energy efficiency equation
Carbon Capturing system	Absorber	$\dot{m}_{fluGas}ex_{fluGas} + \dot{m}_{LA}ex_{LA} = \dot{m}_{cleanGas}ex_{cleanGas} + \dot{m}_{RA}ex_{RA} + \dot{E}x_{dest_{abs}}$	$\eta_{abs,ex} = \frac{\dot{m}_{cleanGas}ex_{cleanGas} + \dot{m}_{RA}ex_{RA}}{\dot{m}_{fluGas}ex_{fluGas} + \dot{m}_{lean}ex_{LA}}$
	Pump	$\dot{m}_{RA1}ex_{RA1} + \dot{W}_{pump} = \dot{m}_{RA2}ex_{RA2} + \dot{E}x_{dest_{Pump}}$	$\eta_{pump,ex} = \frac{\dot{m}_{RA2}ex_{RA2} - \dot{m}_{RA1}ex_{RA1}}{\dot{W}_{pump}}$
	Heat exchanger	$\dot{m}_{LA1}ex_{LA1} + \dot{m}_{RA1}ex_{RA1} = \dot{m}_{LA2}ex_{LA2} + \dot{m}_{RA2}ex_{RA2} + \dot{E}x_{dest_{HX}}$	$\eta_{HX,ex} = \frac{\dot{m}_{LA2}ex_{LA2} + \dot{m}_{RA2}ex_{RA2}}{\dot{m}_{LA1}ex_{LA1} + \dot{m}_{RA1}ex_{RA1}}$
	Regenerator	$\dot{m}_{RA}ex_{RA} + \dot{Q}_{Boiler}\left(1 - \frac{T_0}{T}\right) = \dot{m}_{LA}ex_{LA} + \dot{m}_{CO2}ex_{CO2} + \dot{E}x_{dest_{REGEN}}$	$\eta_{HX,ex} = 1 - \frac{\dot{E}x_{dest_{REGEN}}}{\dot{Q}_{Boiler}\left(1 - \frac{T_0}{T}\right)}$
PEM Hydrogen production system	Heat exchanger 1	$\dot{m}_0ex_0 + \dot{m}_8ex_8 = \dot{m}_1ex_1 + \dot{m}_9ex_9 + \dot{E}x_{dest_{HX1}}$	$\eta_{HX1,ex} = \frac{\dot{m}_1ex_1 + \dot{m}_9ex_9}{\dot{m}_0ex_0 + \dot{m}_8ex_8}$
	Heat exchanger 2	$\dot{m}_1ex_1 + \dot{m}_4ex_4 = \dot{m}_2ex_2 + \dot{m}_5ex_5 + \dot{E}x_{dest_{HX2}}$	$\eta_{HX2,ex} = \frac{\dot{m}_2ex_2 + \dot{m}_5ex_5}{\dot{m}_1ex_1 + \dot{m}_4ex_4}$
	Electric heater	$\dot{m}_2ex_2 + \dot{Q}_{EH}\left(1 - \frac{T_0}{T}\right) = \dot{m}_3ex_3 + \dot{E}x_{dest_{EH}}$	$\eta_{HX,ex} = 1 - \frac{\dot{E}x_{dest_{EH}}}{\dot{Q}_{EH}\left(1 - \frac{T_0}{T}\right)}$
	PEM electrolyzer	$\dot{m}_{H2O}ex_{H2O} + \dot{W}_{PEM} = \dot{m}_{H2}ex_{H2} + \dot{m}_{O2}ex_{O2} + \dot{E}x_{dest_{electrolyzer}}$	$\eta_{PEM,ex} = \frac{\dot{m}_{H2}ex_{H2}}{\dot{W}_{PEM}}$
Methanol synthesis system	H_2 compressor 1	$\dot{m}_1ex_1 + \dot{W}_{comp1,H2} = \dot{m}_2ex_2 + \dot{E}x_{dest_{comp1,H2}}$	$\eta_{comp1,H2,ex} = \frac{\dot{m}_2ex_2 - \dot{m}_1ex_1}{\dot{W}_{comp1,H2}}$
	H_2 compressor 2	$\dot{m}_3ex_3 + \dot{W}_{comp2,H2} = \dot{m}_4ex_4 + \dot{E}x_{dest_{comp2,H2}}$	$\eta_{comp2,H2,ex} = \frac{\dot{m}_4ex_4 - \dot{m}_3ex_3}{\dot{W}_{comp2,H2}}$
	CO_2 compressor 1	$\dot{m}_5ex_5 + \dot{W}_{comp1,CO2} = \dot{m}_6ex_6 + \dot{E}x_{dest_{comp1,CO2}}$	$\eta_{comp1,CO2,ex} = \frac{\dot{m}_6ex_6 - \dot{m}_5ex_5}{\dot{W}_{comp1,CO2}}$
	CO_2 compressor 2	$\dot{m}_7ex_7 + \dot{W}_{comp2,CO2} = \dot{m}_8ex_8 + \dot{E}x_{dest_{comp2,CO2}}$	$\eta_{comp2,CO2,ex} = \frac{\dot{m}_8ex_8 - \dot{m}_7ex_7}{\dot{W}_{comp2,CO2}}$
	H_2 intercooler	$\dot{m}_2ex_2 = \dot{m}_3ex_3 + \dot{E}x_{dest_{IC,H2}}$	$\eta_{IC,H2,ex} = 1 - \frac{\dot{E}x_{dest_{IC,H2}}}{\dot{m}_2ex_2}$
	CO_2 intercooler	$\dot{m}_6ex_6 = \dot{m}_7ex_7 + \dot{E}x_{dest_{IC,CO2}}$	$\eta_{IC,CO2,ex} = 1 - \frac{\dot{E}x_{dest_{IC,CO2}}}{\dot{m}_6ex_6}$
	MeOH reactor 1	$\dot{m}_{CO2}ex_{CO2} + \dot{m}_{H2}ex_{H2} + \dot{m}_{Rec}ex_{Rec} = \dot{m}_{MeOH,1}ex_{MeOH,1} + \dot{m}_{Unrec}ex_{Unrec} + \dot{E}x_{dest,reactor1}$	$\eta_{reactor1,ex} = 1 - \frac{\dot{E}x_{dest_{reactor1}}}{\dot{m}_{CO2}ex_{CO2} + \dot{m}_{H2}ex_{H2} + \dot{m}_{Rece}ex_{Recycle}}$

	MeOH reactor 2	$\dot{m}_{Unrec} ex_{Unrec} + Q_{in}\left(1-\frac{T_0}{T}\right) = \dot{m}_{MeOH,2} ex_{MeOH,2} + \dot{m}_{Rec} ex_{Rec} + \dot{E}x_{dest,Reactor2}$	$\eta_{Reactor2,ex} = 1 - \frac{\dot{E}x_{dest_{reactor2}}}{\dot{m}_{Unrec} ex_{Unrec} + Q_{in}\left(1-\frac{T_0}{T}\right)}$
	MeOH distillation column	$\dot{m}_{MeOH} ex_{MeOH} + \dot{Q}_{reb}\left(1-\frac{T_0}{T}\right) = \dot{m}_{MeOH,pure} ex_{MeOH,pure} + \dot{m}_{H2O} ex_{H2O} + \dot{E}x_{dest,DC1}$	$\eta_{DC1,ex} = 1 - \frac{\dot{E}x_{dest_{DC1}}}{\dot{Q}_{reb}\left(1-\frac{T_0}{T}\right)}$
DME synthesis system	DME reactor	$\dot{m}_{MeOH,Pure} ex_{MeOH,Pure} = \dot{m}_{DME,mixture} ex_{DME,mixture} + \dot{E}x_{dest,DME\ R}$	$\eta_{DME\ R,ex} = 1 - \frac{\dot{E}x_{dest_{DME\ R}}}{\dot{m}_{MeOH,Pure} ex_{MeOH,Pure}}$
	Heat exchanger	$\dot{m}_{23} ex_{23} + \dot{m}_{26} ex_{26} = \dot{m}_{27} ex_{27} + \dot{m}_{24} ex_{24} + \dot{E}x_{dest,HX}$	$\eta_{HX2,ex} = \frac{\dot{m}_{24} ex_{24} + \dot{m}_{27} ex_{27}}{\dot{m}_{23} ex_{23} + \dot{m}_{26} ex_{26}}$
	DME distillation column	$\dot{m}_{DME,mixture} ex_{DME,mixture} + \dot{Q}_{reb}\left(1-\frac{T_0}{T}\right) = \dot{m}_{MeOH,mix} ex_{MeOH,mix} + \dot{m}_{DME,Pure} ex_{DME,Pure} + \dot{Q}_{cond}\left(1-\frac{T_0}{T}\right) + \dot{E}x_{dest,DC2}$	$\eta_{DC2,ex} = 1 - \frac{\dot{E}x_{dest_{DC2}}}{\dot{Q}_{reb}\left(1-\frac{T_0}{T}\right)}$
	Unreacted MeOH distillation column	$\dot{m}_{MeOH,mix} ex_{MeOH,mix} + \dot{Q}_{reb}\left(1-\frac{T_0}{T}\right) = \dot{m}_{MeOH,Rec} ex_{MeOH,Rec} + \dot{m}_{H2O} ex_{H2O} + \dot{Q}_{cond}\left(1-\frac{T_0}{T}\right) + \dot{E}x_{dest,DC3}$	$\eta_{DC3,ex} = 1 - \frac{\dot{E}x_{dest_{DC3}}}{\dot{Q}_{reb}\left(1-\frac{T_0}{T}\right)}$

The activation overpotential can be calculated as

$$V_{act,i} = \left(\frac{RT}{F}\right) sinh^{-1}\left(\frac{J_{el}}{2J_{o,i}}\right) \tag{4.26}$$

where i denotes either anode or cathode, $J_{o,i}$ is exchange current density which can be expressed as

$$J_{o,i} = J_i^{ref} \exp\left(\frac{E_{act,i}}{RT}\right) \tag{4.27}$$

here J_i^{ref} is the pre-exponential factor, and $E_{act,i}$ is the activation energy.

Finally, the Ohmic overpotential in PEM electrolyzer can be expressed as

$$V_{Ohmic} = R_{PEM}\, J_{el} \tag{4.28}$$

where R_{PEM} can be calculated through the following equation

$$R_{PEM} = \int_0^D \frac{1}{\sigma[\varphi(x)]} dx \quad (4.29)$$

where represent ionic conductivity of the membrane, $\varphi(x)$ denotes water content at given membrane thickness and can be expressed as

$$\varphi(x) = \frac{\varphi_a - \varphi_c}{D} x + \varphi_c \quad (4.30)$$

where D represents the membrane thickness.

Local ionic conductivity can be calculated as [46]

$$\sigma[\varphi(x)] = (0.5139\varphi(x) - 0.326)\exp[1268\left(\frac{1}{303} - \frac{1}{T}\right)] \quad (4.31)$$

The operating parameters and assumption used in PEM electrolyzer modeling are listed in Table 3.1

4.3 Thermodynamic Analysis of System 2

The second system produces DME and electricity using waste heat from steel manufacturing plant and renewable energy through thermal solar tower heliostat field. The integrated system is composed of five subsystems, named as thermal solar tower heliostat field, carbon capturing system, SOSE hydrogen production system, methanol synthesis system and DME synthesis system. Thermodynamic analyses represented by energy and exergy balance equations have been performed to assess the performance of each subsystem and the overall integrated system. Mass balance equations and energy balance equations are demonstrated in Table 4.3. Exergy balance equations and exergy efficiency equations are demonstrated in Table 4.4.

For the first subsystem which is thermal solar tower heliostat field, the energy efficiency for thermal solar tower heliostat field is expressed as

$$\eta_{Hel,en} = \frac{\dot{Q}_{SG} + \dot{W}_T}{I_{solar} A_{Hel}} \quad (4.32)$$

where $\dot{Q}_{SG}$ is the heat provided to SOSE steam generator through bled steam, $\dot{W}_T$ is the steam turbine output work, I_{solar} is the solar irradiation, and A_{Hel} is the heliostat field area. While the exergy efficiency for thermal solar tower heliostat field is expressed as

$$\eta_{Hel,ex} = \frac{Ex^{\dot{Q}_{SG}} + \dot{W}_T}{\dot{E}x_{solar}} \tag{4.33}$$

where $Ex^{\dot{Q}_{SG}}$ exergy output in the form of heat, and $\dot{E}x_{solar}$ is the exergy provided by the sun.

The second subsystem is SOSE hydrogen production system, the energy efficiency for SOSE hydrogen production system is expressed as

$$\eta_{SOSE,en} = \frac{\dot{m}_{H2} LHV_{H2}}{\dot{Q}_{EH} + \dot{Q}_{SG} + \dot{W}_{el}} \tag{4.34}$$

where $\dot{Q}_{EH}$ is the heat provided to by electric heater to water. $\dot{Q}_{SG}$ is the heat provided to the water to generate steam and $\dot{W}_e$ is the electrical work provided to the electrolyzer.

And exergy efficiency for SOSE hydrogen production system can be written as

$$\eta_{SOSE,ex} = \frac{\dot{m}_{H2} ex_{H2}}{\dot{E}^{\dot{Q}}{}_{SG} + \dot{E}^{\dot{Q}}{}_{EH} + \dot{E}^{\dot{W}}{}_{el}} \tag{4.35}$$

where $\dot{E}^{\dot{Q}}{}_{EH}$ is the exergy provided by an electric heater in the form of heat, $\dot{E}^{\dot{Q}}{}_{SG}$ is the exergy provided by a steam generator in the form of heat and $\dot{E}^{\dot{W}}{}_{e}$ is the exergy provided to the electrolyzer in the form of heat.

The third system is the DME synthesis system. The energy efficiency of DME synthesis system can be written as

$$\eta_{DME,en} = \frac{\dot{m}_{DME} LHV_{DME}}{Q_{total} + \dot{W}_{Total}} \tag{4.36}$$

where $\dot{m}_{DME}$ is the mass flowrate of produced DME, LHV_{DME} is the lower heating value of the produced DME. The total heat provided during methanol synthesis process is expressed as

$$\dot{Q}_{total} = \dot{Q}_{B9} + \dot{Q}_{B10} + \dot{Q}_{B23} + \dot{Q}_{B14} \tag{4.37}$$

Also, total work can be expressed as follows:

$$\dot{W}_{Total} = \dot{W}_{B1} + \dot{W}_{B2} + \dot{W}_{B12} + \dot{W}_{B15} \tag{4.38}$$

The energy efficiency of methanol synthesis system is can be written as

$$\eta_{DME,ex} = \frac{\dot{m}_{DME} ex_{DME}}{\dot{E}^{\dot{Q}}{}_{Total} + \dot{W}_{Total}} \quad (4.39)$$

where ex_{DME} is the total specific exergy of methanol, $\dot{E}^{\dot{Q}}{}_{Total}$ is the total exergy provided in the form of heat.

The overall energy efficiency for solar thermal based DME production system is expressed as follows:

$$\eta_{ov,en,sys2} = \frac{\dot{m}_{\mathrm{DME}} LHV_{\mathrm{DME}} + \dot{W}_T}{\dot{Q}_{total} + \dot{W}_{Total}} \quad (4.40)$$

where $\dot{Q}_{total}$ can be expressed as follows:

$$\dot{Q}_{total} = \dot{Q}_{EH} + \dot{Q}_{stripper} + \dot{Q}_{B9} + \dot{Q}_{B10} + \dot{Q}_{B23} + \dot{Q}_{B14} + \dot{Q}_{solar} \quad (4.41)$$

Here $\dot{W}_{Total}$ can be expressed as follows:

$$\dot{W}_{Total} = \dot{W}_{p,SOSE} + \dot{W}_{p,ccs} + \dot{W}_{el} + \dot{W}_{B1} + \dot{W}_{B2} + \dot{W}_{B12} + \dot{W}_{B15} \quad (4.42)$$

The overall exergy efficiency for solar thermal based DME production system is expressed as follows:

$$\eta_{ov,ex,sys2} = \frac{\dot{m}_{\mathrm{DME}} ex_{\mathrm{DME}} + \dot{W}_T}{\dot{Ex}^{\dot{Q}}{}_{total} + \dot{W}_{Total}} \quad (4.43)$$

where $\dot{Ex}^{\dot{Q}}{}_{total}$ is the total exergy provided in the form of heat and is expressed as

$$\dot{Ex}^{\dot{Q}}{}_{total} = \dot{Q}_{EH}\left(1 - \frac{T_0}{T}\right) + \dot{Q}_{stripper}\left(1 - \frac{T_0}{T}\right) + \dot{Q}_{B9}\left(1 - \frac{T_0}{T}\right) + \dot{Q}_{B10}\left(1 - \frac{T_0}{T}\right) + \dot{Q}_{B23}\left(1 - \frac{T_0}{T}\right) + \dot{Q}_{B14}\left(1 - \frac{T_0}{T}\right) + \dot{Q}_{solar}\left(1 - \frac{T_0}{T}\right) \quad (4.44)$$

SOSE electrolyzer electrochemical model

The overall electrochemical reaction for water decomposition can be expressed as

$$H_2O \xrightarrow{\Delta H} H_2 + \frac{1}{2}O_2 \quad (4.45)$$

here ΔH is the amount of energy supplied to the electrolyzer and can be written as

$$\Delta H = \Delta G + T\Delta S \quad (4.46)$$

where $T\Delta S$ denotes the thermal energy demand which is more significant in SOSE, and ΔG represent the electrical energy demand (change in Gibbs energy).

Hydrogen production rate through SOSE electrolyzer can be expressed as

$$\dot{N}_{H_2} = \frac{J_{el}}{2F} \tag{4.47}$$

where J_{el} is current density in [A/m^2], F represents Faraday constant.

The electrical work provided to the SOSE electrolyzer is calculated as

$$\dot{W}_{PEM} = J_{el}V \tag{4.48}$$

here V represent the electrolyzer cell potential in Volts and can be calculated as

$$V = V_0 + V_{act,a} + V_{act,c} + V_{con,a} + V_{con,c} + V_{Ohmic} \tag{4.49}$$

where V_o denotes reversible cell potential and can be expressed by Nernst equation:

$$V_0 = \frac{\Delta G}{nF} + \frac{RT}{nF}\ln\left(\frac{(p_{H_2})(p_{O_2})^{0.5}}{p_{H_2O}}\right) \tag{4.50}$$

Here n is the number of moles transferred and P is the partial pressure.

The activation overpotential can be calculated as

$$V_{act,i} = \left(\frac{RT}{F}\right) sinh^{-1}\left(\frac{J_{el}}{2J_{o,i}}\right) \tag{4.51}$$

where i denotes either anode or cathode, $J_{o,i}$ is exchange current density which can be expressed as

$$J_{o,i} = J_i^{ref} \exp\left(\frac{E_{act,i}}{RT}\right) \tag{4.52}$$

here J_i^{ref} is the pre-exponential factor, and $E_{act,i}$ is the activation energy.

The concentration overpotential for anode and cathode can be evaluated by:

$$V_{con,c} = \frac{RT}{2F}\ln\left(\frac{1+\left(\frac{JRTd_c}{2FD_{H2O}^{eff}P_{H2}^{In}}\right)}{1-\left(\frac{JRTd_c}{2FD_{H2O}^{eff}P_{H2O}^{In}}\right)}\right) \tag{4.53}$$

$$V_{con,a} = \frac{RT}{2F} \ln\left[(1 + \left(\frac{JRTd_a}{4FD_{O2}^{eff} P_{O2}^{o}}\right))^{0.5}\right] \quad (4.54)$$

where dc and da represent anode and cathode thickness, D_i^{eff} is the effective diffusion coefficient.

Finally, Ohmic overpotential in SOSE electrolyzer can be expressed as

$$V_{Ohmic} = R_{PEM} J_{el} \quad (4.55)$$

where R_{PEM} can be calculated through the same equations used in PEM model to calculate Ohmic resistance through Eq(4.29),Eq(4.30),Eq(4.31).

The operating parameters and assumption used in PEM electrolyzer modeling are listed in Table 3.2

Table 4.3: Mass balance and energy balance equations for system 2

Sub-system	Component	Mass balance equation	Energy balance equation
Solar heliostat field	Receiver	$\dot{m}_7 = \dot{m}_8$	$\dot{m}_7 h_7 + \dot{Q}_{Rec,Abs} = \dot{m}_8 h_8$
	Pump	$\dot{m}_1 = \dot{m}_2$	$\dot{m}_1 h_1 + \dot{W}_{pump} = \dot{m}_2 h_2$
	Boiler-HX	$\dot{m}_8 + \dot{m}_2 = \dot{m}_7 + \dot{m}_3$	$\dot{m}_8 h_8 + \dot{m}_2 h_2 = \dot{m}_7 h_7 + \dot{m}_3 h_3$
	Turbine	$\dot{m}_3 = \dot{m}_4$	$\dot{m}_3 h_3 = \dot{m}_4 h_4 + \dot{W}_T$
Carbon Capturing system	Absorber	$\dot{m}_{fluGas} + \dot{m}_{LA} = \dot{m}_{Gasout} + \dot{m}_{RA}$	$\dot{m}_{fluGas} h_{fluGas} + \dot{m}_{LA} h_{LA} = \dot{m}_{cleanGas} h_{cleanGas} + \dot{m}_{RA} h_{RA}$
	Pump	$\dot{m}_{RA1} = \dot{m}_{RA2}$	$\dot{m}_{RA1} h_{RA1} + \dot{W}_{pump} = \dot{m}_{RA2} h_{RA2}$
	Heat exchanger	$\dot{m}_{LA1} + \dot{m}_{RA1} = \dot{m}_{LA2} + \dot{m}_{RA2}$	$\dot{m}_{LA1} h_{LA1} + \dot{m}_{RA1} h_{RA1} = \dot{m}_{LA2} h_{LA2} + \dot{m}_{RA2} h_{RA2}$
	Regenerator	$\dot{m}_{RA} = \dot{m}_{CO2} + \dot{m}_{LA}$	$\dot{m}_{RA} h_{RA} + \dot{Q}_{Boiler} = \dot{m}_{LA} h_{LA} + \dot{m}_{CO2} h_{CO2}$
SOSE Hydrogen production	Heat exchangers	$\dot{m}_1 + \dot{m}_{13} = \dot{m}_{20} + \dot{m}_{22}$	$\dot{m}_1 h_1 + \dot{m}_{13} h_{13} = \dot{m}_{20} h_{20} + \dot{m}_{22} h_{22}$
	Steam generator	$\dot{m}_2 = \dot{m}_3$	$\dot{m}_2 h_2 + \dot{Q}_{SG} = \dot{m}_3 h_3$
	Electric heater	$\dot{m}_6 = \dot{m}_7$	$\dot{m}_6 h_6 + \dot{Q}_{EH} = \dot{m}_7 h_7$

	SOSE electrolyzer	$\dot{m}_{H2O} = \dot{m}_{H2} + \dot{m}_{O2}$	$\dot{m}_{H2O}h_{H2O} + \dot{W}_{el} = \dot{m}_{H2}h_{H2} + \dot{m}_{O2}h_{O2}$
Methanol synthesis system	H_2 compressor1	$\dot{m}_1 = \dot{m}_2$	$\dot{m}_1 h_1 + \dot{W}_{comp1,H2} = \dot{m}_2 h_2$
	H_2 compressor 2	$\dot{m}_3 = \dot{m}_4$	$\dot{m}_3 h_3 + \dot{W}_{comp2,H2} = \dot{m}_4 h_4$
	CO_2 compressor1	$\dot{m}_5 = \dot{m}_6$	$\dot{m}_5 h_5 + \dot{W}_{comp1,CO2} = \dot{m}_6 h_6$
	CO_2 compressor2	$\dot{m}_7 = \dot{m}_8$	$\dot{m}_7 h_7 + \dot{W}_{comp2,CO2} = \dot{m}_8 h_8$
	H_2 intercooler	$\dot{m}_2 = \dot{m}_3$	$\dot{m}_2 h_2 = \dot{m}_3 h_3 + \dot{Q}_{IC,H2}$
	CO_2 intercooler	$\dot{m}_6 = \dot{m}_7$	$\dot{m}_6 h_6 = \dot{m}_7 h_7 + \dot{Q}_{IC,CO2}$
	MeOH reactor 1	$\dot{m}_{CO2} + \dot{m}_{H2} + \dot{m}_{Rec} = \dot{m}_{MeOH,1} + \dot{m}_{Unrec}$	$\dot{m}_{CO2}h_{CO2} + \dot{m}_{H2}h_{H2} + \dot{m}_{Rec}h_{Rec} = \dot{m}_{MeOH,1}h_{MeOH,1} + \dot{m}_{Unrec}h_{Unrec} + Q_{out}$
	MeOH reactor 2	$\dot{m}_{Unrec} = \dot{m}_{MeOH,2} + \dot{m}_{Rec2}$	$\dot{m}_{Unrec}h_{Unrec} + Q_{in} = \dot{m}_{MeOH,2}h_{MeOH,2} + \dot{m}_{Rec2}h_{Rec2}$
	MeOH distillation column	$\dot{m}_{MeOH,1} + \dot{m}_{MeOH,2} = \dot{m}_{MeOH,Pure} + \dot{m}_{H2O}$	$\dot{m}_{MeOH,1}h_{MeOH,1} + \dot{m}_{MeOH,2}h_{MeOH,2} + \dot{Q}_{reb,DC1} = \dot{m}_{MeOH,pure}h_{MeOH,pure} + \dot{m}_{H2O}h_{H2O} + \dot{Q}_{cond,DC1}$
DME synthesis system	DME reactor	$\dot{m}_{MeOH,Pure} = \dot{m}_{DME,mixture}$	$\dot{m}_{MeOH,Pure}h_{MeOH,Pure} = \dot{m}_{DME,mix}h_{DME,mix}$
	Heat exchanger	$\dot{m}_{23} + \dot{m}_{26} = \dot{m}_{27} + \dot{m}_{24}$	$\dot{m}_{23}h_{23} + \dot{m}_{26}h_{26} = \dot{m}_{27}h_{27} + \dot{m}_{24}h_{24}$
	DME distillation column	$\dot{m}_{DME,mix} = \dot{m}_{MeOH,mix} + \dot{m}_{DME,Pure}$	$\dot{m}_{DME,mix}h_{DME,mix} + \dot{Q}_{reb,DC2} = \dot{m}_{MeOH,mix}h_{MeOH,mix} + \dot{m}_{DME,Pure}h_{DME,Pure} + \dot{Q}_{cond,DC2}$
	Unreacted MeOH distillation column	$\dot{m}_{MeOH,mix} = \dot{m}_{MeOH,Rec} + \dot{m}_{H2O}$	$\dot{m}_{MeOH,mix}h_{MeOH,mix} + \dot{Q}_{reb,DC3} = \dot{m}_{MeOH,Rec}h_{MeOH,Rec} + \dot{m}_{H2O}h_{H2O} + \dot{Q}_{cond,DC3}$

Table 4.4: Exergy balance and exergy efficiency equations for system 2

Sub-system	Component	Exergy balance equation	Energy efficiency equation
Solar heliostat field	Receiver	$\dot{m}_7 ex_7 + \dot{Q}_{rec,Abs}\left(1-\frac{T_0}{T}\right) = \dot{m}_8 ex_8 + \dot{E}x_{dest,Rec}$	$\eta_{HX,ex} = 1 - \frac{\dot{E}x_{dest_{Rec}}}{\dot{Q}_{rec,Abs}\left(1-\frac{T_0}{T}\right)}$
	Pump	$\dot{m}_1 ex_1 + \dot{W}_{pump} = \dot{m}_2 ex_2 + \dot{E}x_{dest,Pump}$	$\eta_{pump,ex} = \frac{\dot{m}_2 ex_2 - \dot{m}_1 ex_1}{\dot{W}_{pump}}$
	Boiler-HX	$\dot{m}_8 ex_8 + \dot{m}_2 ex_2 = \dot{m}_7 ex_7 + \dot{m}_3 ex_3 + \dot{E}x_{dest_{Boiler}}$	$\eta_{boiler,ex} = \frac{\dot{m}_7 ex_7 + \dot{m}_3 ex_3}{\dot{m}_2 ex_2 + \dot{m}_8 ex_8}$
	Turbine	$\dot{m}_3 ex_3 = \dot{m}_4 ex_4 + \dot{W}_{hpT} + \dot{E}x_{dest,hpT}$	$\eta_{boiler,ex} = \frac{\dot{W}_{hpT}}{\dot{m}_3 ex_3 + \dot{m}_4 ex_4}$
Carbon Capturing system	Absorber	$\dot{m}_{fluGas} ex_{fluGas} + \dot{m}_{LA} ex_{LA} = \dot{m}_{cleanGas} ex_{cleanGas} + \dot{m}_{RA} ex_{RA} + \dot{E}x_{dest_{abs}}$	$\eta_{abs,ex} = \frac{\dot{m}_{cleanGas} ex_{cleanGas} + \dot{m}_{RA} ex_{RA}}{\dot{m}_{fluGas} ex_{fluGas} + \dot{m}_{lean} ex_{LA}}$
	Pump	$\dot{m}_{RA1} ex_{RA1} + \dot{W}_{pump} = \dot{m}_{RA2} ex_{RA2} + \dot{E}x_{dest_{Pump}}$	$\eta_{pump,ex} = \frac{\dot{m}_{RA2} ex_{RA2} - \dot{m}_{RA1} ex_{RA1}}{\dot{W}_{pump}}$
	Heat exchanger	$\dot{m}_{LA1} ex_{LA1} + \dot{m}_{RA1} ex_{RA1} = \dot{m}_{LA2} ex_{LA2} + \dot{m}_{RA2} ex_{RA2} + \dot{E}x_{dest_{HX}}$	$\eta_{HX,ex} = \frac{\dot{m}_{LA2} ex_{LA2} + \dot{m}_{RA2} ex_{RA2}}{\dot{m}_{LA1} ex_{LA1} + \dot{m}_{RA1} ex_{RA1}}$
	Regenerator	$\dot{m}_{RA} ex_{RA} + \dot{Q}_{Boiler}\left(1-\frac{T_0}{T}\right) = \dot{m}_{LA} ex_{LA} + \dot{m}_{CO2} ex_{CO2} + \dot{E}x_{dest_{REGEN}}$	$\eta_{HX,ex} = 1 - \frac{\dot{E}x_{dest_{REGEN}}}{\dot{Q}_{Boiler}\left(1-\frac{T_0}{T}\right)}$
SOSE Hydrogen production system	Heat exchanger 1,2,3,4,5	$\dot{m}_1 ex_1 + \dot{m}_{13} ex_{13} = \dot{m}_{20} ex_{20} + \dot{m}_{22} ex_{22} + \dot{E}x_{dest_{HX1}}$	$\eta_{HX1,ex} = \frac{\dot{m}_{20} ex_{20} + \dot{m}_{22} ex_{22}}{\dot{m}_1 ex_1 + \dot{m}_{13} ex_{13}}$
	Steam generator	$\dot{m}_2 ex_2 + \dot{Q}_{SG} = \dot{m}_3 ex_3 + \dot{E}x_{dest_{SG2}}$	$\eta_{HX2,ex} = \frac{\dot{m}_3 ex_3 + \dot{m}_2 ex_2}{\dot{Q}_{SG}\left(1-\frac{T_0}{T}\right)}$
	Electric heater	$\dot{m}_6 ex_6 + \dot{Q}_{EH}\left(1-\frac{T_0}{T}\right) = \dot{m}_7 ex_7 + \dot{E}x_{dest_{EH}}$	$\eta_{HX,ex} = 1 - \frac{\dot{E}x_{dest_{EH}}}{\dot{Q}_{EH}\left(1-\frac{T_0}{T}\right)}$
	SOSE electrolyzer	$\dot{m}_{H2O} ex_{H2O} + \dot{W}_{SOSE} = \dot{m}_{H2} ex_{H2} + \dot{m}_{O2} ex_{O2} + \dot{E}x_{dest_{SOSE}}$	$\eta_{PEM,ex} = \frac{\dot{m}_{H2} ex_{H2}}{\dot{W}_{SOSE}}$

Methanol synthesis system	H_2 compressor 1	$\dot{m}_1 ex_1 + \dot{W}_{comp1,H2} = \dot{m}_2 ex_2 + \dot{E}x_{dest_{comp1,H2}}$	$\eta_{comp1,H2,ex} = \frac{\dot{m}_2 ex_2 - \dot{m}_1 ex_1}{\dot{W}_{comp1,H2}}$
	H_2 compressor 2	$\dot{m}_3 ex_3 + \dot{W}_{comp2,H2} = \dot{m}_4 ex_4 + \dot{E}x_{dest_{comp2,H2}}$	$\eta_{comp2,H2,ex} = \frac{\dot{m}_4 ex_4 - \dot{m}_3 ex_3}{\dot{W}_{comp2,H2}}$
	CO_2 compressor 1	$\dot{m}_5 ex_5 + \dot{W}_{comp1,CO2} = \dot{m}_6 ex_6 + \dot{E}x_{dest_{comp1,CO2}}$	$\eta_{comp1,CO2,ex} = \frac{\dot{m}_6 ex_6 - \dot{m}_5 ex_5}{\dot{W}_{comp1,CO2}}$
	CO_2 compressor 2	$\dot{m}_7 ex_7 + \dot{W}_{comp2,CO2} = \dot{m}_8 ex_8 + \dot{E}x_{dest_{comp2,CO2}}$	$\eta_{comp2,CO2,ex} = \frac{\dot{m}_8 ex_8 - \dot{m}_7 ex_7}{\dot{W}_{comp2,CO2}}$
	H_2 intercooler	$\dot{m}_2 ex_2 = \dot{m}_3 ex_3 + \dot{E}x_{dest_{IC,H2}}$	$\eta_{IC,H2,ex} = 1 - \frac{\dot{E}x_{dest_{IC,H2}}}{\dot{m}_2 ex_2}$
	CO_2 intercooler	$\dot{m}_6 ex_6 = \dot{m}_7 ex_7 + \dot{E}x_{dest_{IC,CO2}}$	$\eta_{IC,CO2,ex} = 1 - \frac{\dot{E}x_{dest_{IC,CO2}}}{\dot{m}_6 ex_6}$
	MeOH reactor 1	$\dot{m}_{CO2} ex_{CO2} + \dot{m}_{H2} ex_{H2} + \dot{m}_{Rec} ex_{Rec} = \dot{m}_{MeOH,1} ex_{MeOH,1} + \dot{m}_{Unrec} ex_{Unrec} + \dot{E}x_{dest,reactor1}$	$\eta_{reactor1,ex} = 1 - \frac{\dot{E}x_{dest_{reactor1}}}{\dot{m}_{CO2} ex_{CO2} + \dot{m}_{H2} ex_{H2} + \dot{m}_{Rece} ex_{Recycle}}$
	MeOH reactor 2	$\dot{m}_{Unrec} ex_{Unrec} + Q_{in}\left(1 - \frac{T_0}{T}\right) = \dot{m}_{MeOH,2} ex_{MeOH,2} + \dot{m}_{Rec} ex_{Rec} + \dot{E}x_{dest,Reactor2}$	$\eta_{Reactor2,ex} = 1 - \frac{\dot{E}x_{dest_{reactor2}}}{\dot{m}_{Unrec} ex_{Unrec} + Q_{in}\left(1 - \frac{T_0}{T}\right)}$
	MeOH distillation column	$\dot{m}_{MeOH} ex_{MeOH} + \dot{Q}_{reb}\left(1 - \frac{T_0}{T}\right) = \dot{m}_{MeOH,pure} ex_{MeOH,pure} + \dot{m}_{H2O} ex_{H2O} + \dot{E}x_{dest,DC1}$	$\eta_{DC1,ex} = 1 - \frac{\dot{E}x_{dest_{DC1}}}{\dot{Q}_{reb}\left(1 - \frac{T_0}{T}\right)}$
DME synthesis system	DME reactor	$\dot{m}_{MeOH,Pure} ex_{MeOH,Pure} = \dot{m}_{DME,mixture} ex_{DME,mixture} + \dot{E}x_{dest,DME\ R}$	$\eta_{DME\ R,ex} = 1 - \frac{\dot{E}x_{dest_{DME\ R}}}{\dot{m}_{MeOH,Pure} ex_{MeOH,Pure}}$
	Heat exchanger	$\dot{m}_{23} ex_{23} + \dot{m}_{26} ex_{26} = \dot{m}_{27} ex_{27} + \dot{m}_{24} ex_{24} + \dot{E}x_{dest,HX}$	$\eta_{HX2,ex} = \frac{\dot{m}_{24} ex_{24} + \dot{m}_{27} ex_{27}}{\dot{m}_{23} ex_{23} + \dot{m}_{26} ex_{26}}$
	DME distillation column	$\dot{m}_{DME,mix} ex_{DME,mix} + \dot{Q}_{reb}\left(1 - \frac{T_0}{T}\right) = \dot{m}_{MeOH,mix} ex_{MeOH,mix} + \dot{m}_{DME,Pure} ex_{DME,Pure} + \dot{Q}_{cond}\left(1 - \frac{T_0}{T}\right) + \dot{E}x_{dest,DC2}$	$\eta_{DC2,ex} = 1 - \frac{\dot{E}x_{dest_{DC2}}}{\dot{Q}_{reb}\left(1 - \frac{T_0}{T}\right)}$
	Unreacted MeOH distillation column	$\dot{m}_{MeOH,mix} ex_{MeOH,mix} + \dot{Q}_{reb}\left(1 - \frac{T_0}{T}\right) = \dot{m}_{MeOH,Rec} ex_{MeOH,Rec} + \dot{m}_{H2O} ex_{H2O} + \dot{Q}_{cond}\left(1 - \frac{T_0}{T}\right) + \dot{E}x_{dest,DC3}$	$\eta_{DC3,ex} = 1 - \frac{\dot{E}x_{dest_{DC3}}}{\dot{Q}_{reb}\left(1 - \frac{T_0}{T}\right)}$

4.4 Thermodynamic Analysis of System 3

The third system is producing DME, generate electricity, and produce fresh water from seawater. The main energy sources for this system is the thermal energy of the waste exhaust gas for a gas turbine, and electrical work through solar PV panels. This system is composed of six main subsystems, named as gas turbine system, carbon capturing system, Cu-Cl thermochemical hydrogen production cycle, multi-effect Desalination system, Methanol synthesis system, MED synthesis system. This system has been studied thermodynamically through energy and exergy balance equations. Furthermore, energy and exergy efficiency of each subsystem has been evaluated to investigate the major source of energy losses. Mass balance equations and energy balance equations are demonstrated in Table 4.5. Exergy balance equations and exergy efficiency equations are demonstrated in Table 4.6.

The first subsystem is gas turbine system. The energy efficiency for gas turbine system can be expressed as:

$$\eta_{en_{GT}} = \frac{\dot{W}_T - \dot{W}_C}{\dot{Q}_{in}} \tag{4.56}$$

where $\dot{W}_T$ is the generated work by gas turbine, $\dot{W}_C$ is the consumed work by compressor and $\dot{Q}_{in}$ is the heat added in the form of fuel. While the exergy efficiency for gas turbine system can be expressed as:

$$\eta_{ex_{GT}} = \frac{\dot{W}_T - \dot{W}_C}{\dot{Q}_{in}\left(1-\frac{T_0}{T}\right)} \tag{4.57}$$

The second subsystem is the Cu-Cl thermochemical cycle. The energy efficiency for the Cu-Cl cycle can be expressed as:

$$\eta_{en_{CuCl}} = \frac{\dot{m}_{H2} LHV_{H2}}{\dot{Q}_{Total} + \dot{W}_{elec}} \tag{4.58}$$

where $\dot{W}_{elec}$ is the consumed work in electrolysis step, $\dot{Q}_{Total}$ can be expressed as:

$$\dot{Q}_{Total} = \dot{Q}_{B2} + \dot{Q}_{B4} \tag{4.59}$$

The exergy efficiency for the Cu-Cl cycle can be written as:

$$\eta_{ex_{CuCl}} = \frac{\dot{m}_{H2} ex_{H2}}{\dot{Q}_{Total}(1-\frac{T_0}{T_s})+\dot{W}_{elec}} \quad (4.60)$$

The third system is the DME synthesis system. The energy efficiency of DME synthesis system can be written as:

$$\eta_{DME,en} = \frac{\dot{m}_{DME} LHV_{DME}}{Q_{total}+\dot{W}_{Total}} \quad (4.61)$$

where $\dot{m}_{DME}$ is the mass flowrate of produced DME, LHV_{DME} is the lower heating value of the produced DME. The total heat provided during methanol synthesis process is expressed as:

$$\dot{Q}_{total} = \dot{Q}_{B9} + \dot{Q}_{B10} + \dot{Q}_{B23} + \dot{Q}_{B14} \quad (4.62)$$

And total work can be expressed as the following:

$$\dot{W}_{Total} = \dot{W}_{B1} + \dot{W}_{B2} + \dot{W}_{B12} + \dot{W}_{B15} \quad (4.63)$$

And the exergy efficiency of the methanol synthesis system is can be written as:

$$\eta_{DME,ex} = \frac{\dot{m}_{DME} ex_{DME}}{\dot{E}\dot{Q}_{Total}+\dot{W}_{Total}} \quad (4.64)$$

where ex_{DME} is the total specific exergy of methanol, $\dot{E}^{\dot{Q}}{}_{Total}$ is the total exergy provided in the form of heat.

The fourth subsystem is MED desalination system. The performance parameter for desalination systems is measured either by Gain Output Ratio (GOR) or Performance Ratio (PR). GOR for MED system can be written as:

$$GOR = \frac{\dot{m}_d h_{fg}}{\dot{Q}_{in}} \quad (4.65)$$

where $\dot{m}_d$ is the mass flow rate of the produced distilled water, h_{fg} is the enthalpy of vaporization and $\dot{Q}_{in}$ is the heat supplies to the system. And performance ratio (PR) can be expressed as:

$$PR = \frac{\dot{m}_d}{\dot{m}_s} \quad (4.66)$$

where $\dot{m}_s$ is the salt water entering the desalination system.

The overall energy efficiency for solar thermal based DME production system is expressed as the following:

$$\eta_{ov,en,sys3} = \frac{\dot{m}_{\mathrm{DME}}\, LHV_{\mathrm{DME}} + \dot{W}_T + \dot{m}_d h_{fg}}{\dot{Q}_{total} + \dot{W}_{Total}} \tag{4.67}$$

where $\dot{Q}_{total}$ can be expressed as the following:

$$\dot{Q}_{total} = \dot{Q}_{stripper} + \dot{Q}_{B9} + \dot{Q}_{B10} + \dot{Q}_{B23} + \dot{Q}_{B14} + \dot{Q}_{B2} + \dot{Q}_{B4} \tag{4.68}$$

And $\dot{W}_{Total}$ can be expressed as the following:

$$\dot{W}_{Total} = \dot{W}_{p,ccs} + \dot{W}_{elec} + \dot{W}_{B1} + \dot{W}_{B2} + \dot{W}_{B12} + \dot{W}_{B15} \tag{4.69}$$

The overall exergy efficiency for solar thermal based DME production system is expressed as the following:

$$\eta_{ov,ex,sys3} = \frac{\dot{m}_{\mathrm{DME}}\, ex_{\mathrm{DME}} + \dot{E}x_{Des}}{\dot{Ex}_{total} + \dot{W}_{Total}} \tag{4.70}$$

where $\dot{E}x_{Des}$ is the exergy recovered in desalination. $\dot{Ex}_{total}$ is the total exergy provided in the form of heat and is expressed as:

$$\dot{Ex}_{total} = \dot{Q}_{EH}\left(1 - \frac{T_0}{T}\right) + \dot{Q}_{stripper}\left(1 - \frac{T_0}{T}\right) + \dot{Q}_{B9}\left(1 - \frac{T_0}{T}\right) + \dot{Q}_{B10}\left(1 - \frac{T_0}{T}\right)$$
$$+\dot{Q}_{B23}\left(1 - \frac{T_0}{T}\right) + \dot{Q}_{B14}\left(1 - \frac{T_0}{T}\right) + \dot{Q}_{solar}\left(1 - \frac{T_0}{T}\right) \tag{4.71}$$

Table 4.5 Mass balance and energy balance equations for system 3

Sub-system	Component	Mass balance equation	Energy balance equation
Gas Turbine system	Compressor	$\dot{m}_1 = \dot{m}_2$	$\dot{m}_1 h_1 + \dot{W}_{comp} = \dot{m}_2 h_2$
	Combustion chamber	$\dot{m}_2 = \dot{m}_3$	$\dot{m}_2 h_2 + \dot{Q}_{C.C} = \dot{m}_3 h_3$
	Turbine	$\dot{m}_3 = \dot{m}_4$	$\dot{m}_3 h_3 = \dot{W}_T + \dot{m}_4 h_4$
	HRSG	$\dot{m}_4 = \dot{m}_5$	$\dot{m}_4 h_4 = \dot{m}_5 h_5 + \dot{Q}_{HRSG}$
Carbon Capturing system	Absorber	$\dot{m}_{fluGas} + \dot{m}_{LA} = \dot{m}_{Gasout} + \dot{m}_{RA}$	$\dot{m}_{fluGas} h_{fluGas} + \dot{m}_{LA} h_{LA} = \dot{m}_{cleanGas} h_{cleanGas} + \dot{m}_{RA} h_{RA}$
	Pump	$\dot{m}_{RA1} = \dot{m}_{RA2}$	$\dot{m}_{RA1} h_{RA1} + \dot{W}_{pump} = \dot{m}_{RA2} h_{RA2}$
	Heat exchanger	$\dot{m}_{LA1} + \dot{m}_{RA1} = \dot{m}_{LA2} + \dot{m}_{RA2}$	$\dot{m}_{LA1} h_{LA1} + \dot{m}_{RA1} h_{RA1} = \dot{m}_{LA2} h_{LA2} + \dot{m}_{RA2} h_{RA2}$
	Regenerator	$\dot{m}_{RA} = \dot{m}_{CO2} + \dot{m}_{LA}$	$\dot{m}_{RA} h_{RA} + \dot{Q}_{Boiler} = \dot{m}_{LA} h_{LA} + \dot{m}_{CO2} h_{CO2}$
Cu-Cl Thermochemical cycle	Heat exchanger B13	$\dot{m}_1 + \dot{m}_9 = \dot{m}_2 + \dot{m}_{10}$	$\dot{m}_1 h_1 + \dot{m}_9 h_9 = \dot{m}_2 h_2 + \dot{m}_{10} h_{10}$
	Hydrolysis B2	$\dot{m}_2 + \dot{m}_{19} = \dot{m}_4 + \dot{m}_5$	$\dot{m}_2 h_2 + \dot{m}_{19} h_{19} + \dot{Q}_{hydrolysis} = \dot{m}_4 h_4 + \dot{m}_5 h_5$
	Thermolysis B4	$\dot{m}_4 + \dot{m}_6 = \dot{m}_8 + \dot{m}_9$	$\dot{m}_4 h_4 + \dot{m}_6 h_6 + \dot{Q}_{Thermolysis} = \dot{m}_8 h_8 + \dot{m}_9 h_9$
	Heat exchanger B14	$\dot{m}_{16} + \dot{m}_{10} = \dot{m}_{11} + \dot{m}_{17}$	$\dot{m}_{16} h_{16} + \dot{m}_{10} h_{10} = \dot{m}_{11} h_{11} + \dot{m}_{17} h_{17}$
	Electrolysis B8	$\dot{m}_{12} + \dot{m}_{13} = \dot{m}_{15} + \dot{m}_{16}$	$\dot{m}_{12} h_{12} + \dot{m}_{13} h_{13} + \dot{Q}_{in,elec} = \dot{m}_{15} h_{15} + \dot{m}_{16} h_{16}$
	Dryer	$\dot{m}_{12} + \dot{m}_{13} = \dot{m}_{15} + \dot{m}_{16}$	$\dot{m}_{12} h_{12} + \dot{m}_{13} h_{13} = \dot{m}_{15} h_{15} + \dot{m}_{16} h_{16}$
Methanol synthesis system	H_2 compressor1	$\dot{m}_1 = \dot{m}_2$	$\dot{m}_1 h_1 + \dot{W}_{comp1,H2} = \dot{m}_2 h_2$
	H_2 compressor 2	$\dot{m}_3 = \dot{m}_4$	$\dot{m}_3 h_3 + \dot{W}_{comp2,H2} = \dot{m}_4 h_4$
	CO_2 compressor1	$\dot{m}_5 = \dot{m}_6$	$\dot{m}_5 h_5 + \dot{W}_{comp1,CO2} = \dot{m}_6 h_6$
	CO_2 compressor2	$\dot{m}_7 = \dot{m}_8$	$\dot{m}_7 h_7 + \dot{W}_{comp2,CO2} = \dot{m}_8 h_8$
	H_2 intercooler	$\dot{m}_2 = \dot{m}_3$	$\dot{m}_2 h_2 = \dot{m}_3 h_3 + \dot{Q}_{IC,H2}$
	CO_2 intercooler	$\dot{m}_6 = \dot{m}_7$	$\dot{m}_6 h_6 = \dot{m}_7 h_7 + \dot{Q}_{IC,CO2}$
	MeOH reactor 1	$\dot{m}_{CO2} + \dot{m}_{H2} + \dot{m}_{Rec} = \dot{m}_{MeOH,1} + \dot{m}_{Unrec}$	$\dot{m}_{CO2} h_{CO2} + \dot{m}_{H2} h_{H2} + \dot{m}_{Rec} h_{Rec} = \dot{m}_{MeOH,1} h_{MeOH,1} + \dot{m}_{Unrec} h_{Unrec} + Q_{out}$

	MeOH reactor 2	$\dot{m}_{Unrec} = \dot{m}_{MeOH,2} + \dot{m}_{Rec2}$	$\dot{m}_{Unrec}h_{Unrec} + Q_{in} = \dot{m}_{MeOH,2}h_{MeOH,2} + \dot{m}_{Rec2}h_{Rec2}$
	MeOH distillation column	$\dot{m}_{MeOH,1} + \dot{m}_{MeOH,2} = \dot{m}_{MeOH,Pure} + \dot{m}_{H2O}$	$\dot{m}_{MeOH,1}h_{MeOH,1} + \dot{m}_{MeOH,2}h_{MeOH,2} + \dot{Q}_{reb,DC1} = \dot{m}_{MeOH,pure}h_{MeOH,pure} + \dot{m}_{H2O}h_{H2O} + \dot{Q}_{cond,DC1}$
DME synthesis system	DME reactor	$\dot{m}_{MeOH,Pure} = \dot{m}_{DME,mixture}$	$\dot{m}_{MeOH,Pure}h_{MeOH,Pure} = \dot{m}_{DME,mix}h_{DME,mix}$
	Heat exchanger	$\dot{m}_{23} + \dot{m}_{26} = \dot{m}_{27} + \dot{m}_{24}$	$\dot{m}_{23}h_{23} + \dot{m}_{26}h_{26} = \dot{m}_{27}h_{27} + \dot{m}_{24}h_{24}$
	DME distillation column	$\dot{m}_{DME,mix} = \dot{m}_{MeOH,mix} + \dot{m}_{DME,Pure}$	$\dot{m}_{DME,mix}h_{DME,mix} + \dot{Q}_{reb,DC2} = \dot{m}_{MeOH,mix}h_{MeOH,mix} + \dot{m}_{DME,Pure}h_{DME,Pure} + \dot{Q}_{cond,DC2}$
	Unreacted MeOH	$\dot{m}_{MeOH,mix} = \dot{m}_{MeOH,Rec} + \dot{m}_{H2O}$	$\dot{m}_{MeOH,mix}h_{MeOH,mix} + \dot{Q}_{reb,DC3} = \dot{m}_{MeOH,Rec}h_{MeOH,Rec} + \dot{m}_{H2O}h_{H2O} + \dot{Q}_{cond,DC3}$
MED	Overall system	$\dot{m}_f = \dot{m}_d + \dot{m}_b$	$\dot{m}_f h_f + \dot{Q}_s = \dot{m}_d h_d + \dot{m}_b h_b$

Table 4.6 Exergy balance and exergy efficiency equations for system 3

Sub-system	Component	Exergy balance equation	Energy efficiency equation
Solar heliostat field	Compressor	$\dot{m}_1 ex_1 + \dot{W}_{C1} = \dot{m}_2 ex_2 + \dot{E}x_{d,C1}$	$\eta_{ex,c1} = \frac{\dot{E}x_2 - \dot{E}x_1}{\dot{W}_{c1}}$
	Combustion chamber	$\dot{m}_2 ex_2 + \dot{Q}_f\left(1 - \frac{T_0}{T_{cc}}\right) = \dot{m}_3 ex_3 + \dot{E}x_{d,CC}$	$\eta_{ex,cc1} = \frac{\dot{E}x_8 - \dot{E}x_7}{\dot{Q}_{f,1}(1 - \frac{T_o}{T_{cc1}})}$
	Turbine	$\dot{m}_3 ex_3 = \dot{m}_4 ex_4 + \dot{W}_{GT} + \dot{E}x_{dest,GT}$	$\eta_{ex,T1} = \frac{\dot{W}_{T1}}{\dot{E}x_8 - \dot{E}x_9}$
	HRSG	$\dot{m}_4 ex_4 + \dot{m}_{cold\ water} ex_{cold\ water} = m_5 ex_5 + \dot{m}_{hot\ water} ex_{hot\ water} + \dot{E}x_{dest,HRSG}$	$\eta_{ex,CAES} = 1 - \frac{Ex_{d,CAES}}{Ex_{in}}$
Carbon Capturing system	Absorber	$\dot{m}_{fluGas} ex_{fluGas} + \dot{m}_{LA} ex_{LA} = \dot{m}_{cleanGas} ex_{cleanGas} + \dot{m}_{RA} ex_{RA} + \dot{E}x_{dest_{abs}}$	$\eta_{abs,ex} = \frac{\dot{m}_{cleanGas} ex_{cleanGas} + \dot{m}_{RA} ex_{RA}}{\dot{m}_{fluGas} ex_{fluGas} + \dot{m}_{lean} ex_{LA}}$
	Pump	$\dot{m}_{RA1} ex_{RA1} + \dot{W}_{pump} = \dot{m}_{RA2} ex_{RA2} + \dot{E}x_{dest_{Pump}}$	$\eta_{pump,ex} = \frac{\dot{m}_{RA2} ex_{RA2} - \dot{m}_{RA1} ex_{RA1}}{\dot{W}_{pump}}$
	Heat exchanger	$\dot{m}_{LA1} ex_{LA1} + \dot{m}_{RA1} ex_{RA1} = \dot{m}_{LA2} ex_{LA2} + \dot{m}_{RA2} ex_{RA2} + \dot{E}x_{dest_{HX}}$	$\eta_{HX,ex} = \frac{\dot{m}_{LA2} ex_{LA2} + \dot{m}_{RA2} ex_{RA2}}{\dot{m}_{LA1} ex_{LA1} + \dot{m}_{RA1} ex_{RA1}}$

	Regenerator	$\dot{m}_{RA}ex_{RA} + \dot{Q}_{Boiler}\left(1-\frac{T_0}{T}\right) = \dot{m}_{LA}ex_{LA} + \dot{m}_{CO2}ex_{CO2} + \dot{E}x_{dest_{REGEN}}$	$\eta_{HX,ex} = 1 - \frac{\dot{E}x_{dest_{REGEN}}}{\dot{Q}_{Boiler}\left(1-\frac{T_0}{T}\right)}$
Cu-Cl Thermochemical cycle	Heat exchanger B13	$\dot{m}_1ex_1 + \dot{m}_9ex_9 = \dot{m}_2ex_2 + \dot{m}_{10}ex_{10} + \dot{E}x_{dest_{B13}}$	$\eta_{B13,ex} = \frac{\dot{m}_2ex_2 + \dot{m}_{10}ex_{10}}{\dot{m}_1ex_1 + \dot{m}_9ex_9}$
	Hydrolysis B2	$\dot{m}_2ex_2 + \dot{m}_{19}ex_{19} + \dot{Q}_{hydrolysis} = \dot{m}_4ex_4 + \dot{m}_5ex_5 + \dot{E}x_{dest_{SG2}}$	$\eta_{B2,ex} = \frac{\dot{m}_4ex_4 + \dot{m}_5ex_5}{\dot{Q}_{hydrolysis}\left(1-\frac{T_0}{T}\right)}$
	Thermolysis B4	$\dot{m}_4ex_4 + \dot{m}_6ex_6 + \dot{Q}_{thermolysis}\left(1-\frac{T_0}{T}\right) = \dot{m}_7ex_7 + \dot{E}x_{dest_{thermolysis}}$	$\eta_{B4,ex} = 1 - \frac{\dot{E}x_{dest_{thermolysis}}}{\dot{Q}_{thermolysis}\left(1-\frac{T_0}{T}\right)}$
	Heat exchanger B14	$\dot{m}_{16}ex_{16} + \dot{m}_{10}ex_{10} = \dot{m}_{11}ex_{11} + \dot{m}_{17}ex_{17} + \dot{E}x_{dest_{B14}}$	$\eta_{B13,ex} = \frac{\dot{m}_{16}ex_{16} + \dot{m}_{10}ex_{10}}{\dot{m}_{11}ex_{11} + \dot{m}_{17}ex_{17}}$
	Electrolysis B8	$\dot{m}_{12}ex_{12} + \dot{m}_{13}ex_{13} + \dot{W}_{in,elec} = \dot{m}_{15}ex_{15} + \dot{m}_{16}ex_{16} + \dot{E}x_{dest_{electrolysis}}$	$\eta_{B8,ex} = 1 - \frac{\dot{E}x_{dest_{electrolysis}}}{\dot{Q}_{electrolysis}\left(1-\frac{T_0}{T}\right)}$
	Dryer	$\dot{m}_{12}ex_{12} + \dot{m}_{13}ex_{13} = \dot{m}_{15}ex_{15} + \dot{m}_{16}ex_{16} + \dot{E}x_{dest_{dryer}}$	$\eta_{Dryer,ex} = \frac{\dot{m}_{16}ex_{16} + \dot{m}_{15}ex_{15}}{\dot{m}_{12}ex_{12} + \dot{m}_{13}ex_{13}}$
Methanol synthesis system	H_2 compressor1	$\dot{m}_1ex_1 + \dot{W}_{comp1,H2} = \dot{m}_2ex_2 + \dot{E}x_{dest_{comp1,H2}}$	$\eta_{comp1,H2,ex} = \frac{\dot{m}_2ex_2 - \dot{m}_1ex_1}{\dot{W}_{comp1,H2}}$
	H_2 compressor 2	$\dot{m}_3ex_3 + \dot{W}_{comp2,H2} = \dot{m}_4ex_4 + \dot{E}x_{dest_{comp2,H2}}$	$\eta_{comp2,H2,ex} = \frac{\dot{m}_4ex_4 - \dot{m}_3ex_3}{\dot{W}_{comp2,H2}}$
	CO_2 compressor1	$\dot{m}_5ex_5 + \dot{W}_{comp1,CO2} = \dot{m}_6ex_6 + \dot{E}x_{dest_{comp1,CO2}}$	$\eta_{comp1,CO2,ex} = \frac{\dot{m}_6ex_6 - \dot{m}_5ex_5}{\dot{W}_{comp1,CO2}}$
	CO_2 compressor2	$\dot{m}_7ex_7 + \dot{W}_{comp2,CO2} = \dot{m}_8ex_8 + \dot{E}x_{dest_{comp2,CO2}}$	$\eta_{comp2,CO2,ex} = \frac{\dot{m}_8ex_8 - \dot{m}_7ex_7}{\dot{W}_{comp2,CO2}}$
	H_2 intercooler	$\dot{m}_2ex_2 = \dot{m}_3ex_3 + \dot{E}x_{dest_{IC,H2}}$	$\eta_{IC,H2,ex} = 1 - \frac{\dot{E}x_{dest_{IC,H2}}}{\dot{m}_2ex_2}$
	CO_2 intercooler	$\dot{m}_6ex_6 = \dot{m}_7ex_7 + \dot{E}x_{dest_{IC,CO2}}$	$\eta_{IC,CO2,ex} = 1 - \frac{\dot{E}x_{dest_{IC,CO2}}}{\dot{m}_6ex_6}$
	MeOH reactor 1	$\dot{m}_{CO2}ex_{CO2} + \dot{m}_{H2}ex_{H2} + \dot{m}_{Rec}ex_{Rec} = \dot{m}_{MeOH,1}ex_{MeOH,1} + \dot{m}_{Unrec}ex_{Unrec} + \dot{E}x_{dest,reactor1}$	$\eta_{reactor1,ex} = 1 - \frac{\dot{E}x_{dest_{reactor1}}}{\dot{m}_{CO2}ex_{CO2} + \dot{m}_{H2}ex_{H2} + \dot{m}_{Rece}ex_{Rec}}$
	MeOH reactor 2	$\dot{m}_{Unrec}ex_{Unrec} + Q_{in}\left(1-\frac{T_0}{T}\right) = \dot{m}_{MeOH,2}ex_{MeOH,2} + \dot{m}_{Rec}ex_{Rec} + \dot{E}x_{dest,Reactor2}$	$\eta_{Reactor2,ex} = 1 - \frac{\dot{E}x_{dest_{reactor2}}}{\dot{m}_{Unrec}ex_{Unrec} + Q_{in}\left(1-\frac{T_0}{T}\right)}$

	MeOH distillation column	$\dot{m}_{MeOH} ex_{MeOH} + \dot{Q}_{reb}\left(1-\frac{T_0}{T}\right) = \dot{m}_{MeOH,pure} ex_{MeOH,pure} + \dot{m}_{H2O} ex_{H2O} + \dot{E}x_{dest,DC1}$	$\eta_{DC1,ex} = 1 - \frac{\dot{E}x_{dest_{DC1}}}{\dot{Q}_{reb}\left(1-\frac{T_0}{T}\right)}$
DME synthesis system	DME reactor	$\dot{m}_{MeOH,Pure} ex_{MeOH,Pure} = \dot{m}_{DME,mixture} ex_{DME,mixture} + \dot{E}x_{dest,DME\ R}$	$\eta_{DME\ R,ex} = 1 - \frac{\dot{E}x_{dest_{DME\ R}}}{\dot{m}_{MeOH,Pure} ex_{MeOH,Pure}}$
	Heat exchanger	$\dot{m}_{23} ex_{23} + \dot{m}_{26} ex_{26} = \dot{m}_{27} ex_{27} + \dot{m}_{24} ex_{24} + \dot{E}x_{dest,HX}$	$\eta_{HX2,ex} = \frac{\dot{m}_{24} ex_{24} + \dot{m}_{27} ex_{27}}{\dot{m}_{23} ex_{23} + \dot{m}_{26} ex_{26}}$
	DME distillation column	$\dot{m}_{DME,mixture} ex_{DME,mixture} + \dot{Q}_{reb}\left(1-\frac{T_0}{T}\right) = \dot{m}_{MeOH,mix} ex_{MeOH,mix} + \dot{m}_{DME,Pure} ex_{DME,Pure} + \dot{Q}_{cond}\left(1-\frac{T_0}{T}\right) + \dot{E}x_{dest,DC2}$	$\eta_{DC2,ex} = 1 - \frac{\dot{E}x_{dest_{DC2}}}{\dot{Q}_{reb}\left(1-\frac{T_0}{T}\right)}$
	Unreacted MeOH distillation column	$\dot{m}_{MeOH,mix} ex_{MeOH,mix} + \dot{Q}_{reb}\left(1-\frac{T_0}{T}\right) = \dot{m}_{MeOH,Rec} ex_{MeOH,Rec} + \dot{m}_{H2O} ex_{H2O} + \dot{Q}_{cond}\left(1-\frac{T_0}{T}\right) + \dot{E}x_{dest,DC3}$	$\eta_{DC3,ex} = 1 - \frac{\dot{E}x_{dest_{DC3}}}{\dot{Q}_{reb}\left(1-\frac{T_0}{T}\right)}$
MED	Overall system	$\dot{m}_f ex_f + \dot{Q}_s\left(1-\frac{T_0}{T}\right) = \dot{m}_d ex_d + \dot{E}x_{dest,MED}$	$\eta_{MED,ex} = 1 - \frac{\dot{E}x_{dest_{MED}}}{\dot{Q}_s\left(1-\frac{T_0}{T}\right)}$

Chapter 5 : Results and Discussion

In this chapter, the main results of thermodynamic analyses and simulations are presented. Each section discusses the results of one of the three proposed DME production system. The results exhibit the energy requirement and performance of each subsystem as well as for the overall systems.

5.1 Results for System 1

The proposed photovoltaic based DME production system is studied including energy and exergy performance. Results of thermodynamic analyses and process simulations for the first system are presented in this section. All chemical processes such as methanol and DME synthesis and carbon capturing process are analyzed using Aspen plus process simulation software. However, chemical exergy, exergy destructions, and exergy efficiencies analyses have been performed using programmed Excel sheet. While hydrogen production electrochemical process has been analyzed using Engineering Equation Solver (EES).

The overall performance results of DME production plant are discussed in this section. The study considers energy efficiency, exergy efficiency, and exergy destruction rate. Moreover, the study evaluates the operational energy requirements either in the form of work or heat. The major overall results of system 1 are listed in Table 5.1.

Table 5.1 Overall system 1 results summary

DME production plant parameters	Value
Energy efficiency	40.46 %
Exergy efficiency	52.81 %
DME production rate	1879.15 kg/day
Heat requirement for the production of 1 mol/s of DME	804.95 kW
Electric work rate requirement for production of 3 mol/s of hydrogen	1074.1 kW
Boiler heat duty for carbon capturing of 1 mol/s of carbon dioxide	312.09 kW
The pressure of the produced DME	940 kPa
The temperature of the produced DME	42 ^{o}C
Exergy destruction rate	675.63 kW

A production rate of 0.0217 kg/s for a plant that is running 24 hours a day would result in a production capacity of 1879.15 kg/day. This plant would require a waste heat recovery of 379.94 kW, electric work of 1146.45 kW and feed water at a rate of 0.054 kg/s. The overall energy efficiency of the first proposed DME production system is 40.46 %. While the overall exergy efficiency of the DME production system is 52.81 %.

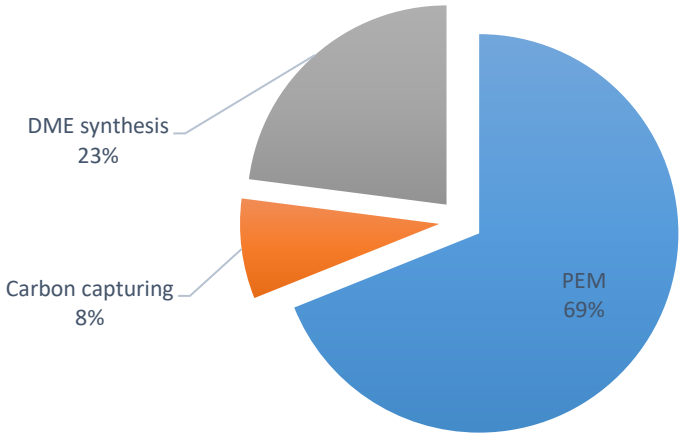

Figure 5.1 Distribution of exergy destruction over the three subsystems

Figure 5.1 shows the exergy destruction contribution of each subsystem. The figure indicates that most of the exergy destruction is occurring in the PEM electrolyzer due to the overpotential and thermal losses. However, minimum exergy destruction is taking place at the carbon capturing system.

The performance of PEM hydrogen production subsystem is discussed here, the system is composed of two heat exchangers for heat recovery, electric heater, and PEM electrolyzer. The heat duty, work consumption, exergy destruction, and exergy efficiency are demonstrated in Figure 5.2.

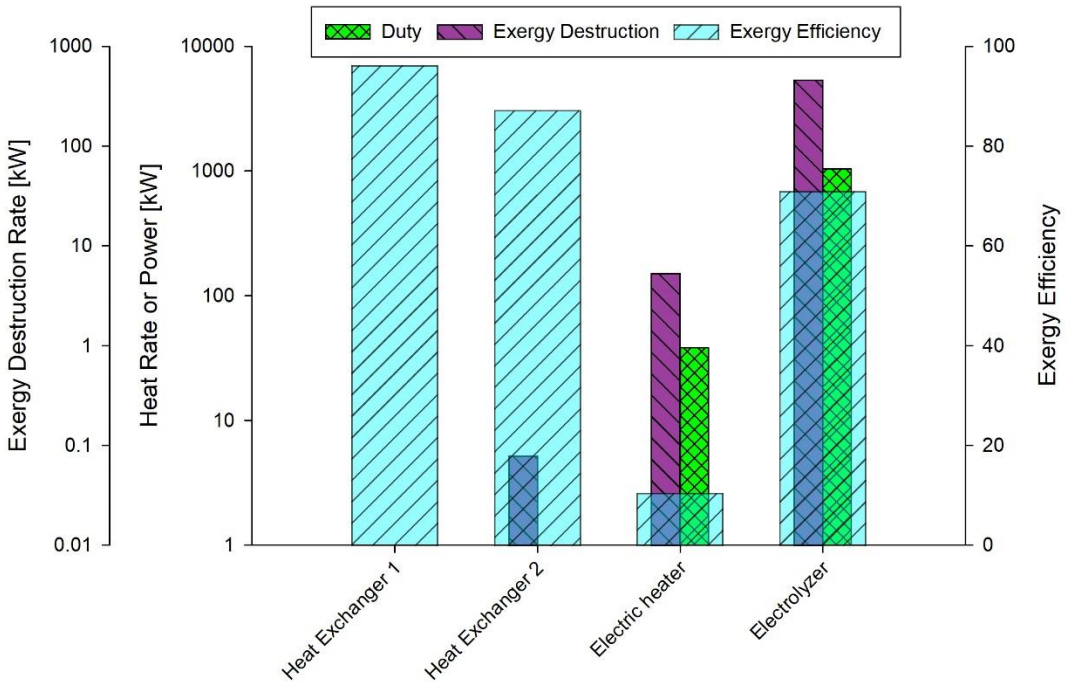

Figure 5.2 Heat duty, work consumption, exergy destruction, and exergy efficiency for PEM electrolyzer subsystem

The maximum exergy destruction rate is occurring at the electrolyzer due to the chemical irreversibility and over potential losses such as Ohmic, activation, and concentration losses which is rejected to the surrounding in the form of heat. The energy efficiency of the PEM hydrogen production subsystem is 69.5 %. While the exergy efficiency of the PEM hydrogen production subsystem is 70.5 %. Different parametric studies have been conducted to study the effect of operating parameters on the performance of the hydrogen production system. Electrolyzer working temperature has a significant effect on the electrolyzer performance. Figure 5.3 show the effect of electrolyzer working temperature on the cell potential. As the working temperature of the electrolyzer increases the cell potential decreases due to the decrease in the overpotential losses. As a result, exergy destruction rate for electrolyzer decreases as accordingly and energy and exergy efficiencies increase as demonstrated in Figure 5.4.

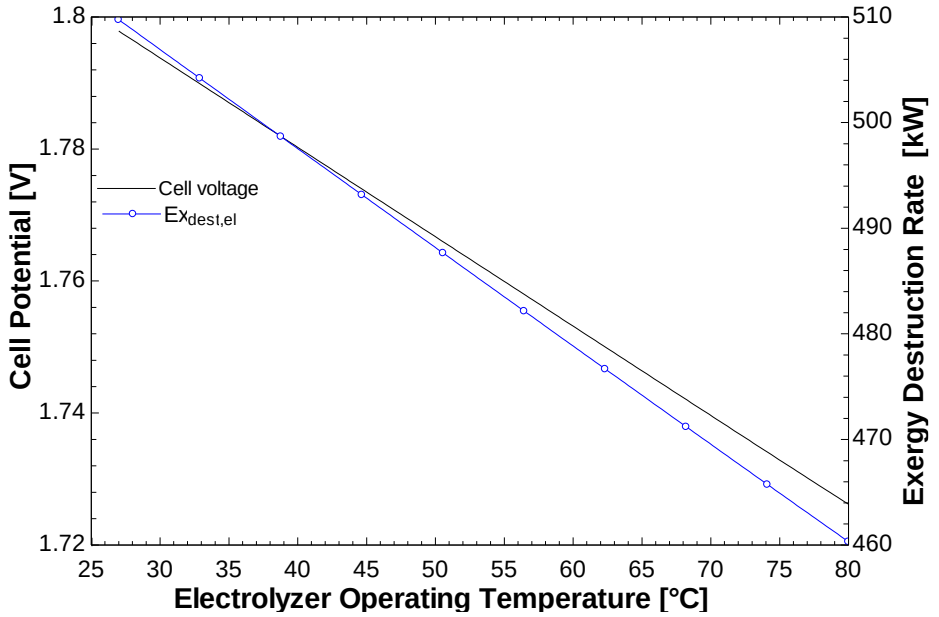

Figure 5.3 Effect of electrolyzer working temperature on the cell potential and exergy destruction

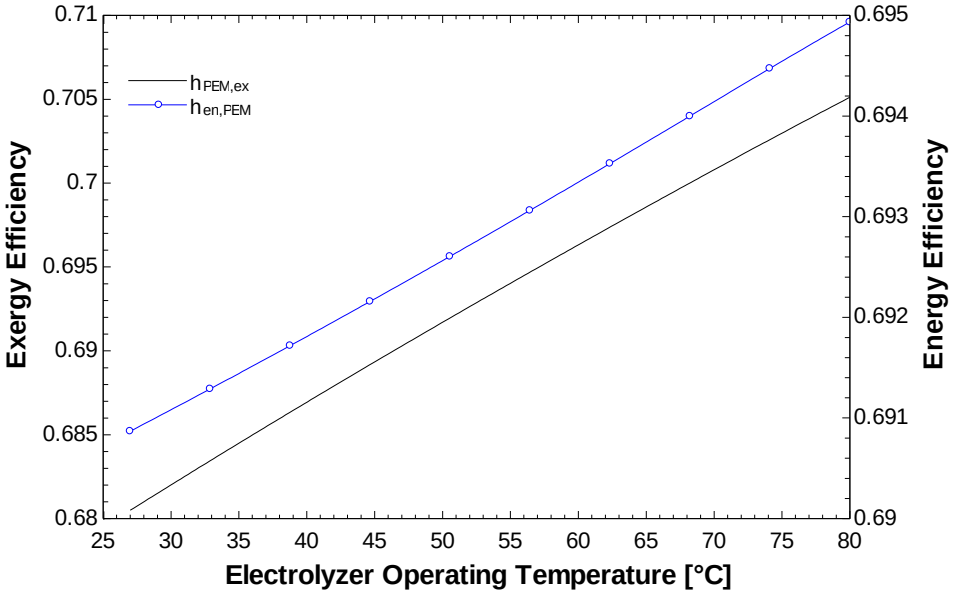

Figure 5.4 Effect of electrolyzer working temperature on energy and exergy efficiencies

Also, current density has a significant effect on the performance of the hydrogen production system. Figure 5.5 shows the effect of increasing current density on the cell potential at different working temperatures. As the applied current density increases, cell potential increases accordingly due to the increase in the different overpotentials as shown in Figure 5.6. The working temperature has an obvious influence on the cell potential increase with increasing current density. The lower the working temperature the higher cell

potential increase is achieved. Consequently, the applied current density has a significant impact on the energy and exergy efficiency of the hydrogen production system. Figure 5.7 shows the effect of increasing the applied current density on the energy and exergy efficiency of the hydrogen production system as well as the effect on the exergy destruction rate of the electrolyzer.

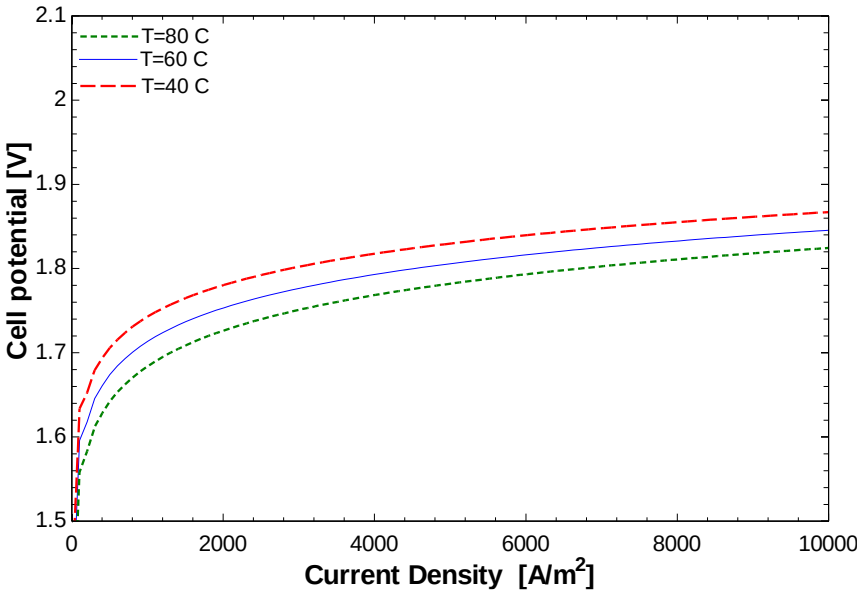

Figure 5.5 Effect of increasing current density on the cell potential at different working temperatures

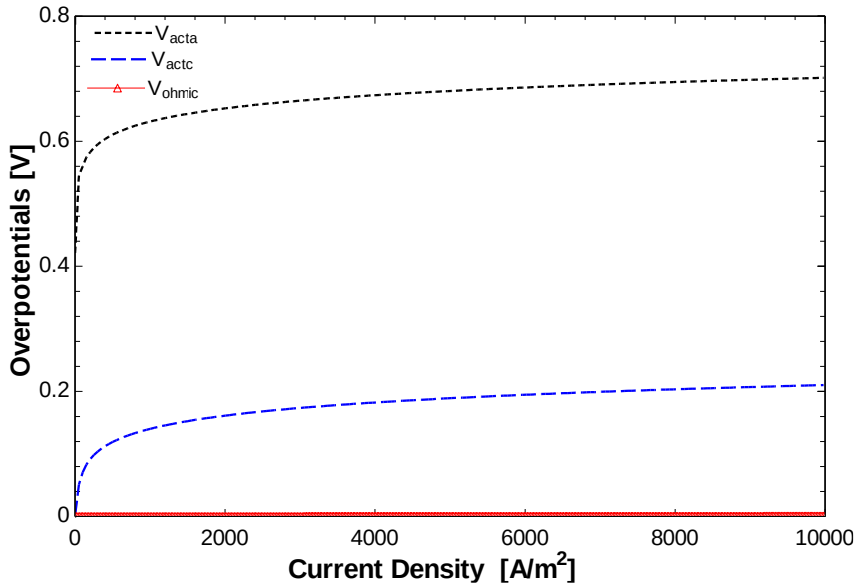

Figure 5.6 Effect of increasing current density on the overpotentials at different working temperatures

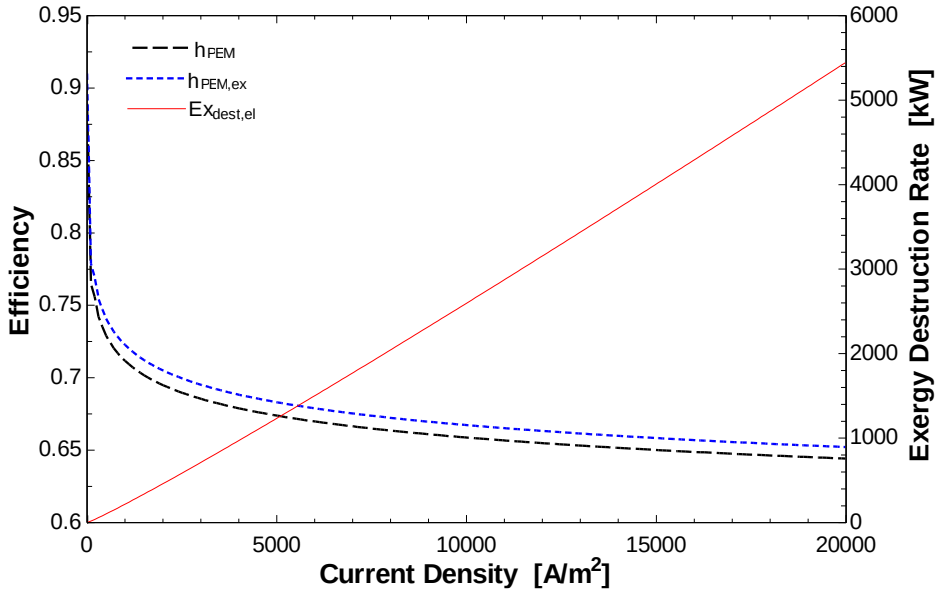

Figure 5.7 Effect of increasing the applied current density on the energy and exergy efficiency and exergy destruction in the electrolyzer

Figure 5.8 shows the consumption of electrical work and thermal heat along with the produced hydrogen energy. As can be concluded from the figure, the energy consumption becomes relatively higher than produced hydrogen energy as the applied current density increases.

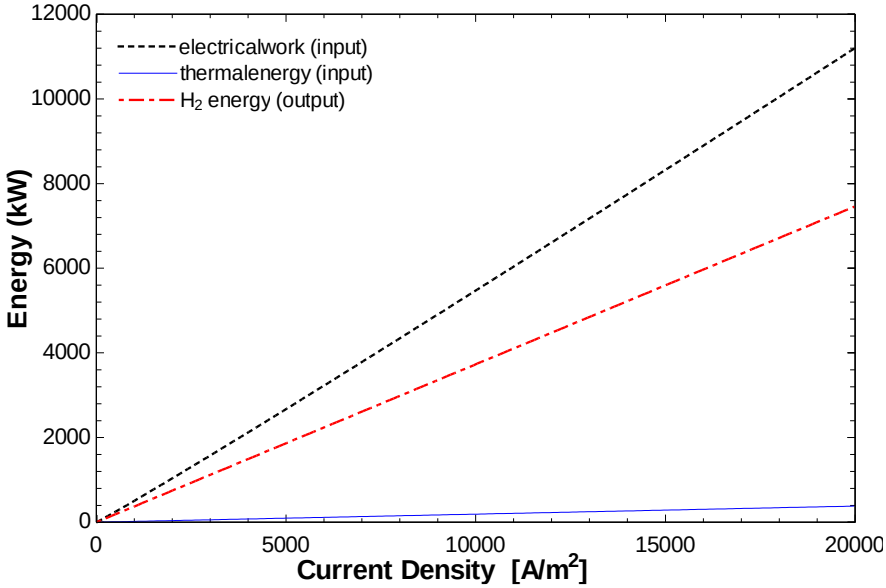

Figure 5.8 Consumption of electrical work and thermal energy along with the produced hydrogen energy

The analyses results and parametric study display good matching with the study presented by Ni et al. [11] except that the efficiency is slightly higher than Ni work due to the enhanced heat recovery from the electrolyzer products.

For carbon capturing subsystem, the system is composed of an absorber, pump, heat exchanger, and regenerator or regenerator. The operating conditions and flue gas composition are tabulated in Table 5.2. The heat duty, exergy destruction, and exergy efficiency are listed in Figure 5.9.

Table 5.2 Cement furnace flue gas conditions

Parameter		Value
Temperature		371°C [21]
Pressure		120 kPa
Total flow		5.07 kg/s
Mole Fraction	H_2O	16 %
	CO_2	18.41 %
	N_2	75.28 %
	O_2	4.7 %

Source: [54]

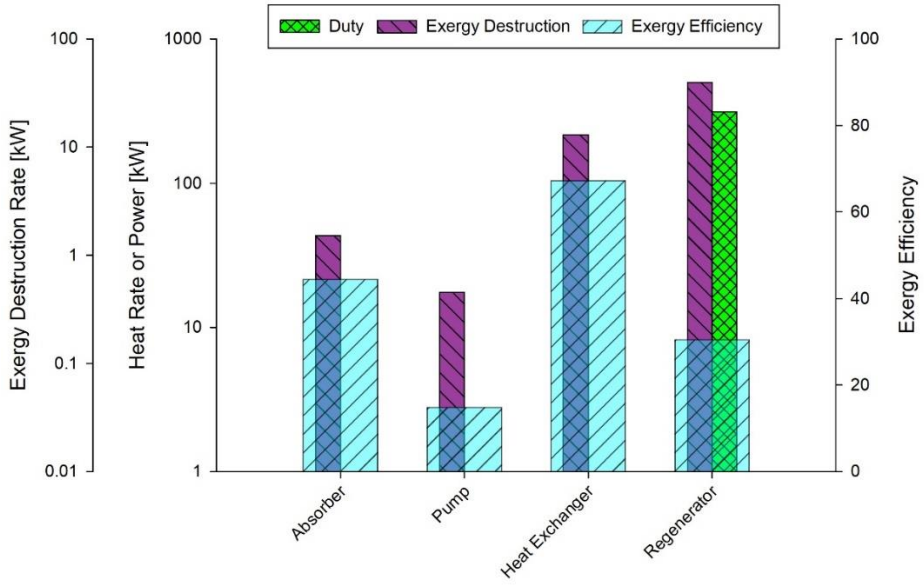

Figure 5.9 Heat duty, exergy destruction, and exergy efficiency for carbon capturing subsystem 1.

The maximum exergy destruction rate is taking place in the regenerator due to chemical irreversibility and the waste heat rejected to the surrounding through the condenser. The maximum exergy efficiency is at the heat exchanger which is 68.3 %, since there are not much exergy losses in this component. The heat recovery system is providing heat to the different components in a specific order to maintain the proper temperature required in each component.

MeOH and DME synthesis subsystems are discussed here. The system is composed of two compressors for hydrogen feed stream with intercooler between them, another two compressors four carbon dioxide feed stream with intercooler between them. Two methanol reactors with a conversion rate of 47% [55], Cooler and flash chamber after each reactor, methanol-water distillation column, heat exchanger, DME reactor with a conversion rate of 80% [41], pre distillation cooler, DME-water distillation column and unreacted methanol-water distillation column. A summary of heat duties, heat produced, work consumption are presented in Figure 5.10.

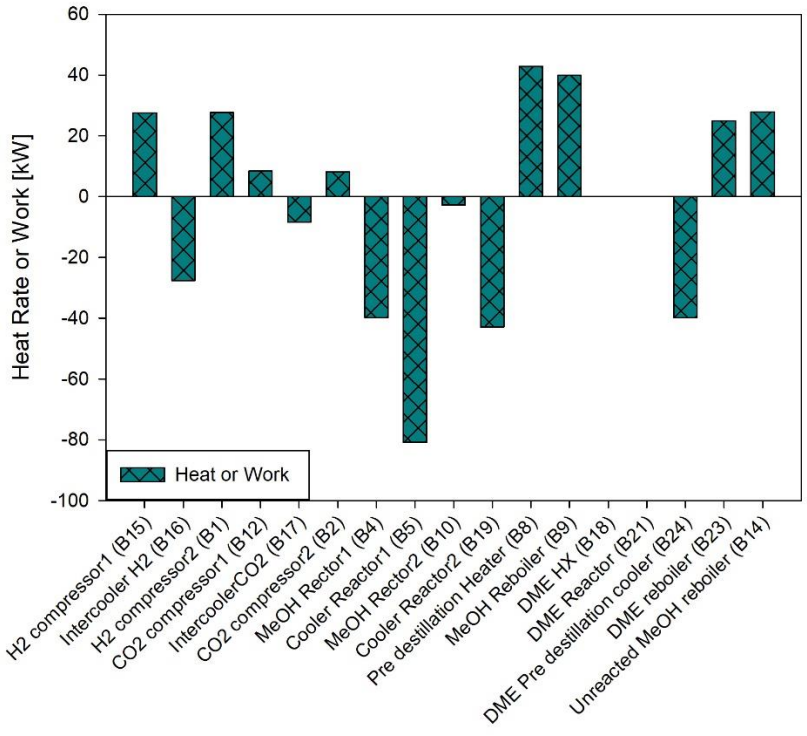

Figure 5.10 Heat and power consumption or production for DME synthesis.

A summary of exergy analysis has been demonstrated in Figure 5.11 showing exergy transfer from or to the system, exergy destruction and exergy efficiency for each component of the DME synthesis system.

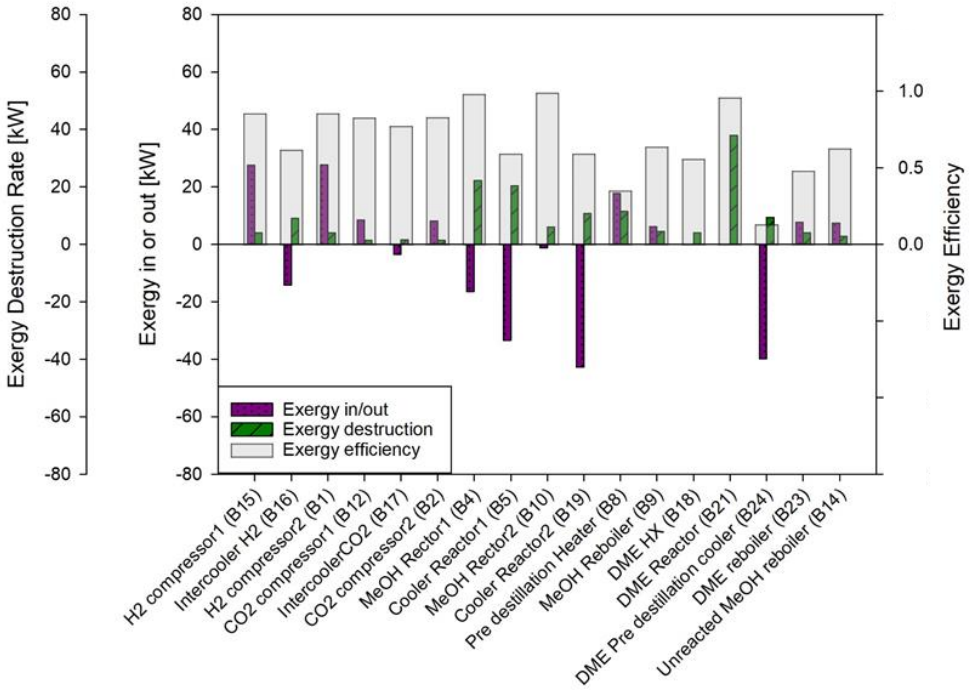

Figure 5.11 Exergy destruction rates, and exergy efficiencies for DME synthesis subsystem

Exergy destruction rate appears to be maximum at the reactors as expected due to the chemical irreversibility. However, the maximum exergy efficiency is still taking place at the reactors due to the fact that total exergy of the output products is very close to the total exergy of the input reactants. Compressors have relatively high exergy efficiency since they are assumed to be working adiabatically. The energy efficiency of DME synthesis from hydrogen and carbon dioxide is 71.39 % which is very close to the values obtained by Clausen et Al. [56] and Reed [57]. While the exergy efficiency of DME synthesis was calculated to be 80.7 %.

Design and sizing of distillation columns have been selected based on McCabe and Thiele graphical method explained in Perry`s Handbook [58] and shown in Figure 5.12 and Figure 5.13. The summary of distillation column design results is demonstrated in Table 5.3.

Table 5.3 Distillation column design parameters

Parameter	CH_3OH-H_2O DC#1	DME-CH_3OH-H_2O DC#2 [41]	CH_3OH-H_2O DC#3
Number of stages	17	36	20
Feed stage	6	24	8
Reflux ratio	1.04	1.6	2.78
Distillate to feed	0.5	0.385	0.3

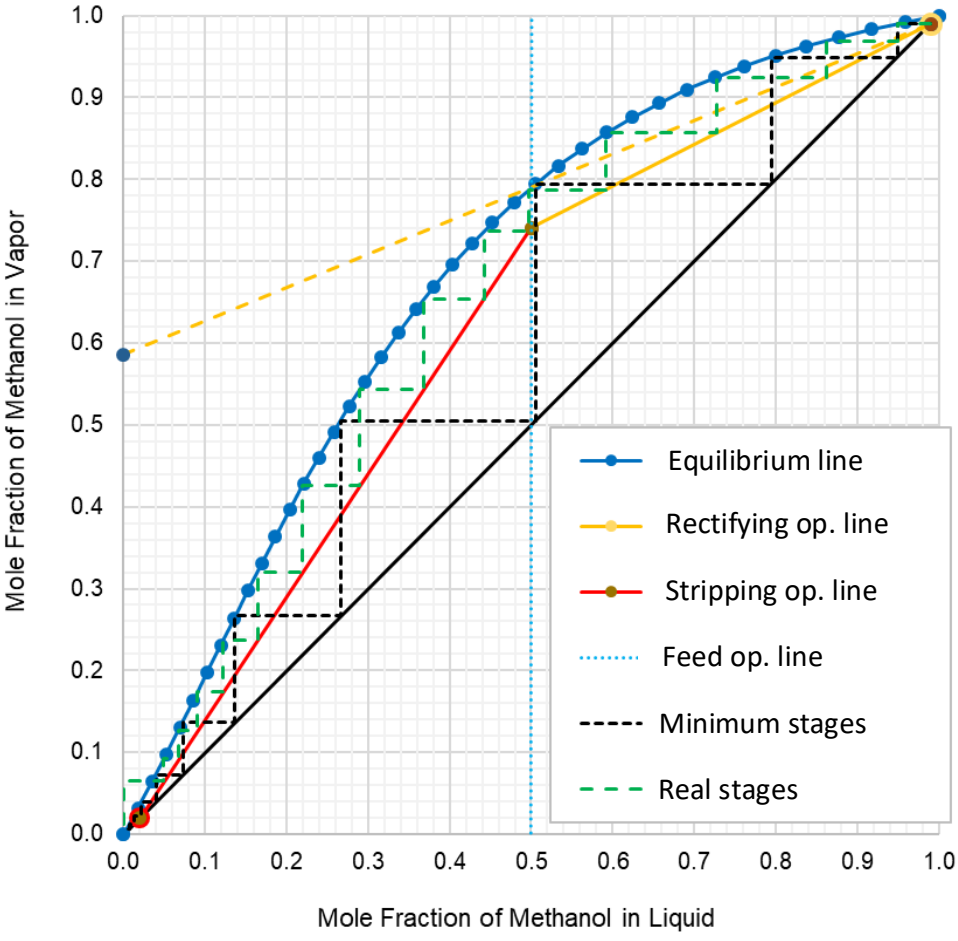

Figure 5.12 Distillation column 1 design using the graphical method.

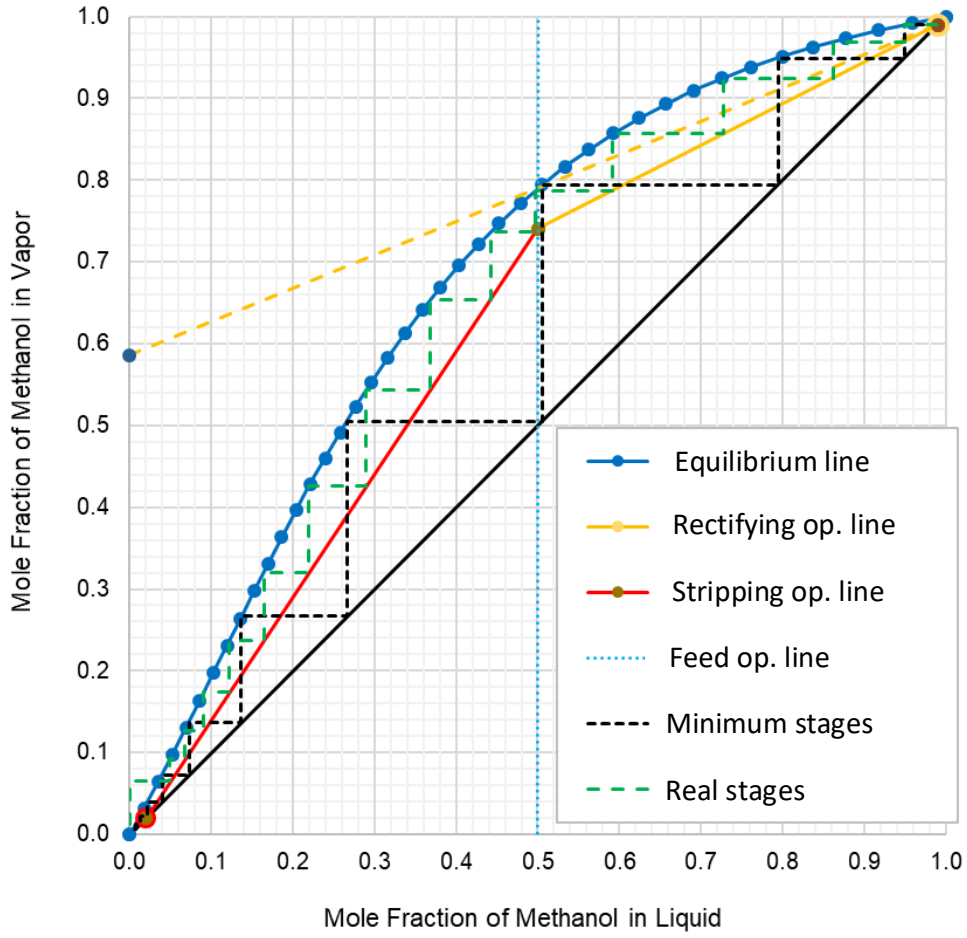

Figure 5.13 Distillation column 2 design using the graphical method.

5.2 Results for System 2

The second system which is solar thermal based DME production system has been studied thermodynamically through energy and exergy analyses. Results of the overall performance such exergy destruction rate, DME production rates, energy outputs, overall energy and exergy efficiencies are presented in this section. Moreover, the overall system energy requirements are discussed in this section. All the chemical processes such as methanol synthesis and DME production, and carbon capturing process are simulated through Aspen plus process simulation software. Though, stream results have been exported to a programmed excel sheet to include chemical exergy analyses and calculation of exergy destruction rates and exergy efficiencies of each component. However, the solid oxide steam electrolyzer hydrogen production subsystem and solar heliostat field

subsystem is modeled using EES. The main overall results of the system are tabulated in Table 5.4.

Table 5.4 Overall results summary of system 2

DME production plant parameters	Value
Energy efficiency	28.75 %
Exergy efficiency	32.54 %
DME production rate	3758.3 kg/day
Heat requirement for the production of 1 mol/s of DME	901.65 kW
Electric work rate requirement for production of 6 mol/s of hydrogen	1409.28 kW
Boiler heat duty for carbon capturing of 2 mol/s of carbon dioxide	479.3 kW
Amount of work produced by the steam turbine	1688.2 kW
The pressure of the produced DME	940 kPa
The temperature of the produced DME	40 ^{o}C
Exergy destruction rate	7651.90 kW

The system is capable of producing 3758.29 kg/day if the plant is operating 24 hours a day at a rate of 0.0435 kg/s. The plant is also able to extract a net energy of 3.221 MWh per day from the steam turbine. The system requires 615 kW of waste heat to be recovered from the waste flue gas, a total electric work of 1553.98 kW and feed water at a rate of 0.108 kg/s. The overall energy efficiency of the second DME production system is 28.75 %. While the overall exergy efficiency of the second DME production system is 32.54 %.

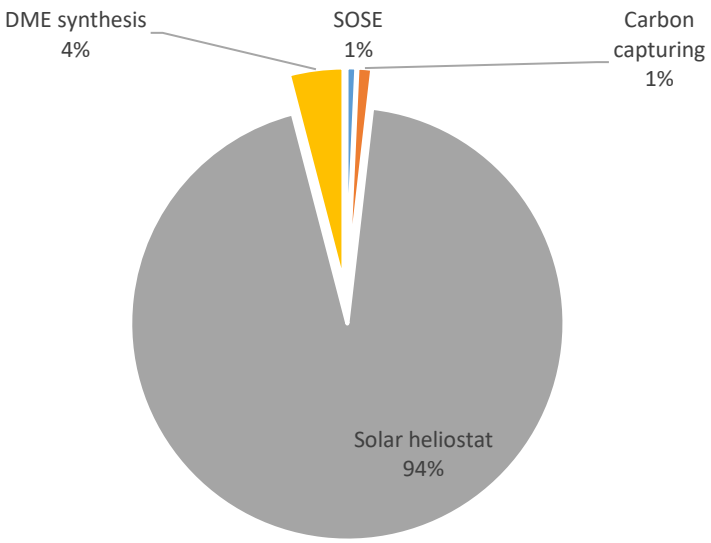

Figure 5.14 Distribution of exergy destruction over the four subsystem

Table 5.5 Solar heliostat working parameters

Parameters	Value
Solar radiation	0.8 kW/m^2
Field efficiency [52]	75 %
Receiver efficiency [52]	90 %
Area of heliostat	10,000 m^2
Receiver area	21.2 m^2
Pump efficiency	90 %
Heat Exchanger effectiveness	95 %
Turbine isentropic efficiency	80 %
Heat supplied to SOSE	120 kW
Source temperature	4,500 K
Steam mass flow rate	1 kg/s
Thermal fluid mass flow rate	7.14 kg/s
Turbine inlet pressure	12,600 kPa

The distribution of exergy destruction among the different subsystems of system 2 is demonstrated in Figure 5.14. Most of the exergy destruction is taking place in solar heliostat subsystem due to the huge amount of heat losses at very high temperature.

The results of solar heliostat energy subsystem are discussed here. The system is composed of heliostat field mirrors, thermal energy storage, heat exchanger (boiler), turbine and condenser. Thermal energy storage is incorporated in the system for the necessity to operate 24 hrs/day. However, thermal storage analysis can be found in Al-Sulaiman [59]. The input working parameters and assumptions are listed in Table 5.5

Energy and exergy analyses have been performed to investigate the energy and exergy losses through the different components by evaluating the energy and exergy efficiency and calculating exergy destruction rates. The results of energy and exergy analyses for solar heliostat field system are shown in Table 5.6.

Table 5.6 Summary of energy and exergy analyses for solar heliostat subsystem

Component		Received (kW)	Delivered (kW)	Energy efficiency	Source temperature (K)	Exergy in or out (kW)	Exergy destruction (kW)	Exergy efficiency
Heliostat field		8000	6000	0.750	4500	7470.222	1868	0.7499
Central receiver		6000	5400	0.900	833	3853.541	2531	0.5482
Boiler heat		5400	4056	0.751	807	2558.245	1608	0.6223
Power cycle	HP turbine	3232	1405	0.522	-	1405	257.4	0.8452
	LP turbine		283.2		-	283.2	56.61	0.8334
	Condenser		2128		372.6	426.0569	878.6	
	Pump	28.05			-	28.05	2.685	0.9043

Figure 5.15 demonstrates a visual comparison of energy analyses performed on solar heliostat field system showing energy received, delivered and energy efficiency of each component in the solar heliostat subsystem.

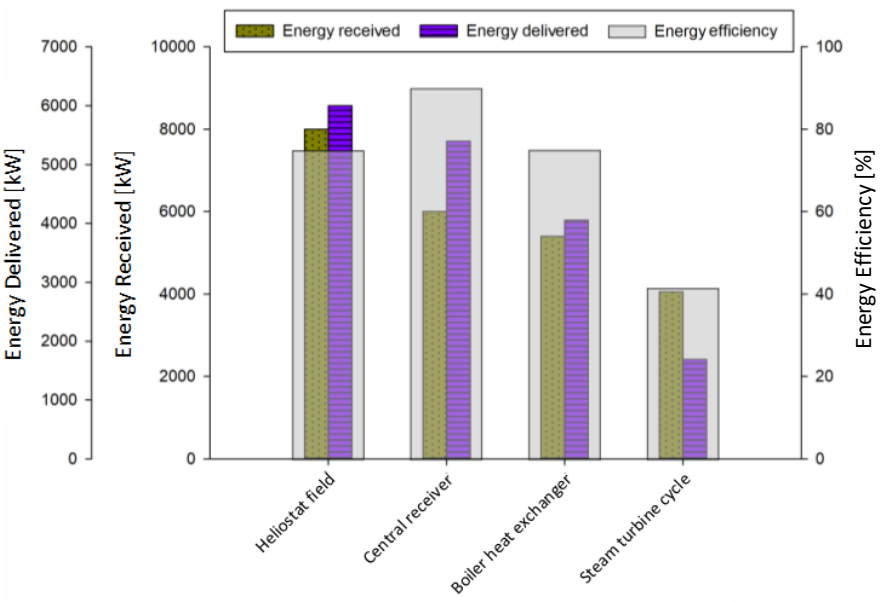

Figure 5.15 Energy received or delivered and energy efficiency for solar heliostat subsystem.

Exergy analyses results are also plotted in Figure 5.16 to visualize the amount of exergy delivered to each component and the amount of exergy destruction in each component.

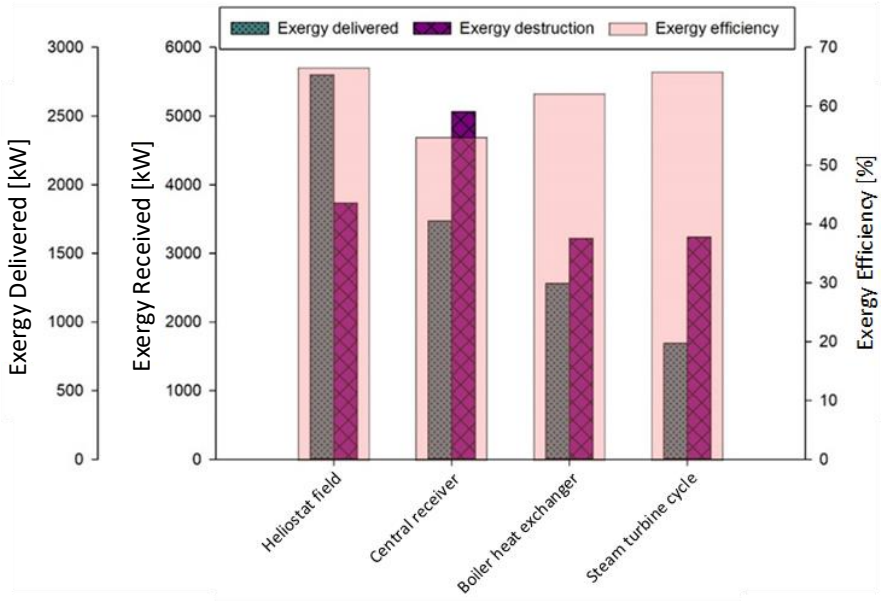

Figure 5.16 Exergy delivered, destruction, efficiencies for solar heliostat field

The power cycle seems to have the minimum energy efficiency due to the major heat rejection through the condenser. The maximum exergy destruction rate is occurring at the central receiver because heat is being lost at a very high temperature which indicates high

exergy loss. The energy efficiency for the solar heliostat subsystem is 23.75% while the exergy efficiency for the solar heliostat subsystem is 23.1% which is almost similar to the results obtained by Xu et al. [52]. Parametric studies have been performed on the operating parameters to investigate the maximum possible performance. Figure 5.17 shows the effect of different solar irradiation values on the system work output and efficiencies. As solar irradiation increases, the turbine work output significantly increases. However, energy and exergy efficiencies drop due to the increased losses.

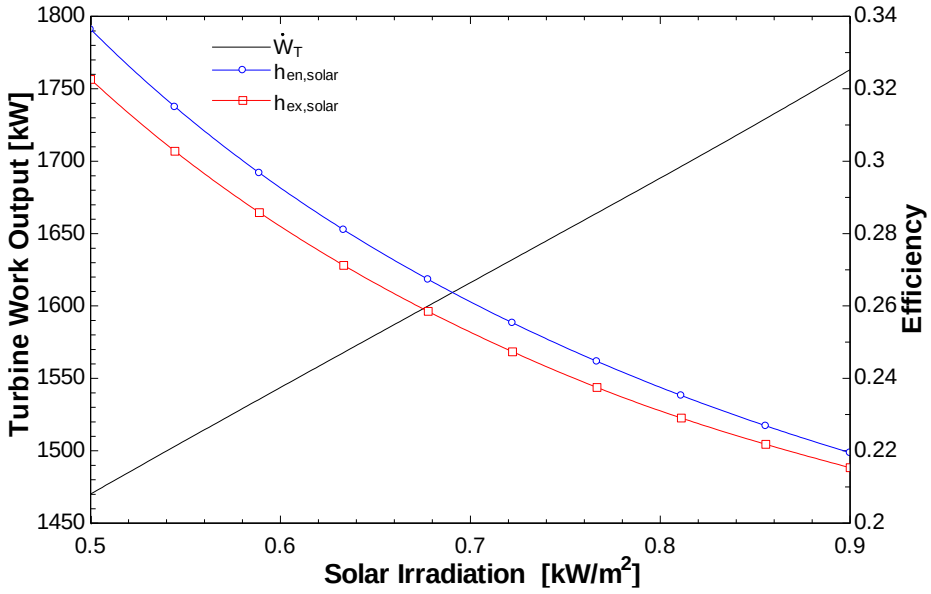

Figure 5.17 Effect of different solar irradiation values on the system work output and efficiencies

Figure 5.18 shows the effect of increasing turbine inlet pressure on the system performance. As the turbine inlet pressure increases, the turbine work output considerably increases. As a result, energy and exergy efficiency also increase. However, the increase in efficiencies was insignificant due to the increase in pump work demand with increasing the turbine inlet pressure.

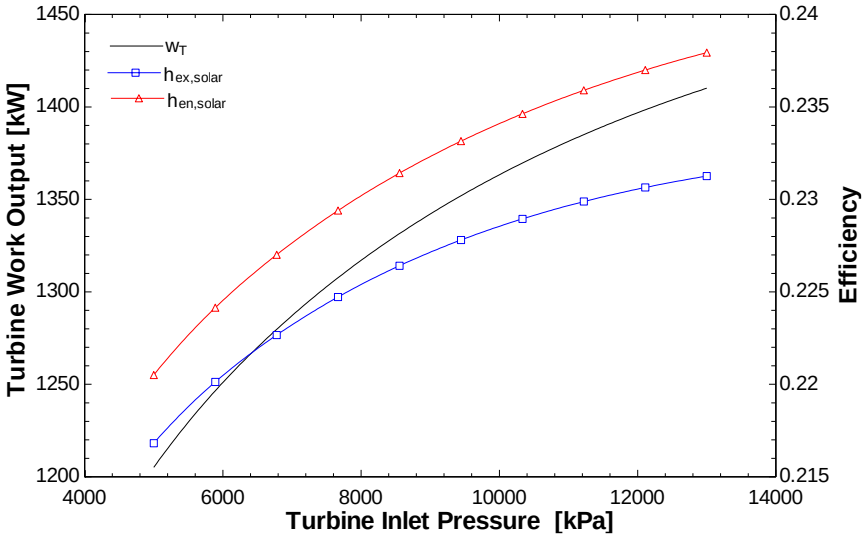

Figure 5.18 Effect of increasing turbine inlet pressure on the system performance.

The parametric studies also considered the effect of mass flow rate on the system performance. Figure 5.19 shows the effect of increasing steam mass flow rate on the turbine work output and turbine inlet temperature. As the steam mass flow rate increases, the turbine work output decreases due to the consequent decrease in turbine inlet temperature. Figure 5.20 shows the effect of increasing steam mass flow rate on both energy and exergy efficiency. The results show that both efficiencies decrease with increasing steam mass flow rate due to the decrease in turbine work output and increase in pump work demand.

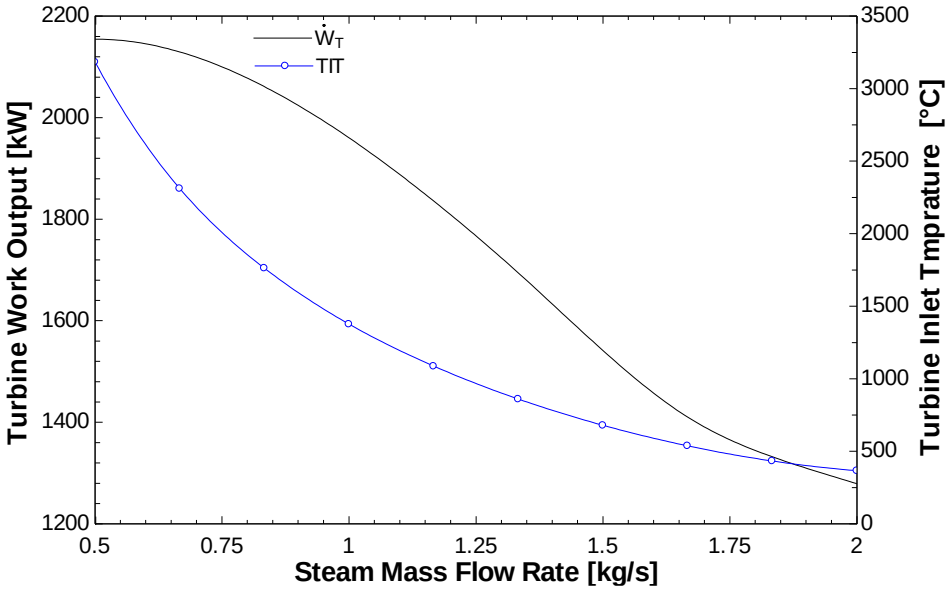

Figure 5.19 Effect of increasing steam mass flow rate on the turbine work output and turbine inlet temperature.

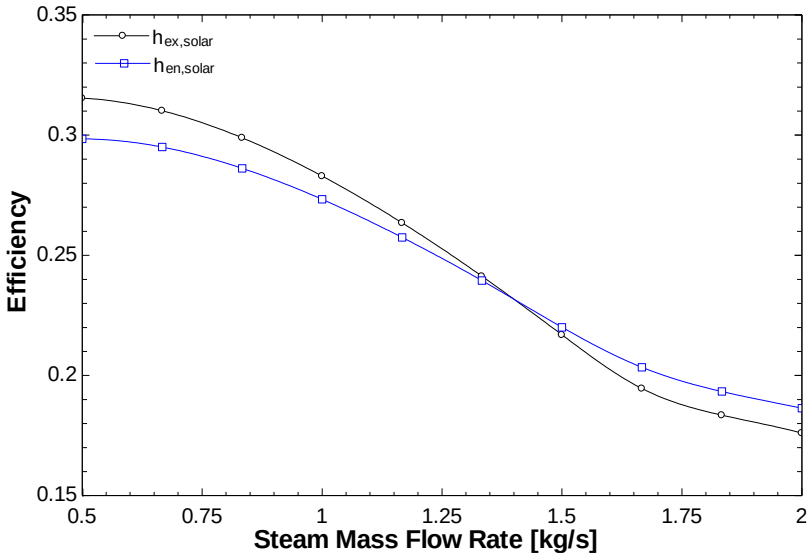

Figure 5.20 Effect of increasing steam mass flow rate on both energy and exergy efficiency.

The performance of solid oxide steam electrolyzer (SOSE) is discussed here. The main feature that distinguishes SOSE from PEM is that great portion of the electrochemical energy demand can be replaced with thermal energy as shown in Figure 5.21. Providing steam at very high temperature to the electrolyzer reduces the electrical work provided to the electrolyzer. Moreover, thermal energy provided to the electrolyzer, can be partially recovered from the product streams through preheating the feed stream. Consequently, the overall efficiency of the hydrogen production system is expected to increase.

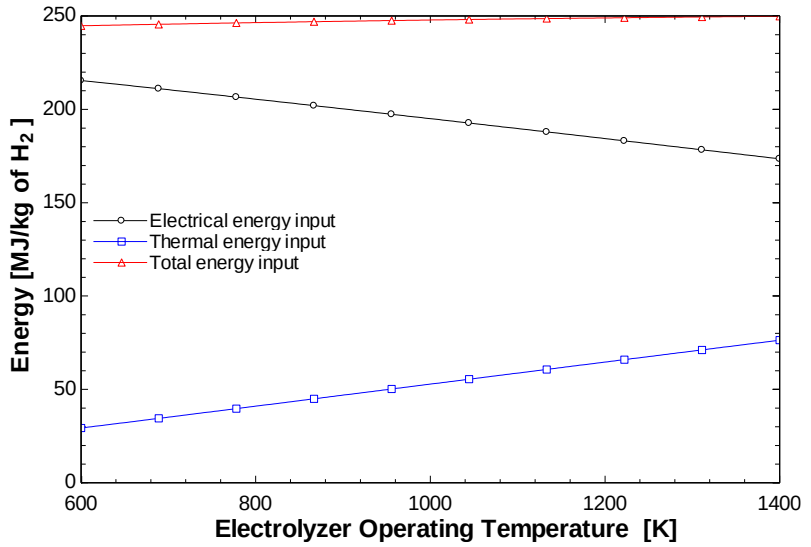

Figure 5.21 Different forms of energy demand for hydrogen production at different temperatures of the electrolyzer.

The SOSE hydrogen production system is composed of five heat exchangers, steam generator, electric heater, water pump and electrolyzer. The heat duty, work consumption, exergy destruction, and exergy efficiency are plotted in Figure 5.22.

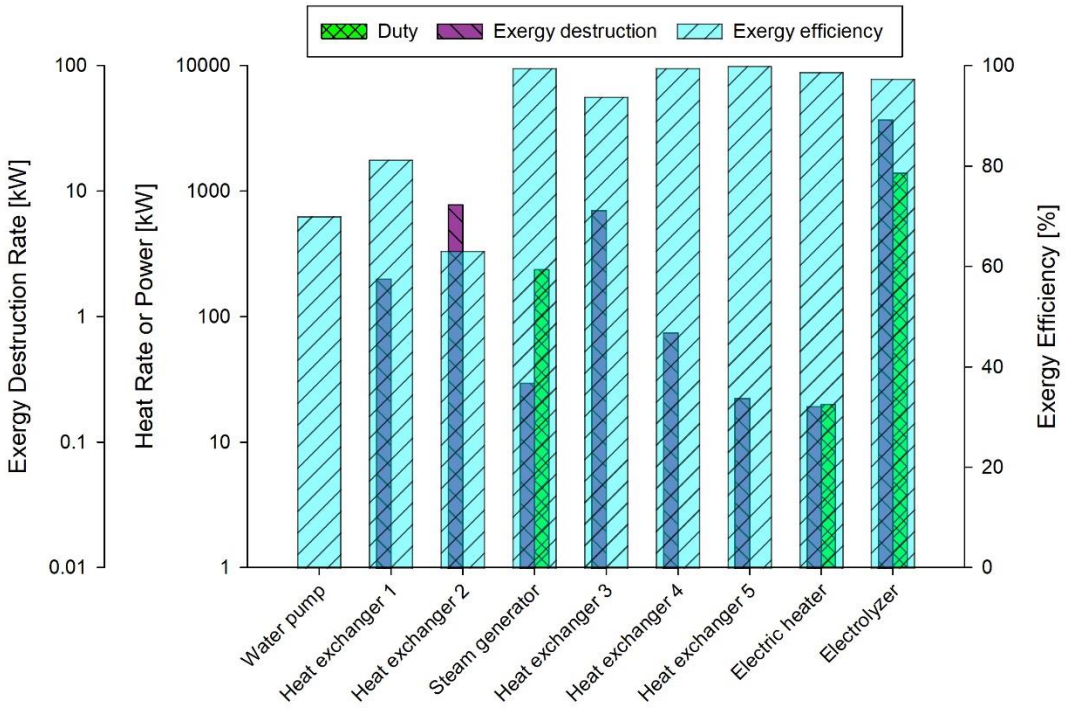

Figure 5.22 Exergy destruction and efficiencies for SOSE.

The maximum exergy destruction rate is again occurring at the electrolyzer due to the thermal heat losses, chemical irreversibility and overpotential losses. The exergy destruction rate for SOSE electrolyzer is relatively lower compared to PEM electrolyzer due to the substantial heat recovery from the product streams. The overall energy efficiency for hydrogen production subsystem is 90.5 %. While the overall exergy efficiency for the overall hydrogen production subsystem is 95.8 % which are relatively close to the results obtained by Alzahrani et al. [48]. Parametric studies have been carried on the effect of applied current density on the cell overpotential losses and the overall cell potential. Figure 5.23 shows the effect of current density on the overpotential losses and overall cell potential. It can be concluded that current density has a significant effect on Ohmic losses as it considerably increases with the increase of applied current density. The other

overpotential losses are also increased by increasing the applied current density. However, concentration overpotential has less influence by increasing current density.

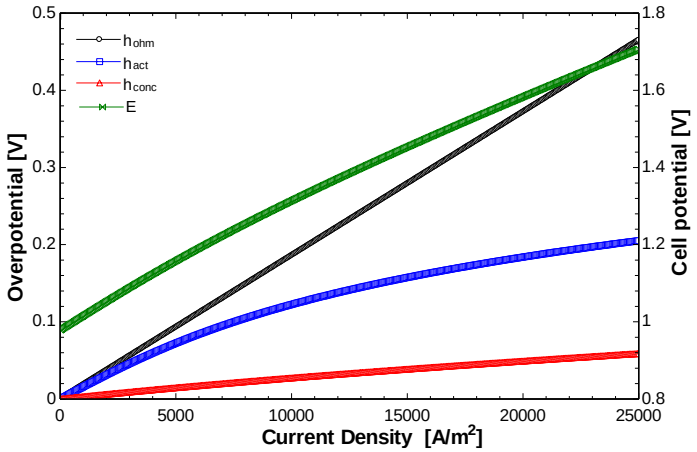

Figure 5.23 Effect of current density on the overpotential losses and overall cell potential.

As a result of the increase of overpotential due to increasing current density, the overall cell potential consequently increases as shown in Figure 5.23. However, the rate of increase in the overall cell potential is significantly affected by the working temperature. Figure 5.24 shows the effect of current density on the cell potential at different working temperatures. This figure implies that the rate of increase of cell potential substantially decreases by increasing the SOSE electrolyzer working temperature. The reduction in cell potential increase as the working temperature increase diminishes as the working temperature increases.

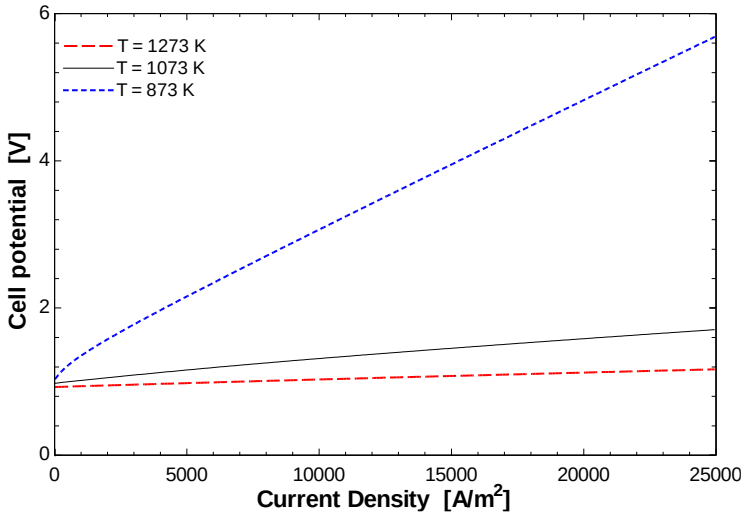

Figure 5.24 Effect of current density on the cell potential at different working temperatures.

Figure 5.25 exhibits the major effect of operating temperature on the overpotentials. As the working temperature increases, the overpotentials significantly decreases and reduces the overall cell potential as a consequence. The results also emphasize the reduction of cell potential at a higher temperature in Figure 5.24.

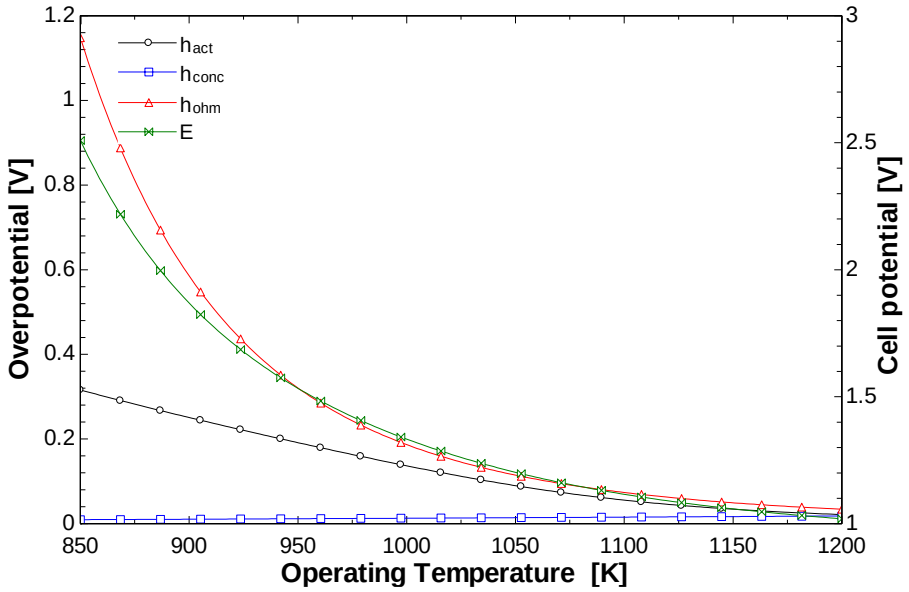

Figure 5.25 Effect of operating temperature on the overpotentials.

For carbon capturing subsystem, the system has the same configuration as the first system. However, the operating parameters are different due to the difference in flue gas temperatures and compositions. The operating flue gas parameters are listed in Table 5.7. The energy and exergy analyses results are charted in Figure 5.26

Table 5.7 Steel furnace flue gas conditions

Parameter		Value
Temperature		982 ^{o}C [21]
Pressure		120 kPa
Total flow		2.48 kg/s
Mole Fraction	H_2O	1.16 %
	CO_2	23.4 %
	N_2	70.28 %
	O_2	4.7 %

Source: [54]

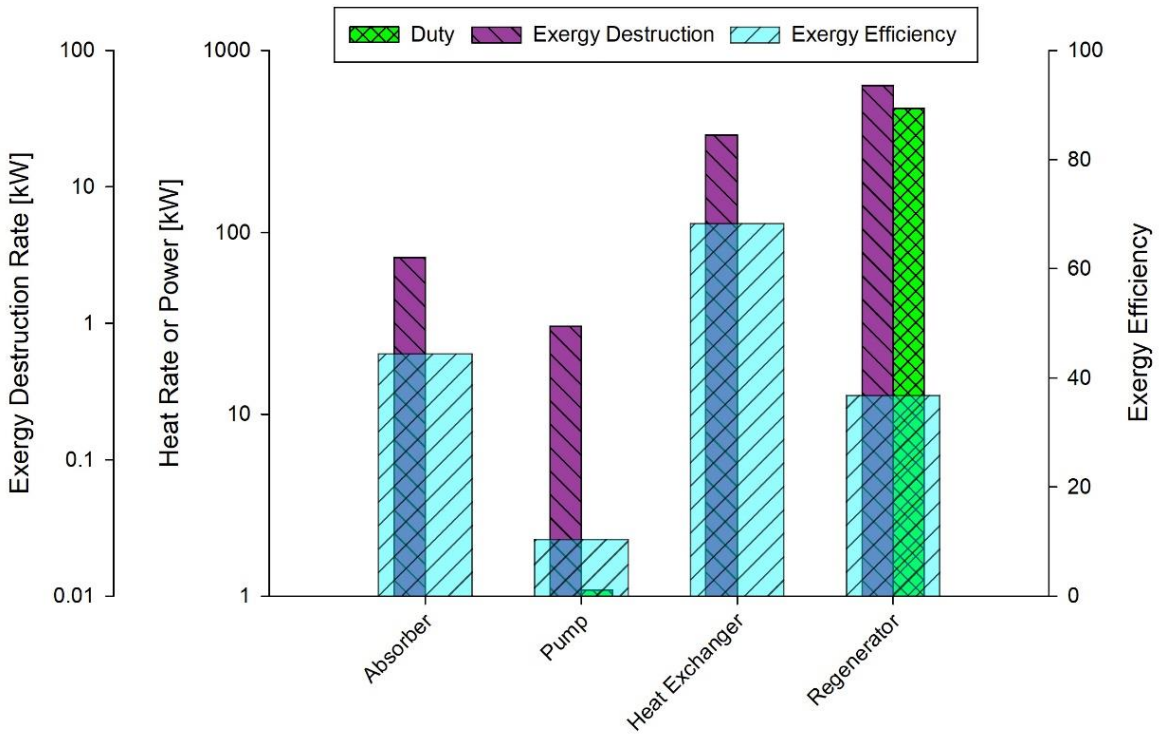

Figure 5.26 Exergy analyses for carbon capturing subsystem.

The maximum exergy destruction is again occurring at the regenerator due to the waste heat rejection through the condenser. However, the amount of exergy destruction in this subsystem is relatively higher than the previous system due to the higher mass flow rate of flue gas and solvent. The exergy efficiencies for all the components are almost the same except for the regenerator it is quite lower due to the higher losses in this case and higher boiler heat duty.

For MeOH and DME synthesis results, the system is composed of the same components that system 1is developed from like, compressors, intercoolers, reactors, distillation columns and flashing chambers. However, the thermodynamic performance variables are different from the performance variable of system 1 due to having different production rates. The energy efficiency of DME synthesis from hydrogen and carbon dioxide is 71.39 % which is very close to the values obtained by Clausen et Al. [56] and Reed [57]. While the exergy efficiency of DME synthesis was calculated to be 80.7 %. Figure 5.27 shows a summary of the amount of energy consumed and released during the DME synthesis

process. The maximum heat rejection is occurring at the methanol reactors cooler. As a result, heat released from this two components has been recovered to be used in pre distillation heater and DME distillation column.

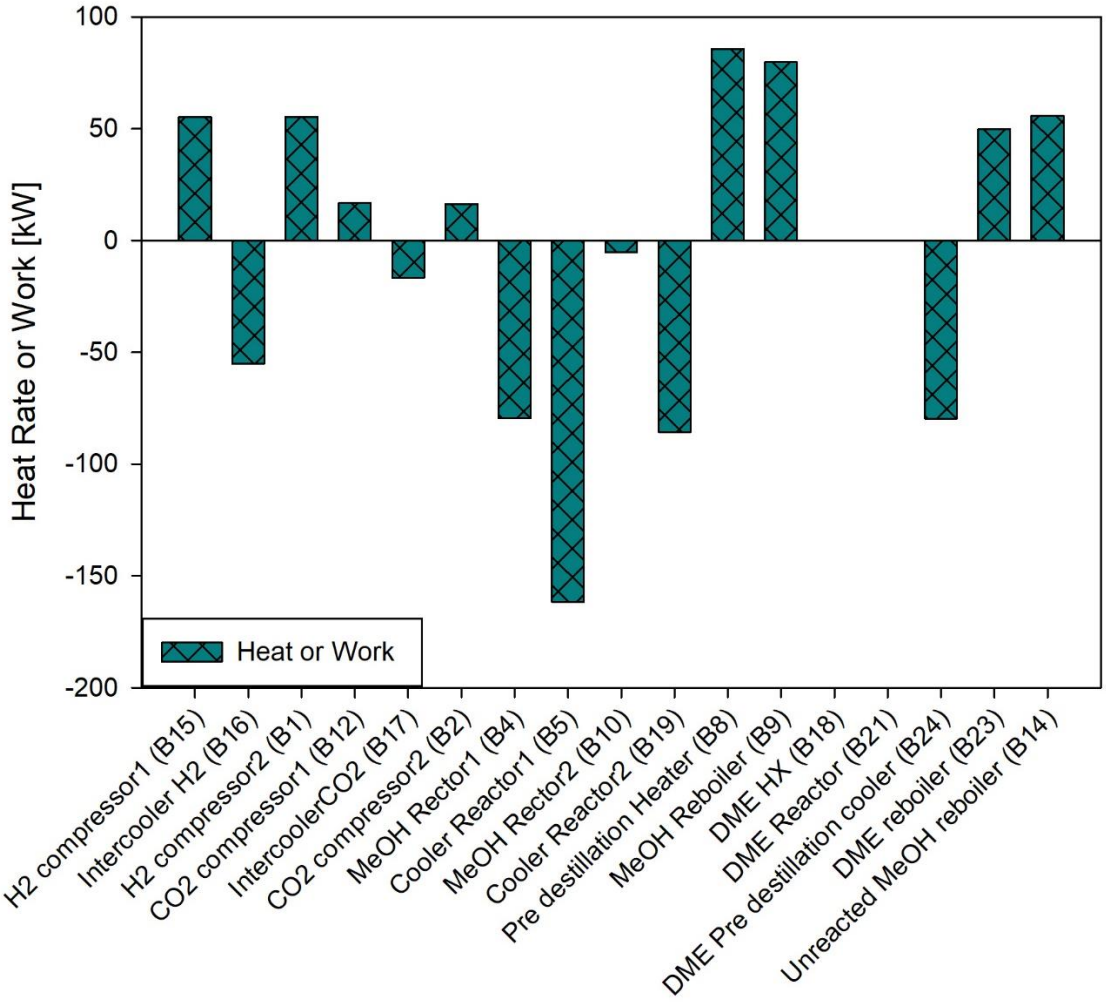

Figure 5.27 Energy analysis result for DME production.

Figure 5.28 demonstrates the different exergy performance variables of each component of MeOH and DME synthesis system. Again, exergy destruction rates are maximum at the reactors. On the other hand, minimum exergy efficiency is taking place at the rector coolers because of the high amount of heat rejected at a very high temperature.

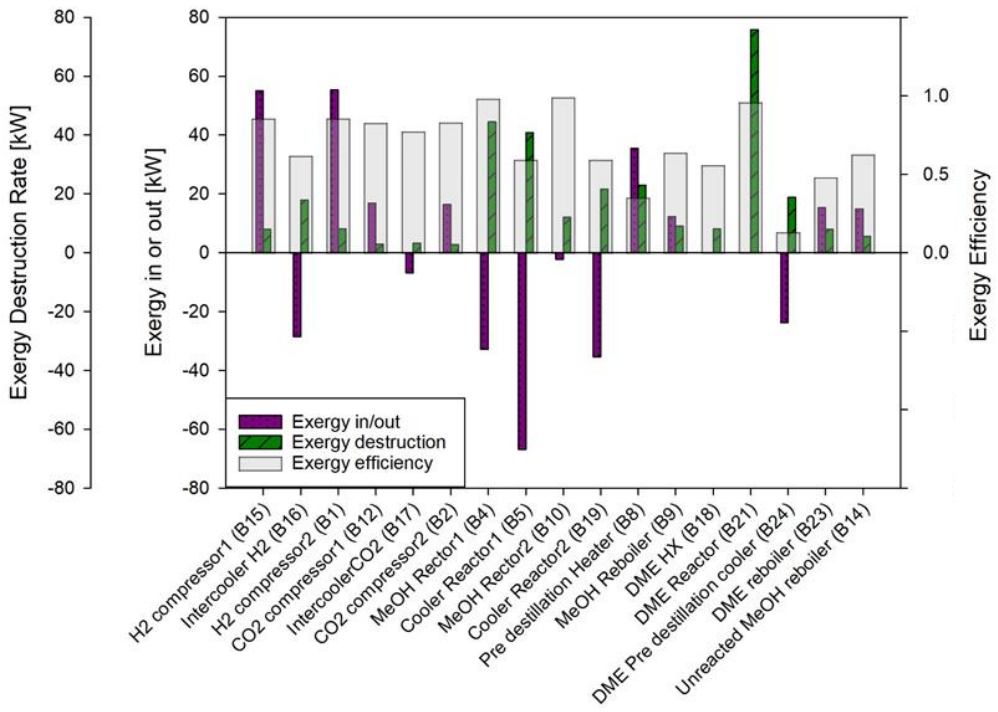

Figure 5.28 Exergy analyses results for DME synthesis

Sizing and design results for distillation columns are the same since the feed conditions, temperature, compositions are the same except that feed flowrates are different.

5.3 Results for System 3

The third system which is solar thermochemical based DME production system results are presented in this section. Performance of each subsystem, energy requirement, exergy destruction rates and the associated input parameters are presented. Moreover, the results of the overall system performance are discussed in terms of energy and exergy efficiencies, exergy destruction rates, energy inputs, DME production rate, And electric power generation. Chemical processes have been simulated using Aspen plus process simulation software. Results then have been exported to formulated Excel sheet to carry the chemical exergy analyses. However, gas turbine and multi-effect desalination modeling have been performed through EES software. The overall performance parameters of the system are listed in table 5.8

Table 5.8 Overall system 3 results summary

DME production plant parameters	Value
Energy efficiency	39.72 %
Exergy efficiency	55.2 %
DME production rate	1879.15 kg/day
Heat requirement for the production of 1 mol/s of DME	4324.40 kW
Electric work rate requirement for production of 3 mol/s of hydrogen	189 kW
Boiler heat duty for carbon capturing of 1 mol/s of carbon dioxide	430.5 kW
Amount of work produced by the gas turbine	10 MW
The mass flow rate of fresh water produced	9.176 kg/s
The pressure of the produced DME	940 kPa
The temperature of the produced DME	40 ^{o}C
Exergy destruction rate	5961.96 kW

The system is capable of producing 0.0217 kg/s. Hence, if the plant is operating 24 hours per day, the daily production rate will be 1,879.15 kg/day. Moreover, the plant is also able to generate 233.71 MWh of energy per day from the gas turbine and produce a net of 788.14 ton/day of fresh water through the MED desalination system. The overall energy efficiency of the third DME production system is 39.72%. Likewise, the overall exergy efficiency of the third DME production system is 55.2 %.

Figure 5.29 shows the distribution of exergy destruction between the different subsystems of the multi-generation system. Most of the exergy destruction is taking place in the gas turbine subsystem due to the high irreversibility occurring in the combustion process and gas turbine.

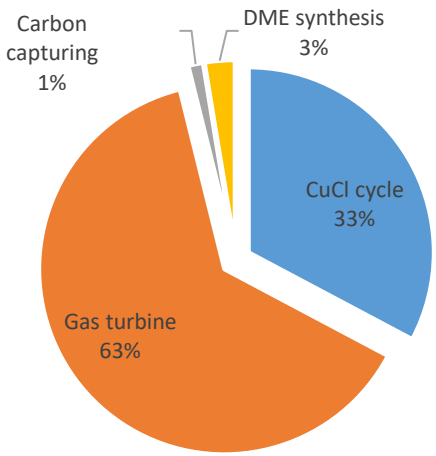

Figure 5.29 Exergy destruction distribution over the four subsystems

The results of the gas turbine subsystem are discussed here. The system is composed of compressor, combustion chamber and turbine. Energy and exergy analyses are performed on each component of the system to examine the specific exergy losses from each component and calculate exergy destruction rate and exergy efficiency as well as overall energy efficiency of the subsystem. The results summary of energy and exergy analyses is presented in Figure 5.30.

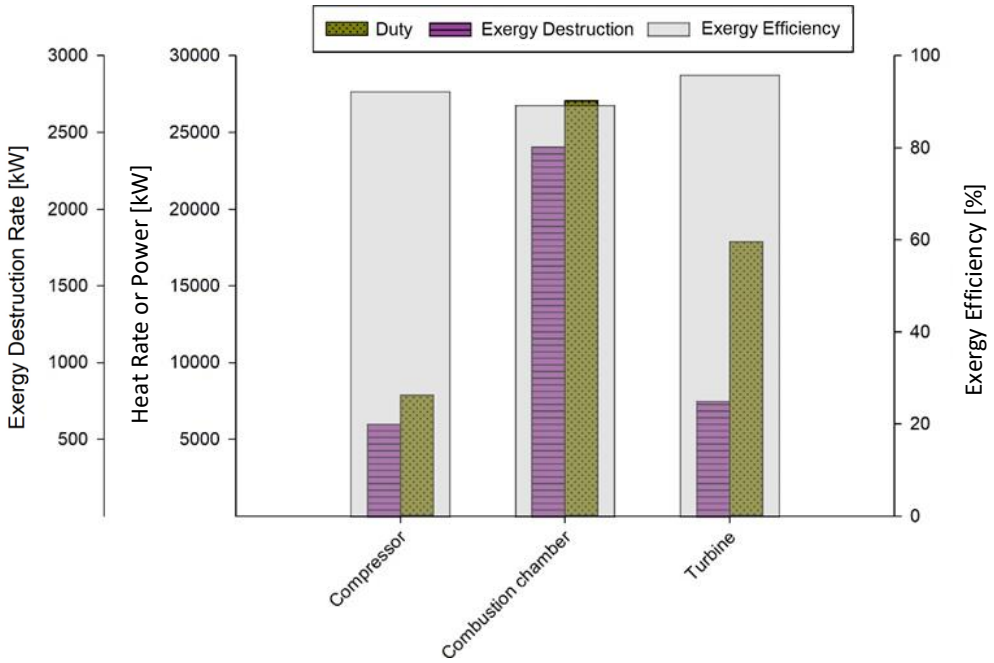

Figure 5.30 Exergy analyses results for gas turbine subsystem

The maximum exergy destruction in gas turbine subsystem is taking place in the combustion chamber due to the significant exergy loss during the combustion process. Consequently, combustion chamber has the minimum exergy efficiency value. The net work output of the gas turbine subsystem is 10 MW at a pressure ratio fixed at 14 and turbine inlet temperature set as 1600ºC. The energy efficiency of the overall gas turbine subsystem is 36.95%. While the exergy efficiency of the overall gas turbine subsystem is 43.94%.

Parametric studies have been performed to study the effect of the different operating parameters on the gas turbine subsystem performance as well as on the exhaust gas temperature. Figure 5.31 shows the effect of compressor pressure on the system inputs and outputs in addition to the exhaust temperature. As the compressor pressure ratio increases, both compressor work and turbine work increase linearly at the same rate of increase. However, as the compressor pressure ratio increases, the rate of heat input to the combustion chamber significantly decreases due to the fact that temperature of compressed air exiting the compressor gets higher as the compressor pressure ratio increases. As a result, the heat duty on combustion chamber significantly drops. On the other hand, as the compressor pressure ratio increases, the exhaust gasses temperature significantly drops –at a fixed turbine inlet temperature- due to the larger pressure range of expansion that allows the gasses to get cooler during the expansion process inside the turbine.

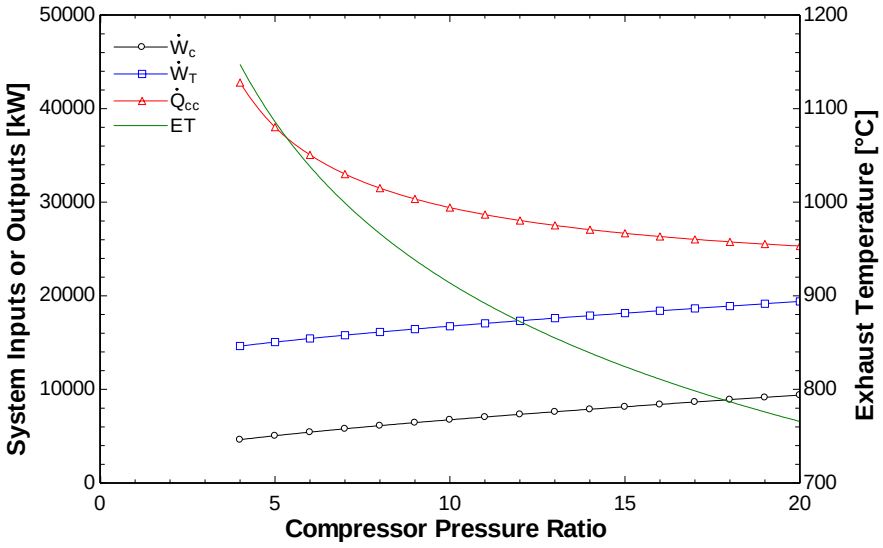

Figure 5.31 Effect of compressor pressure on the system inputs and outputs in addition to the exhaust temperature

Furthermore, the parametric studies have considered the effect of compressor pressure ratio on the performance from the exergy aspect. Figure 5.32 shows the effect of compressor pressure ratio on exergy destruction rate and exergy efficiency of each component. The study concluded that exergy destruction rate significantly reduced due to the decrease in heat duty and losses. As a result, the exergy efficiency for the combustion chamber increases. The exergy destruction rate for turbine slightly increases with increasing compressor pressure ratio which leads to a minor decrease in turbine exergy efficiency. Similarly, compressor exergy destruction rate slightly decreases with increasing compressor pressure ratio which leads to minor exergy efficiency increase.

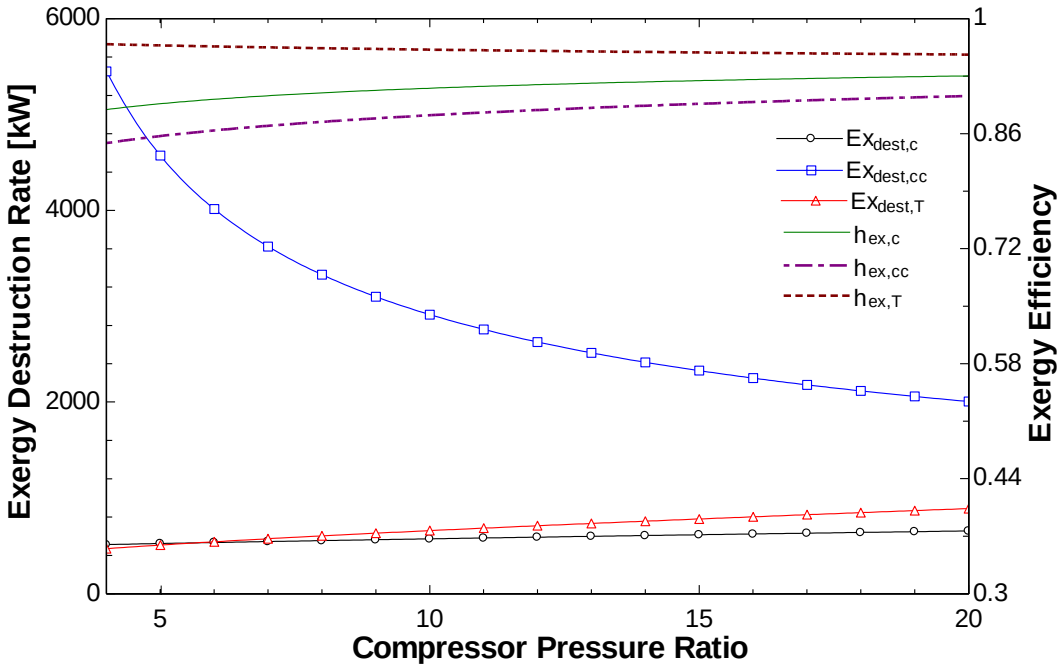

Figure 5.32 Effect of compressor pressure ratio on exergy destruction rate and exergy efficiency of each component

The study also considers the effect of compressor pressure ratio on the overall energy and exergy efficiency and back work ratio. Figure 5.33 depicts the effect of compressor pressure ratio on system efficiencies and back work ratio. The results have shown that both energy and exergy efficiencies have remarkably increased with increasing compressor pressure ratio. However, back work ratio, which is the ratio of compressor work to turbine work is increasing as well imply that a greater portion of the generated work is consumed by compressor as the pressure ratio increase.

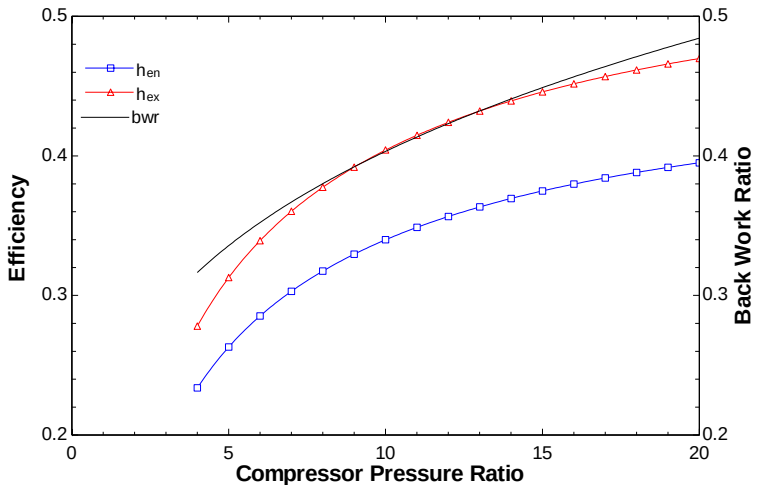

Figure 5.33 Effect of compressor pressure ratio on system efficiencies and back work ratio

Another parametric study is conducted on the effect of the turbine inlet temperature on the gas turbine system performance. Figure 5.34 shows the effect of varying turbine inlet temperature on system inputs and outputs in addition to the back work ratio. The results show that turbine work output increases linearly at a very high rate as the turbine inlet temperature increases because of the higher energy content of air at turbine inlet temperature. Combustion chamber heat duty increases as expected due to increasing the turbine inlet temperature. Compressor work does not change with increasing turbine inlet temperature since pressure ratio is kept constant. Exhaust temperature significantly increases linearly at a high rate of increase.

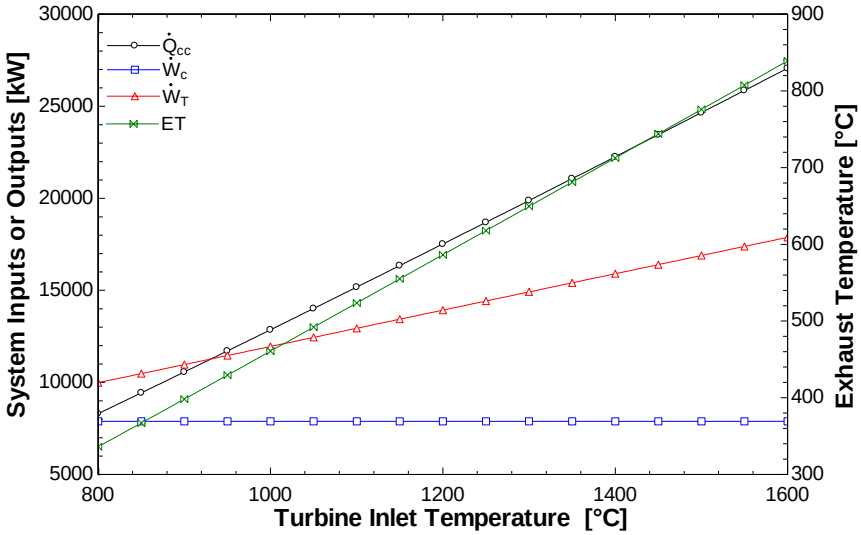

Figure 5.34 Effect of varying turbine inlet temperature on system inputs and outputs in addition to the back work ratio

From exergy point of view, parametric studies have considered the effect of increasing turbine inlet temperature on exergy destruction rate and exergy efficiency of each component in the gas turbine subsystem. Figure 5.35 depicts the effect of increasing turbine inlet temperature on exergy destruction rates and exergy efficiencies. Exergy destruction rate for combustion chamber is linearly increasing at a high rate is the turbine inlet temperature increase due to the increasing heat duty and exergy losses during combustion. Consequently, the exergy efficiency for the combustion chamber drops as the turbine inlet temperature increases. Exergy destruction rate for turbine slightly decreases as the turbine inlet temperature increases which result in a minor increase in exergy efficiency for the turbine. Exergy destruction rate and exergy efficiency for compressor does not change with increasing turbine inlet temperature.

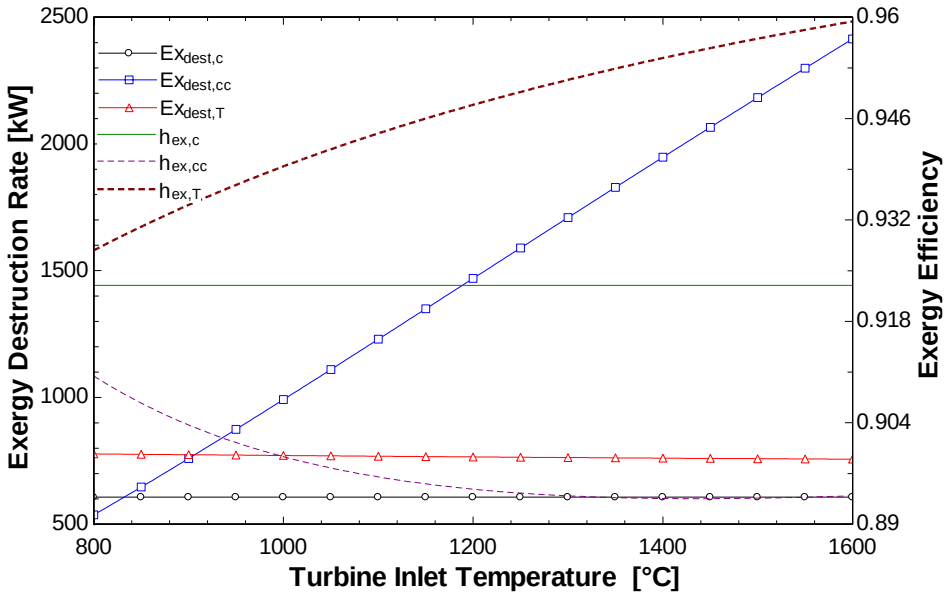

Figure 5.35 Effect of increasing turbine inlet temperature on exergy destruction rates and exergy efficiencies

Finally, the study examined the effect of increasing turbine inlet temperature on overall efficiencies and back work ratio. Figure 5.36 shows the effect of increasing turbine inlet temperature on the overall performance. The study revealed that both energy and exergy efficiencies increase as the turbine inlet temperature increases. However, the rate of efficiency increase diminishes as the temperature gets higher. The back work ratio significantly reduces linearly as the turbine inlet temperature increase.

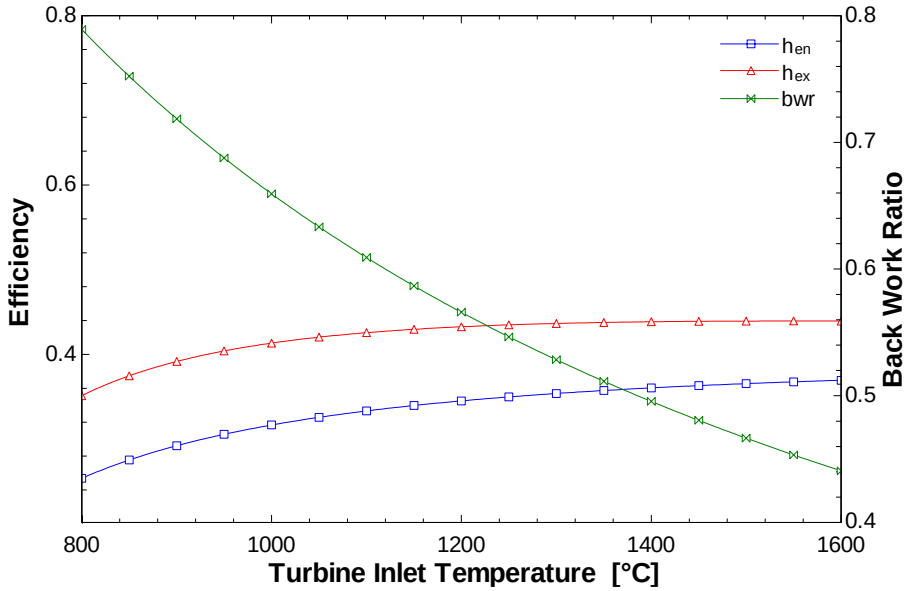

Figure 5.36 Effect of increasing turbine inlet temperature on the overall performance

The parametric study results of gas turbine operating parameters indicate close matching with a previously published study performed by Dinali et al. [60].

The Cu-Cl thermochemical hydrogen production cycle results are discussed here. The subsystem is composed of thermolysis reactor to react water with Cupper Dichloride, thermolysis where copper oxychloride decomposes to oxygen and copper chloride, electrolyzer where hydrochloric acid reacts with copper chloride to produce hydrogen and dryer to separate the water from the Cupper Dichloride. Energy and exergy analyses have been performed on each step of the cupper chlorine hydrogen production cycle. Exergy destruction rate and exergy efficiency have been calculated for each step of the cycle. Figure 5.37 exhibits the exergy destruction rates along with exergy efficiency for each step. The overall energy efficiency for the Cu-Cl thermochemical hydrogen production cycle is 41.57%. While the overall energy efficiency for the Cu-Cl thermochemical hydrogen production cycle is 62.3 %. The results obtained shows very good matching with the results concluded by Al-zareer et al. [61] as 40.1% and 60.2% respectively.

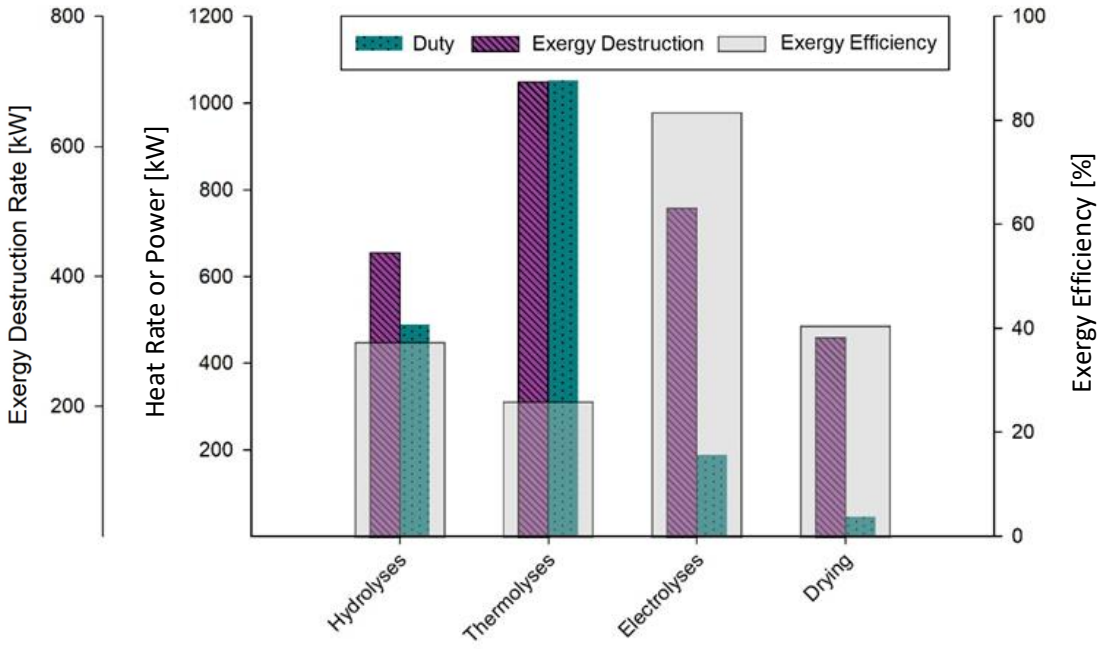

Figure 5.37 Energy and exergy analyses results for Cu-Cl cycle

For carbon capturing subsystem, the system configuration is the same as the first and second systems except that the operating conditions are different due to the difference in flue gas compositions and temperatures. Flue gas conditions and compositions are listed in Table 5.9. Energy and exergy analyses results are listed in Figure 5.38.

Table 5.9 Gas turbine flue gas conditions.

Parameter		Value
Temperature		840 ^{o}C
Pressure		120 kPa
Total flow		19.46 kg/s
Mole Fraction	H_2O	1.6 %
	CO_2	23.41 %
	N_2	70.28 %
	O_2	4.71 %

Source: [54]

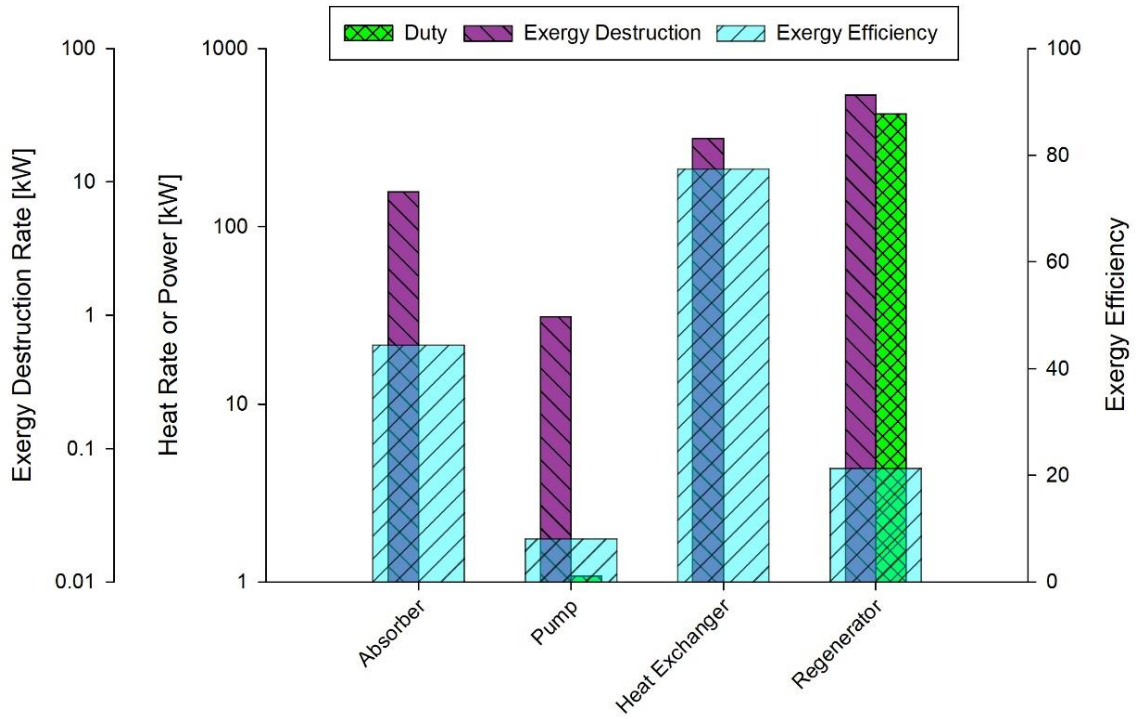

Figure 5.38 Exergy analyses results for carbon capturing subsystem.

The regenerator reboiler duty has remarkably increased due to the increase in solvent mass flow rate which requires more heat to reject the CO_2 gas. As a result, regenerator will have a higher exergy destruction rate compared to the previous carbon capturing subsystems. Maximums exergy efficiency is taking place at the heat exchanger as there are no exergy losses.

MeOH and DME synthesis results are introduced here. The flowsheet for DME synthesis in the third system is the same as in system 2 and 3, except that the hydrogen stream is coming from the Cu-Cl cycle instead of the electrolyzer. The thermodynamic analyses results are shown in Figure 5.39 and Figure 5.40. The summary of energy analyses in terms of work and heat are illustrated in Figure 5.39, the negative heat bars imply that heat has been released from that component.

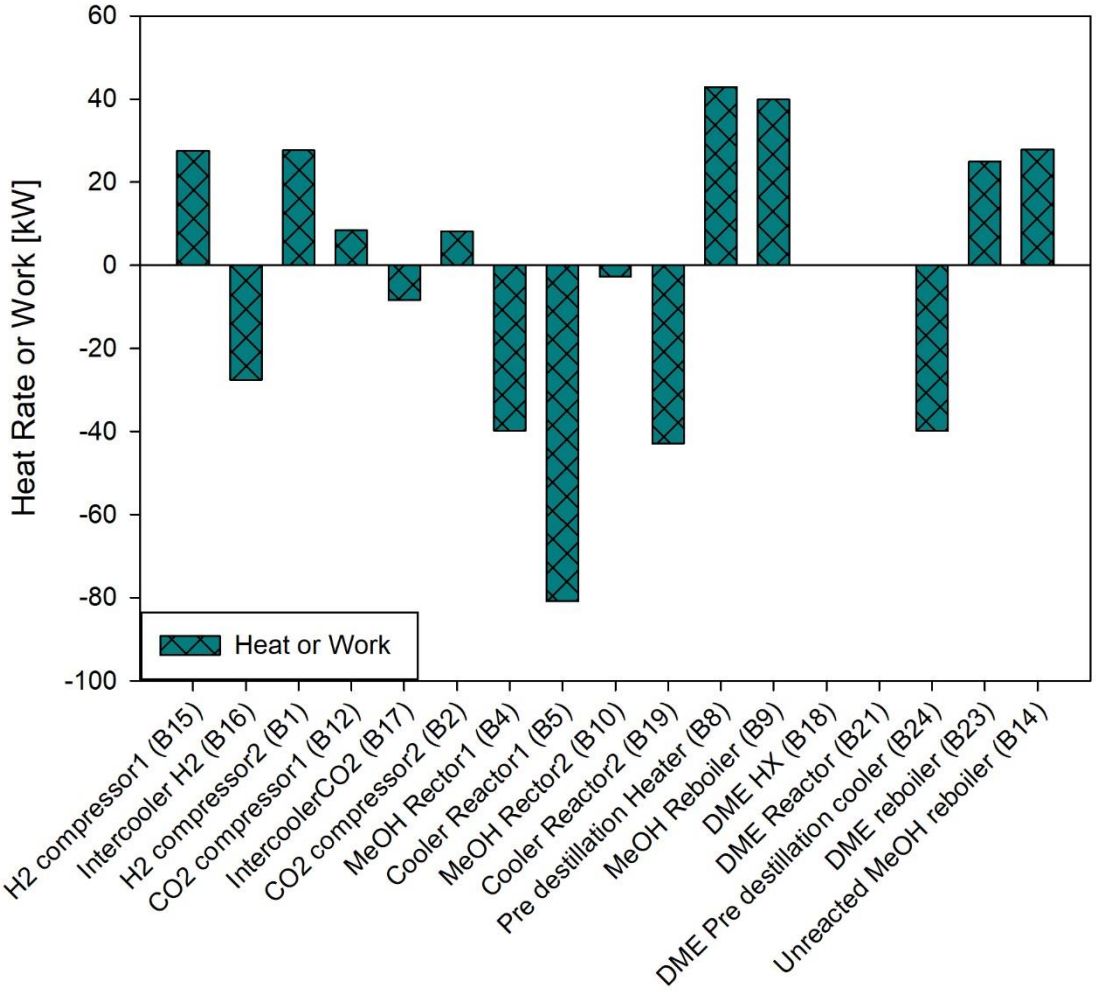

Figure 5.39 Energy analyses results for DME production subsystem.

The summary of exergy analysis results has been exhibited in Figure 5.40. The figure shows exergy transfer and exergy destruction in addition to exergy efficiency. Exergy transfer bars with the minus sign imply that exergy has been released in the form of heat.

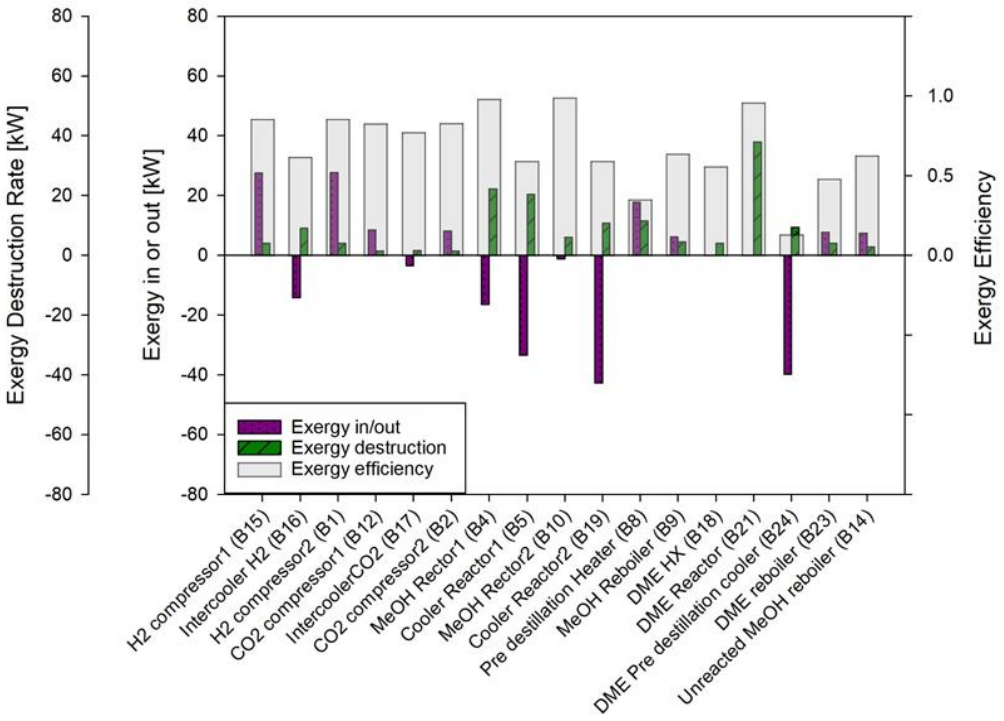

Figure 5.40 Exergy analyses results for DME synthesis subsystem

The energy and exergy analyses results for DME synthesis in system 3 are very close to the results in DME synthesis subsystem in system 1 because they have similar production rate and require almost the same amount of heat and work. The energy efficiency of DME synthesis from hydrogen and carbon dioxide is 71.4 %. While the exergy efficiency of DME synthesis was calculated to be 80.7 %.

Multi-effect desalination subsystem is discussed here. The system is composed of eight different evaporating chambers connected in series with seven feed water preheaters to recover the heat from distilled water and heat feed water in addition to the last stage condenser and brine heat recovery heat exchanger. Energy balance analyses have been performed to investigate the performance of the MED subsystem. Table 5.10 shows the operating parameters used and results for the MED subsystem analyses.

Table 5.10 MED subsystem operating parameters.

Parameter	Value
Number of stages	8
Feed water temperature	25 ^{o}C
Feed water salinity	42000 ppm
Feed water flow rate	22.94 kg/s
Motive steam flow rate	1 kg/s
Motive steam temperature	140 ^{o}C
Brine exit temperature	40 ^{o}C
Rejected brine salinity	70000 ppm
Brine water flow rate	13.76 kg/s
Distilled water flow rate	9.176 kg/s

The detailed mass flow of distilled water, brine water and brine salinity in each stage are plotted in Figure 5.41. The mass flow of distilled water in each effect is almost the same except that it slightly decreases in the last few effects. Figure 5.42 shows the temperature of each effect as well as the temperature drop in each effect. The effect temperature significantly decreases as we go towards the last effects due to the temperature drop. Figure 5.43 demonstrates the overall heat transfer coefficient at the different effects as well as the surface area at each effect. The heat transfer coefficient decreases as we go towards the last effects due to the decrease in motive steam or vapor temperature. The surface areas of each effect are very close to each other except that they slightly decrease as we go towards the last effects due to the decrease in brine mass flow rate.

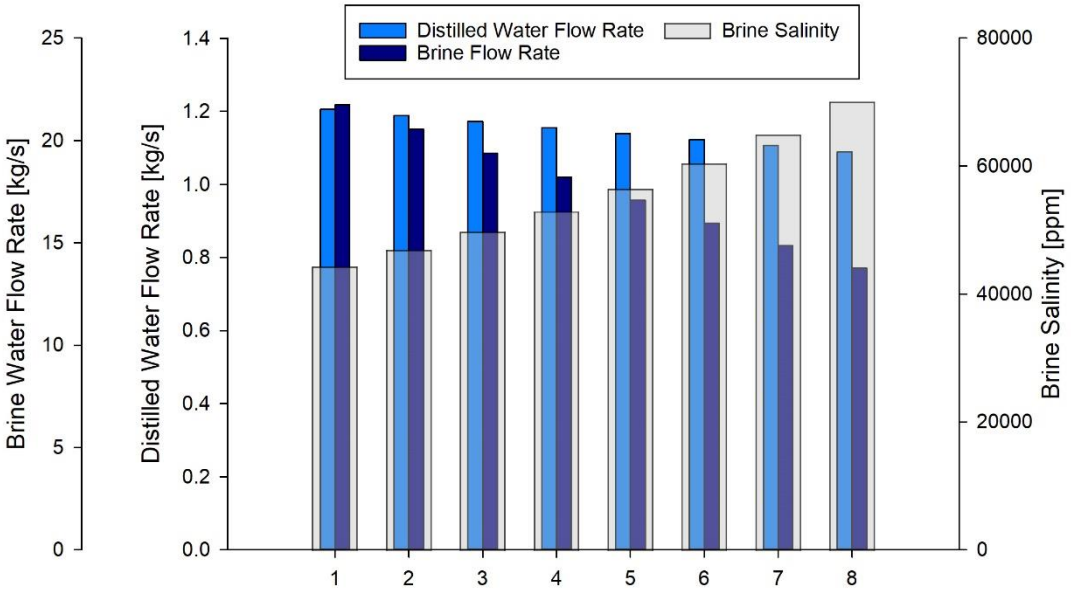

Figure 5.41 Distilled water, brine water flow over the different desalination effects.

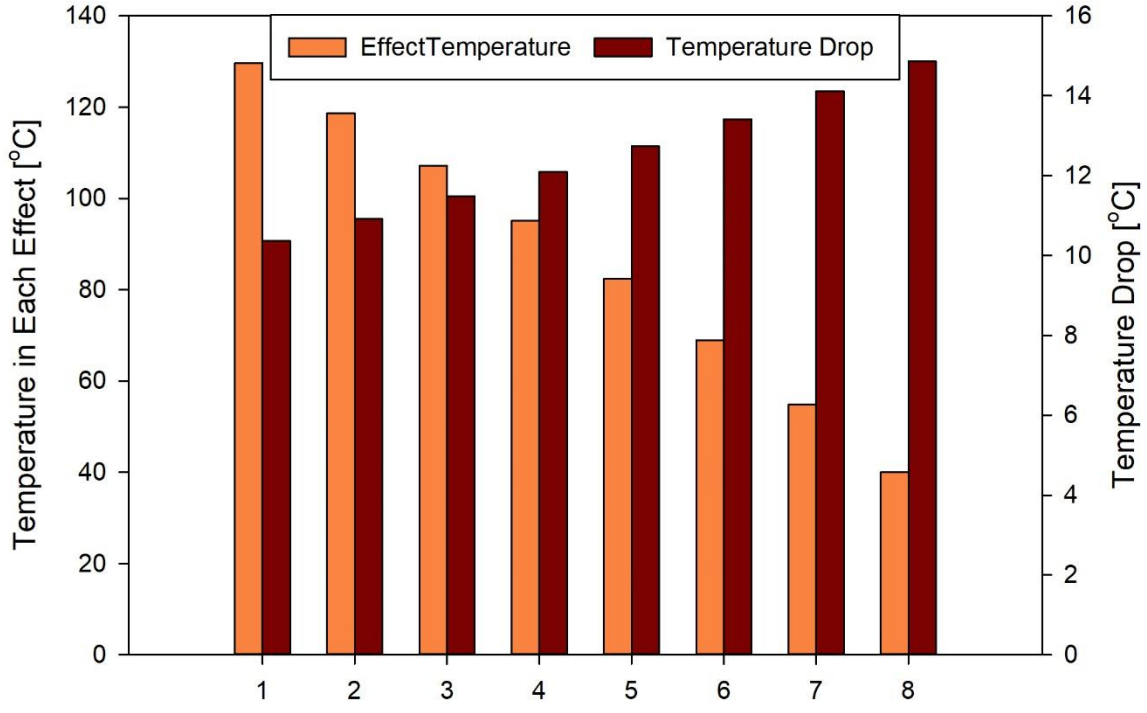

Figure 5.42 Temperature and temperature drop in each effect.

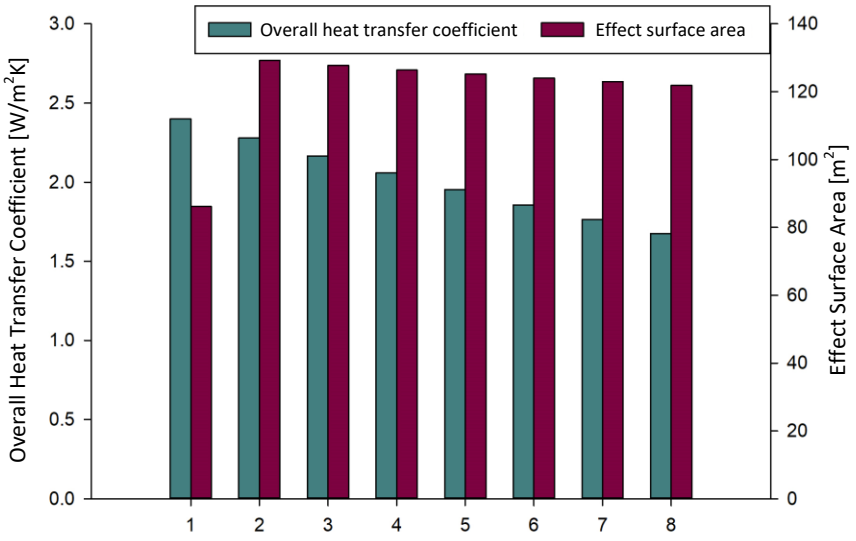

Figure 5.43 Heat transfer coefficient surface area over the different desalination effects.

Parametric studies have been performed to investigate the effect of operating and design parameters on the performance of the MED subsystem. Figure 5.44 shows the effect of motive steam temperature on the distilled water flow rate at a different number of stages. The results show that the distilled water flow slightly decreases as the motive steam temperature increases. However, increasing the number of stages significantly increases the distilled water flow rate as shown in Figure 5.45.

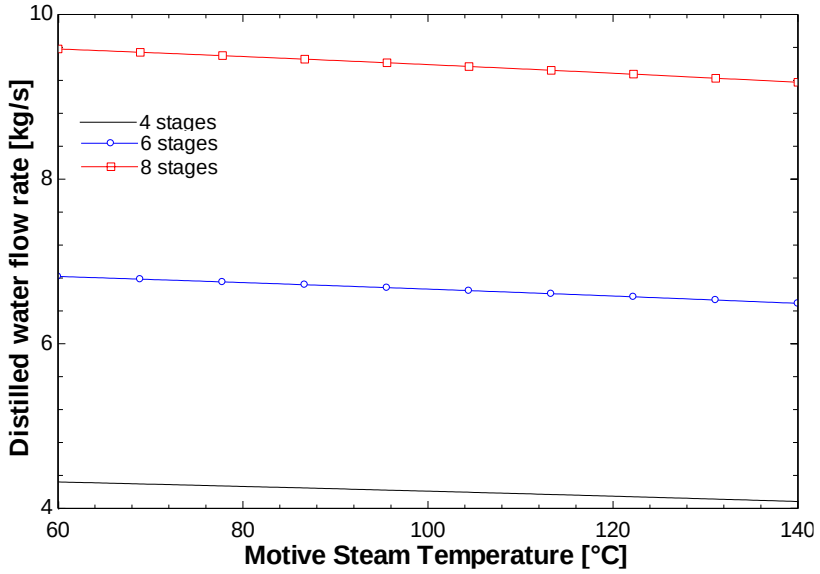

Figure 5.44 Effect of motive steam temperature on the distilled water flow rate at a different number of stages.

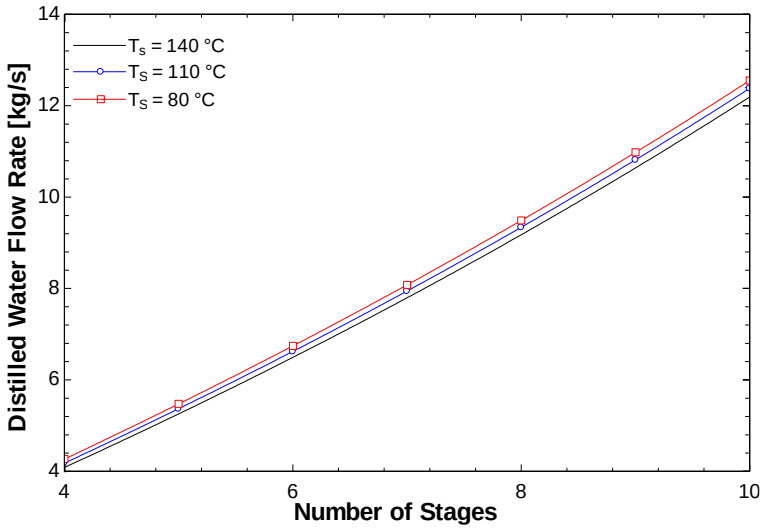

Figure 5.45 Effect of number of stages on the distilled water flow rate at different motive steam temperatures.

The parametric studies also considered the effect of motive steam temperature on performance ratio which is the ratio between heat recovered to evaporate the distillate water to the heat provided by the motive steam. Figure 5.46 shows the effect of increasing the motive steam temperature on performance ratio at a different number of stages. The results show that performance ratio slightly decreases as motive steam temperature increases due to the fact that saturated steam has less enthalpy of evaporation as the temperature of the steam increases. However, the performance ratio significantly increases as the number of stages increase as shown in Figure 5.47.

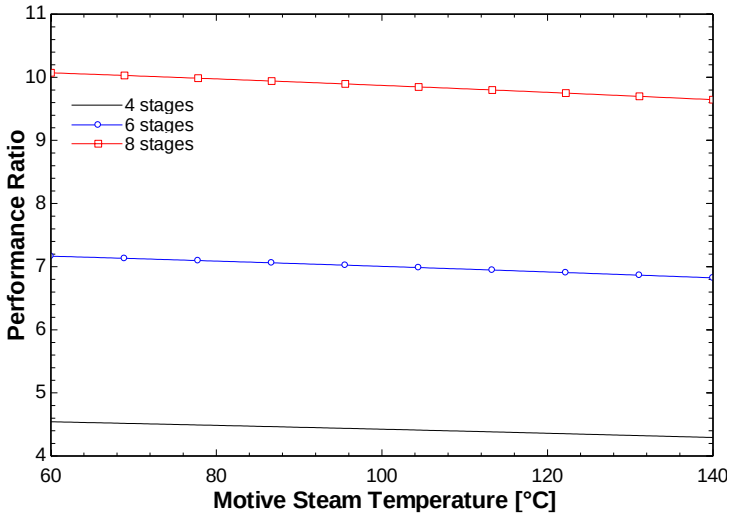

Figure 5.46 Effect of increasing the motive steam temperature on performance ratio at a different number of stages.

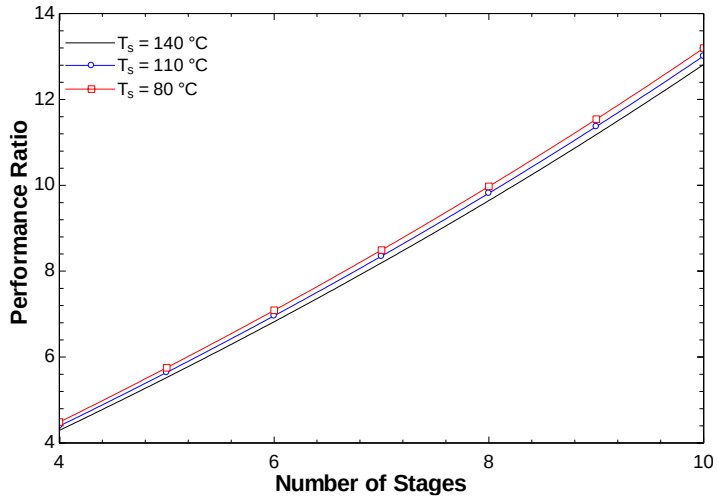

Figure 5.47 Effect of number of stages on performance ratio at different motive steam temperatures.

The last performance parameter to be investigated is the specific area which is the ratio between the summation of all effects surface area and condenser to the mass flow rate of the distilled water. Figure 5.48 shows the effect of motive steam temperature on the specific area. The results conclude that as the motives steam temperature increases, the specific area significantly decreases. However, the rate of reduction in the specific area decreases as the motive steam temperature approaches a high temperature. Furthermore, the number of stages does not affect the specific area at high temperature. However, the difference in specific area between different number of stages becomes significant when the motive steam temperature reduces as shown in Figure 5.49.

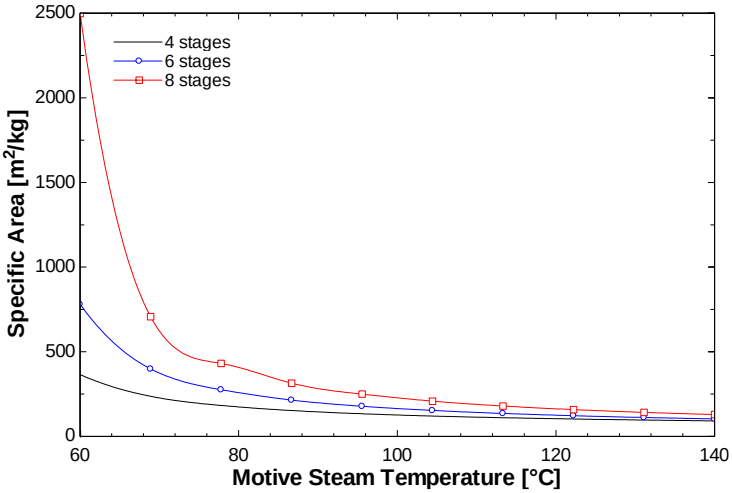

Figure 5.48 Effect of motive steam temperature on the specific area at a different number of stages.

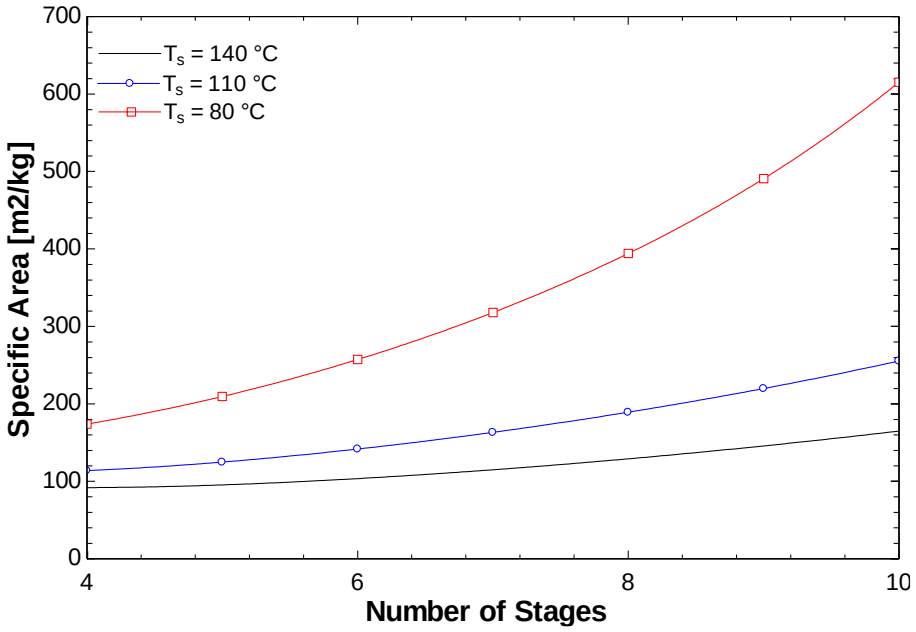

Figure 5.49 Effect of number of stages on the specific area at different motive steam temperatures.

5.4 Systems Comparison

The system comparison is shown in Figure 5.50 which shows a comparison of the overall energy and exergy efficiencies for the three different systems. System 2 represents the minimum energy and exergy efficiencies among the three different systems with 28.75% energy efficiency and 32.54% exergy efficiency. However, it does not imply that system 2 is inefficient because most of the thermal losses are taking place in solar heliostat between sun and boiler. Also, the source temperature considered in this study is 4500 K which significantly reduce exergy efficiency as well. The other two systems have very close energy and exergy efficiencies. However, system 3 has excess produced work in addition to covering the work demand unlike system 1 which is only covering the electrical work demand of the system.

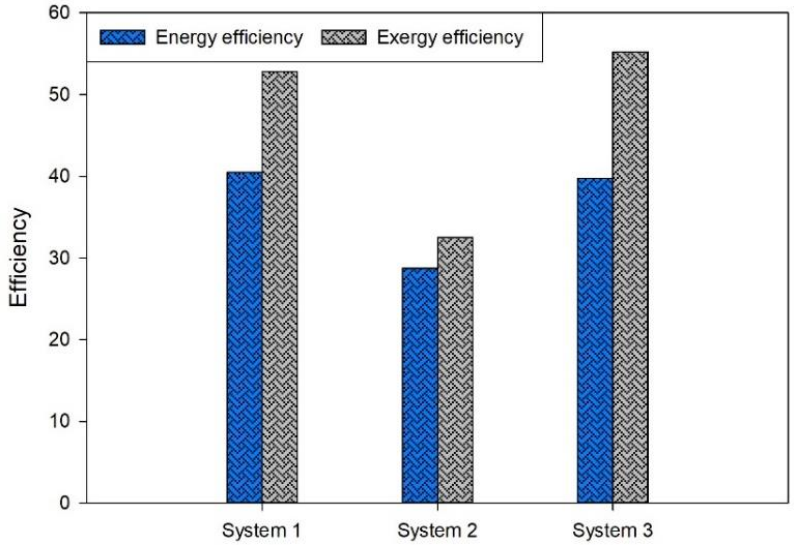

Figure 5.50 Comparison of the three systems energy and exergy efficiency.

Figure 5.51 shows the different forms of energy demand required by each system of the three DME production systems. The electrical work demand resulted to be minimum in the third system then, system 2 electrical work demand is higher and system 1 requires the maximum electrical work demand. On the other hand, system 1 has the minimum heat demand among the three systems then, system 2 requires a relatively higher amount of heat and system requires the maximum amount of heat among the threes DME production systems.

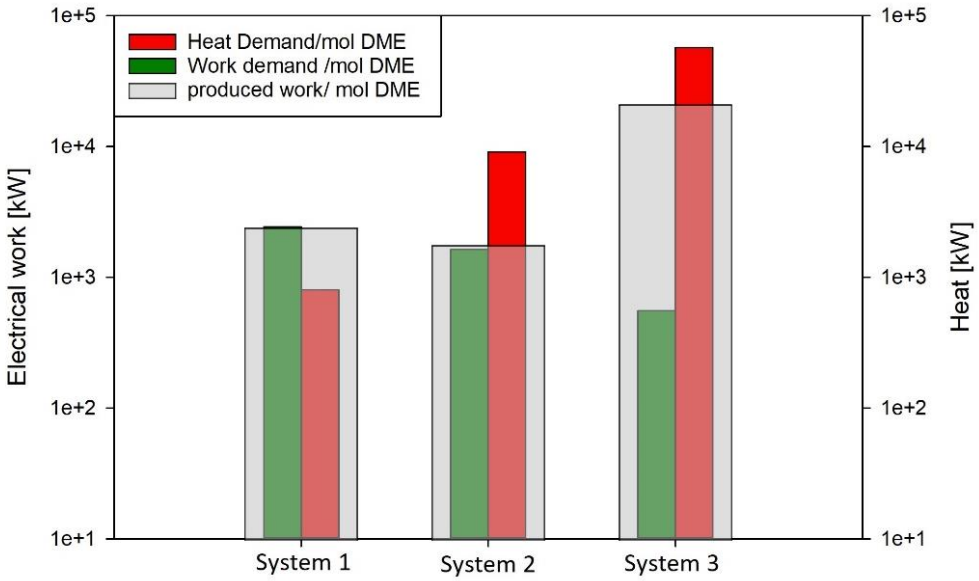

Figure 5.51 Comparison of heat and electrical work demand in each system.

Further comparison is made between the three developed systems and the conventional DME production plant and presented in Table 5.11 in terms of efficiency, energy demand and carbon emissions at a fixed production rate of 1 mol/sec of DME. The results revealed that the conventional plant has the maximum efficiency in producing DME from biomass feedstock. However, the conventional plant relies on fossil fuels as an energy source to operate the plant, unlike the developed systems operate by renewable energy and waste heat. Furthermore, conventional DME plant emits greenhouse gasses due to the dependence on fossil fuel. In contrast, the developed systems produce zero emissions and capture carbon dioxide from the flue gasses as well. Emission analysis is performed based on the best case scenario where natural gas was assumed as the equivalent fuel used for heating. As noticed from the table, conventional DME production plant does not contribute to saving carbon emissions rather it emits around 11.7 tons of carbon dioxide per day.

Table 5.11 Comparison of the developed systems with conventional DME plant

Parameter	System 1	System 2	System 3	Conventional plant
Efficiency (%)	40.5	28.8	39.7	55 [62]
Energy required (kJ/mol DME)	3276	4617	3342	2412
CO_2 emission saving (ton/day)	19.68	26.18	20.00	-

Chapter 6 : Conclusions and Recommendations

This chapter is discussing the main findings and results of the analyses implemented on the three different systems developed in this study, followed by detailed conclusions. Further, a number of recommendations are suggested for continuing future studies.

6.1 Conclusions

This study has considered different forms of renewable energy to be integrated with different waste heat flue gasses through heat recovery and carbon capturing subsystems to investigate the potential of dimethyl-ether production in a more environmentally friendly manner. This research has assessed the performance of the three proposed DME production systems from various sources of waste heat and renewable energy. The three proposed systems utilize the produced hydrogen from water and the captured carbon dioxide from the flue gas to produce methanol through carbon hydrogenation process and then produce DME from methanol through a methanol dehydration process. The three proposed systems have been simulated using Aspen Plus process simulation software, in addition to EES. The performance analyses for the proposed system were purely based on energy and exergy efficiencies. The results presented that the second system which is the solar thermal based DME production system has the lowest energy and exergy efficiencies due to the huge thermal losses in the heliostat field. However, the second system has huge potential to have almost double the production rate of the other two systems. An important aspect that can influence the selection of the system is the obtainability of the main energy resources and the electricity or heat demand required in each system.

The main findings of the research are presented below:

- The overall energy and exergy efficiencies of system 1 are 40.5 %, 52.8 % respectively, with a capacity to produce 1879.2 kg/day of DME.
- The overall energy and exergy efficiencies of system 2 are 28.8%, 32.5% respectively.
- System 2 has the capacity to produce 3758.3 kg/day of DME, and generate 1688 kW of electricity to feed the plant and excess electricity for domestic or industrial use.

- The overall energy and exergy efficiencies of system 3 are 39.7%, 55.2 % respectively.
- System 3 has the capacity to produce 1879.2 kg/day of DME, generate 10 MW of electricity to feed the plant and excess electricity for domestic or industrial use, and provide fresh water at a rate of 9.2 kg/s.

6.2 Recommendations

In this thesis, three conceptual designs of DME production have been proposed. The three systems have been thermodynamically modeled and simulated. Every system is integrated with a different form of renewable energy and waste heat flue gas resource. A number of recommendations have been listed for further investigations. These recommendations are listed as follows:

- The presently developed three systems for DME production should be built and experimentally tested.
- The sustainability dimensions of the proposed systems should be investigated by considering energy and exergy efficiencies.
- The economic analyses and feasibility studies for the proposed systems should be performed for possible applications.
- The systems should be further developed to consider the production of more useful outputs.
- More efficient heat recovery systems should be investigated in order to maximize the energy and exergy efficiencies.
- Further investigation should be conducted on the Cu-Cl cycle through more experimental data to find the reaction kinetics and obtain the optimum operating conditions.
- The multi-objective optimization studies should be performed for the three proposed systems in terms of the system parameters and operating conditions.

References

[1] Salcedo B. U.S. Energy Information Administration, “Monthly Energy Review. vol. 35. 2018. doi:10.1002/da.22823.

[2] BP. Statistical Review of World Energy. 2018.

[3] Bridgwater A. Renewable fuels and chemicals by thermal processing of biomass. Chem Eng J 2003;91:87–102. doi:10.1016/S1385-8947(02)00142-0.

[4] Munasinghe PC, Khanal SK. Biomass-derived syngas fermentation into biofuels. Biofuels 2011;101:79–98. doi:10.1016/B978-0-12-385099-7.00004-8.

[5] Mori D, Hirose K. Recent challenges of hydrogen storage technologies for fuel cell vehicles. Int J Hydrogen Energy 2009;34:4569–74. doi:10.1016/j.ijhydene.2008.07.115.

[6] Patten, J.; McWha T. Dimethyl Ether Fuel Literature Review. NRC Publications Archive. 2015.

[7] Rajeshwar K, McConnel R, Licht S. Solar hydrogen generation: Toward a renewable energy future. 2008. doi:10.1007/978-0-387-72810-0.

[8] Deiman JR. Water electrolysis. Water 2008;2:1–195. doi:PSO-F&U 2006-1-6287.

[9] Gandía LM, Oroz R, Ursúa A, Sanchis P, Diéguez PM. Renewable hydrogen production: Performance of an alkaline water electrolyzer working under emulated wind conditions. Energy and Fuels 2007;21:1699–706. doi:10.1021/ef060491u.

[10] Ni M, Leung MKH, Leung DYC. Electrochemistry Modeling of Proton Exchange Membrane (PEM) Water Electrolysis for Hydrogen Production. Whec 2006;16:13–6. doi:10.1016/j.jpowsour.2009.10.095.

[11] Ni M, Leung MKH, Leung DYC. Energy and exergy analysis of hydrogen production by a proton exchange membrane (PEM) electrolyzer plant. Energy Convers Manag 2008;49:2748–56. doi:10.1016/j.enconman.2008.03.018.

[12] Germany W. Electrochemical High Temperature Technology for hydrogen production or direct electricity generation 1988;13:283–7.

[13] Houaijia A, Roeb M, Monnerie N, Sattler C. Solar power tower as heat and electricity source for a solid oxide electrolyzer: a case study. Int J Energy Res 2015;39:1120–30. doi:10.1002/er.3316.

[14] Rosen MA. Advances in hydrogen production by thermochemical water decomposition: A review. Energy 2010;35:1068–76. doi:10.1016/j.energy.2009.06.018.

[15] Doizi D, Dauvois V, Roujou JL, Delanne V, Fauvet P, Larousse B, et al. Total and partial pressure measurements for the sulphur-iodine thermochemical cycle. Int J Hydrogen Energy 2007;32:1183–91. doi:10.1016/j.ijhydene.2006.11.039.

[16] Duigou A Le, Borgard JM, Larousse B, Doizi D, Allen R, Ewan BC, et al.

HYTHEC: An EC funded search for a long term massive hydrogen production route using solar and nuclear technologies. Int J Hydrogen Energy 2007;32:1516–29. doi:10.1016/j.ijhydene.2006.10.047.

[17] Forsberg C. Lowering Peak Temperatures For Nuclear Thermochemical Production Of Hydrogen. Oak Ridge National Laboratory. 2008.

[18] Naterer G, Suppiah S, Lewis M, Gabriel K, Dincer I, Rosen MA, et al. Recent Canadian advances in nuclear-based hydrogen production and the thermochemical Cu-Cl cycle. Int J Hydrogen Energy 2009;34:2901–17. doi:10.1016/j.ijhydene.2009.01.090.

[19] Naterer GF. Second Law viability of upgrading waste heat for thermochemical hydrogen production. Int J Hydrogen Energy 2008;33:6037–45. doi:10.1016/j.ijhydene.2008.08.010.

[20] Orhan MF, Dincer I, Rosen MA. Design of systems for hydrogen production based on the Cu-Cl thermochemical water decomposition cycle: Configurations and performance. Int J Hydrogen Energy 2011;36:11309–20. doi:10.1016/j.ijhydene.2011.02.034.

[21] Inc B. Waste Heat Recovery: Technology Opportunities in the US Industry. 2008. doi:10.1017/CBO9781107415324.004.

[22] Jouhara H, Khordehgah N, Almahmoud S, Delpech B, Chauhan A, Tassou SA. Waste heat recovery technologies and applications. Therm Sci Eng Prog 2018;6:268–89. doi:10.1016/j.tsep.2018.04.017.

[23] Semkov K, Mooney E, Connolly M, Adley C. Efficiency improvement through waste heat reduction. Appl Therm Eng 2014;70:716–22. doi:10.1016/j.applthermaleng.2014.05.030.

[24] Ishaq H, Dincer I, Naterer GF. Exergy-based thermal management of a steelmaking process linked with a multi-generation power and desalination system 2018;159:1206–17.

[25] Ishaq H, Dincer I, Naterer GF. New trigeneration system integrated with desalination and industrial waste heat recovery for hydrogen production. Appl Therm Eng 2018;142:767–78. doi:10.1016/j.applthermaleng.2018.07.019.

[26] Ishaq H, Dincer I, Naterer GF. Industrial heat recovery from a steel furnace for the cogeneration of electricity and hydrogen with the copper-chlorine cycle. Energy Convers Manag 2018;171:384–97. doi:10.1016/j.enconman.2018.05.039.

[27] Gude VG. Energy storage for desalination processes powered by renewable energy and waste heat sources. Applied Energy. 2015;137:877–98.

[28] Quoilin S, Declaye S, Tchanche BF, Lemort V. Thermo-economic optimization of waste heat recovery Organic Rankine Cycles. Appl Therm Eng 2011;31:2885–93. doi:10.1016/j.applthermaleng.2011.05.014.

[29] Wang ZQ, Zhou NJ, Guo J, Wang XY. Fluid selection and parametric optimization

of organic Rankine cycle using low temperature waste heat. Energy 2012;40:107–15. doi:10.1016/j.energy.2012.02.022.

[30] Bell LE. Cooling, Heating, Generating Power, and Recovering Waste Heat with Thermoelectric Systems. Am Assoc Adv Sci 2016;321:1457–61.

[31] Brückner S, Liu S, Miro L, Radspieler M, Cabeza LF, Lävemann E. Industrial Waste Heat Recovery Technologies: an Economic Analysis of Heat Transformation Technologies. Entwurf 2014;151:1–37.

[32] International Energy Agency. Tracking Industrial Energy Efficiency and CO_2 Emissions 2007.

[33] Tanaka NI. Energy Technology Perspectives Scenarios & Strategies To 2050. 2010. doi:10.1049/et:20060114.

[34] van Straelen J, Geuzebroek F, Goodchild N, Protopapas G, Mahony L. CO_2 capture for refineries, a practical approach. Int J Greenh Gas Control 2010;4:316–20. doi:10.1016/j.ijggc.2009.09.022.

[35] Olaleye AK, Wang M. Conventional and advanced exergy analysis of post-combustion CO_2 capture based on chemical absorption integrated with supercritical coal-fired power plant. Int J Greenh Gas Control 2017;64:246–56. doi:10.1016/j.ijggc.2017.08.002.

[36] Arachchige USPR, Melaaen MC. Aspen plus simulation of CO_2 removal from coal and gas fired power plants. Energy Procedia 2012;23:391–9. doi:10.1016/j.egypro.2012.06.060.

[37] Chen WH, Lin BJ, Lee HM, Huang MH. One-step synthesis of dimethyl ether from the gas mixture containing CO_2 with high space velocity. Appl Energy 2012;98:92–101. doi:10.1016/j.apenergy.2012.02.082.

[38] Tokay KC, Dogu T, Dogu G. Dimethyl ether synthesis over alumina based catalysts. Chem Eng J 2012;184:278–85. doi:10.1016/j.cej.2011.12.034.

[39] Xu M, Lunsford JH, Goodman DW, Bhattacharyya A. Synthesis of dimethyl ether (DME) from methanol over solid-acid catalysts. Appl Catal A Gen 1997;149:289–301. doi:10.1016/S0926-860X(96)00275-X.

[40] Hosseininejad S, Afacan A, Hayes RE. Catalytic and kinetic study of methanol dehydration to dimethyl ether. Chem Eng Res Des 2012;90:825–33. doi:10.1016/j.cherd.2011.10.007.

[41] Bai Z, Ma H, Zhang H, Ying W, Fang D. Process simulation of dimethyl ether synthesis via methanol vapor phase dehydration. Pol J Chem Tech Polish J Chem Technol 2013;15:122–7. doi:10.2478/pjct-2013-0034.

[42] Ng KL., Chadwick D., Toseland BA. Kinetics and modelling of dimethyl ether synthesis from synthesis gas. Chem Eng Sci 1999;54:3587–92. doi:10.1016/S0009-2509(98)00514-4.

[43] Hsi-Jen Chen , Chei-Wei Fan C-SY. Analysis, Synthesis, and Design of a One-Step Dimethyl Ether Production via a Thermodynamic Approach. Construction 2013;2:449–56.

[44] You Q, Liu Z, Li W, Zhou X. Synthesis of dimethyl ether from methane mediated by HBr. J Nat Gas Chem 2009;18:306–11. doi:10.1016/S1003-9953(08)60122-X.

[45] Azizi Z, Rezaeimanesh M, Tohidian T, Rahimpour MR. Dimethyl ether: A review of technologies and production challenges. Chem Eng Process Process Intensif 2014;82:150–72. doi:10.1016/j.cep.2014.06.007.

[46] Siddiqui O, Dincer I. Analysis and performance assessment of a new solar-based multigeneration system integrated with ammonia fuel cell and solid oxide fuel cell-gas turbine combined cycle. J Power Sources 2017;370:138–54. doi:10.1016/j.jpowsour.2017.10.008.

[47] Matzen M, Alhajji M, Demirel Y. Chemical storage of wind energy by renewable methanol production: Feasibility analysis using a multi-criteria decision matrix. Energy 2015;93:343–53. doi:10.1016/j.energy.2015.09.043.

[48] AlZahrani AA, Dincer I. Modeling and performance optimization of a solid oxide electrolysis system for hydrogen production. Appl Energy 2018;225:471–85. doi:10.1016/j.apenergy.2018.04.124.

[49] Ni M, Leung MKH, Leung DYC. Energy and exergy analysis ofhydrogen production by solid oxide steam electrolyzer plant. Int J Hydrogen Energy 2007;32:4648–4660. doi:10.1016/j.enconman.2008.03.018.

[50] AlZahrani AA, Dincer I. Thermodynamic and electrochemical analyses of a solid oxide electrolyzer for hydrogen production. Int J Hydrogen Energy 2017;42:21404–13. doi:10.1016/j.ijhydene.2017.03.186.

[51] Dincer I, Naterer GF. Overview of hydrogen production research in the Clean Energy Research Laboratory (CERL) at UOIT. Int J Hydrogen Energy 2014;39:20592–613. doi:10.1016/j.ijhydene.2014.06.074.

[52] Xu C, Wang Z, Li X, Sun F. Energy and exergy analysis of solar power tower plants. Appl Therm Eng 2011;31:3904–13. doi:10.1016/j.applthermaleng.2011.07.038.

[53] Zamfirescu C, Dincer I, Naterer GF. Thermophysical properties of copper compounds in copper-chlorine thermochemical water splitting cycles. Int J Hydrogen Energy 2009;35:4839–52. doi:10.1016/j.ijhydene.2009.08.101.

[54] Last G V, Schmick M. Identification and Selection of Major Carbon Dioxide Stream Compositions. Rep Prep US Dep Energy 2011.

[55] Matzen M, Alhajji M. Chemical storage of wind energy by renewable methanol production : Feasibility analysis using a multi-criteria decision matrix 2015;93. doi:10.1016/j.energy.2015.09.043.

[56] Clausen LR, Houbak N, Elmegaard B. Technoeconomic analysis of a methanol plant based on gasification of biomass and electrolysis of water 2010.

doi:10.1016/j.energy.2010.02.034.

[57] Thomas R. Reed. Efficiencies of Methanol Production from Gas, Coal, Waste or Wood. Methanol Div f MIT Energy Lab 2000:4801–7.

[58] Perry RH, Green DW. Perry's chemical engineers' handbook. McGraw-Hill; 2008.

[59] Al-Sulaiman FA, Dincer I, Hamdullahpur F. Exergy modeling of a new solar driven trigeneration system. Sol Energy 2011;85:2228–43. doi:10.1016/j.solener.2011.06.009.

[60] Dinali MN, Dincer I. Development and analysis of an integrated gas turbine system with compressed air energy storage for load leveling and energy management. Energy 2018. doi:10.1016/j.energy.2018.08.094.

[61] Al-Zareer M. Conceptual development and analysis of multiple integrated hydrogen production plants with Cu-Cl cycle. 2016.

[62] Birk U, Røngaard L, Munkholt J, Arendt P, Degn A. Production of methanol/DME from biomass EFP06. vol. 12. 2018.